**POLITECNICO**

MILANO 1863

SCUOLA DI INGEGNERIA INDUSTRIALE
E DELL'INFORMAZIONE

TESI DI LAUREA MAGISTRALE IN
MECHANICAL ENGINEERING
INGEGNERIA MECCANICA

Author: **Matteo Arici**

# An application of the Unknown Input Observer to the estimation of railway track irregularities

Student ID: 10569587
Advisor: Egidio di Gialleonardo
Co-advisor: Stefano Alfi
Academic Year: 2022-23

# Abstract

This Thesis work has as its main objective the implementation of an algorithm for the reconstruction of the railway track geometry in the time domain, in all its three main components of vertical, lateral and roll irregularity, through the employment of accelerometers on board of a in-service train, specifically the "Meneghino" train employed on the Milan Underground. The chosen algorithm is the U.I.O. (Unknown Input Observer), a deterministic observer, which unlike a stochastic one (for example, a Kalman Filter-type observer) has no requirement or previous knowledge of statistical quantities of the to-be-estimated displacement, so to make a direct application of the system more practical. At first, the algorithm has been tested on some trial systems so that general character considerations could be made to be successively applied on gradually more complex models; then, such results have been applied on a linearized model of the examined vehicle, and compared with those of a multibody simulation provided by the Politecnico di Milano for their validation. First, the U.I.O. has been applied to estimate vertical dynamics through the employment of a 10 D.o.F. simplified model; the relations between multiple delayed inputs have been analyzed through Padé Approximation, and an algorithm to take vehicle variable velocity into account has been developed. Then, an application of the algorithm for the estimation of roll and lateral irregularity of the railtrack was tried; to this end, a 21 D.o.F. lateral model was developed, that took into account friction and elastic wheel-track contact dynamics. After a thorough model validation, estimation was conducted through the application of an upgraded version of the previously utilized frame and more advanced filtering techniques; furthermore, some considerations were made about the main similarities and differences between this case and the high-speed ones mainly found in literature.

**Key-words:** U.I.O., Track Irregularity

# Sommario

Il presente lavoro di tesi si prefigge come obiettivo l'implementazione di un algoritmo per la ricostruzione dell'irregolarità di binario nel dominio del tempo, nelle tre componenti fondamentali di scostamento verticale, laterale e di rollio, tramite misurazioni di accelerometri a bordo di un treno in servizio, nello specifico il modello Meneghino impiegato nella Metropolitana di Milano. L'algoritmo scelto è l'U.I.O. (Unknown Input Observer), un osservatore deterministico, che contrariamente ad un osservatore stocastico (es., di tipo Kalman Filter) è privo della necessità di conoscenza pregressa di quantità statistiche della deformazione da stimare, in modo da favorire un'applicazione diretta del sistema. In un primo momento l'algoritmo è stato testato su sistemi di prova per trarne considerazioni di carattere generale da poter poi applicare in modelli via via più complessi; nella seconda fase, tali risultati sono stati applicati ad un modello linearizzato del veicolo in esame, e confrontati con quelli di una simulazione multibody concessa dal Politecnico di Milano per la loro validazione. In primo luogo, l'U.I.O. è stato applicato alla stima della dinamica verticale attraverso un modello semplificato a 10 gradi di libertà; i legami tra multipli ingressi con ritardo sono stati analizzati tramite l'Approssimazione di Padé, e si è sviluppato un algoritmo che tenga conto della velocità variabile del veicolo. Quindi, si è provato ad applicare tale algoritmo alla stima di rollio e irregolarità laterale del binario; a tal scopo, si è sviluppato un modello laterale a 21 gradi di libertà che tenesse conto delle dinamiche di attrito e contatto elastico ruota-rotaia. Dopo un'accurata validazione del modello, la stima è stata effettuata attraverso l'applicazione di una versione migliorata dell'infrastruttura precedentemente utilizzata e tecniche di filtraggio più avanzate; inoltre, alcune considerazioni vengono fatte sulle somiglianze e le differenze fra questo caso e quelli ad alta velocità ritrovabili per lo più in letteratura.

**Parole chiave:** U.I.O., Irregolarità di Binario

# Contents

# Introduction

Rail vehicles are one of the main means of transportation for both people and goods. In Italy alone, despite tire-based transport (especially for goods) still being dominant, every year train networks account for almost half a billion passengers and 100 million tonnes of transported goods [1]. Needless to say, a correct and prehemptive maintenance of the rail network is paramount to maintain its functionality; in order to grant both safety and comfort, and also to correctly plan maintenance (instead of having to periodically stop circulation for corrective measures), it is thus of fundamental importance to provide an updated monitoring of the tracks misalignment from nominal conditions, both in terms of vertical and transversal irregularity.

All that has been said is especially true when dealing with point-to-point connections limited to one track per direction (as it is often the case), and even more when the trains we are dealing with are not long range inter-urban ones, but local vehicles for which a prolonged stop could mean the paralysis of one or more sectors of a city. One such example is the Milan Metro, which alone is responsible for the movement of almost 1 million passengers every day (in the face of a 3 million population), and for which even a few hours of stop would result in an immense economical and reputational damage. To furtherly exacerbate the issue, the windows for operating such monitoring without affecting circulation are very tight, as the 4 to 6 hours of nighttime service stop must also account for system reactivation, effectively reducing the available time to a couple hours maximum.

Unfortunately, underground and local trains feature many peculiar aspects which make it almost impossible to run monitoring vehicles like has been done since long on conventional and high-speed networks: short intervals between the trains and the stations, together with highly variable travel speed and rarely straight trajectory arewhat is arguably the main drive to the necessity of finding alternative way to monitor the track geometry. Due to a very simple application of economy of scale, while a nationwide train network may have economical advantages in maintaining a diagnostic fleet in service, such a limited-scale urban network (the largest in Italy, but still just a metro service) cannot afford a constant monitoring and mainly has to rely on externally provided services.

To this end, in this work one alternative way of dealing with the issue will be analyzed, through the employment of the very in-service trains providing on-board measurements (mainly virtue of accelerometers) which will be processed to

reconstruct the irregularity of the track; this requires an algorithm to be done, and among the many available options the one called Unknown Input Observer (U.I.O.) has been chosen for this particular instance. The U.I.O. is a so-called Model-based Algorithm which can be used to reconstruct a non-deterministic input (in this case, the track geometry) through the employment of a linearized model of the system (the train) on which measurements – acceleration measurations in this study case – are carried on. After a brief introduction of the problem and how it is currently solved in other environments (Section 1), the first part of the thesis (Section 2) will thus be centered around the presentation of the U.I.O. algorithm and its employment on a couple of simple study cases, so that general considerations can be deduced about the data sets to be used for the analysis; some alternative ways of dealing with the problem of noise-induced derivation discontinuities will also be described.

After this theoretical introduction, the U.I.O. will be applied on the actual model of the considered metro train in order to reconstruct the geometry of the track by comparing the estimation results with the employment of a multibody model faithfully replicating the behaviour of the real vehicle; first, in Section 3, the system will be focused on the reconstruction of vertical displacement through the use of a 10 D.o.F. linear system. Padé Approximation will be employed to take into account multiple delayed inputs, and in this occasion the limitations on its use will be explored. The relative simplicity of the model will also be exploited to analyze some further aspects, such as the reconstruction of a disturbance while the vehicle changes velocity during travel, or while traversing a curved track section. The results will thus be compared with the ones generated by a multibody simulation provided by PoliMi, both in terms of time history and spectrum, to demonstrate the effectiveness of the method.

Section 4, instead, will be centered around transversal dynamics, thus featuring more complex physics due to the friction contact dynamics; the system to estimate roll and lateral irregularity will be a 21 D.o.F. with externally imposed track roll angle, replicating conditions found in similar works found in literature. The severe limitations and issues associated with the operation of such a system at the low speed of an underground train, opposed to the conditions of high-speed trains on which the aforementioned works are centered around, will be explored in detail, trying to appropriately upgrade both the algorithm and the post-processing techniques in order to refine estimation.

Last, a resume of the advantages and limitations of the U.I.O. applied on low-speed local trains will be presented, in order to finally determine whether the analyzed method is adequate for the solution of the problem, or other algorithms could be more apt to the task.

# 1  State of the Art

The importance of monitoring the geometry of railtracks is well beyond the academic interests of this thesis, but is paramount to allow the correct and continuous circulation of rail-based vehicles. In particular, there are no less than three aspects which make disturbance tracking so essential, that will be discussed in detail in section 1.1 below; in section 1.2, instead, an overview of the currently employed methods to operate track geometry monitoring will be presented, along with a description of the particular study case that will be dealt with in the rest of the work.

## 1.1.  Reasons behind Track Monitoring

The first paramount aspect is safety. By monitoring the profile of the railtracks, certain potentially destructive trends can be prehemptively repaired, such as heat-related tracks' misalignment from nominal position during particularly hot summers, or consumption of the track surface. Moreover, by knowing the exact profile of tracks it is possible to increase logistic efficiency by allowing trains to limit speeds only when traversing particularly disturbed sections.

The second aspect is the most obvious when dealing with passengers' transportation, and it is of course their comfort; there are, in fact, precise norms which exactly deal with the allowed limits for vibrational behaviour of vehicles, in order not to negatively affect the travellers' comfort – or worse, their health. These limits, described by standard ISO2631, correlate every vibrational frequency and acceleration amplitude with a maximum exposure time over which human body starts to show signs of fatigue; by increasing this acceleration thresholds by 6dB, the actual limits for health safety can be obtained, while reducing them by 10dB, an equally important upper bound can be identified, namely the "reduced comfort boundary" – the acceleration limit over which for a passenger becomes difficult to perform activities like reading or writing, effectively pretty reasonable pastimes for public transportation users. Figure 1.1 reports one such graph, called "Janeway Comfort Criterion", in this particular case referring to vertical acceleration; similar diagrams can however be found in the norms for other directions of solicitation:
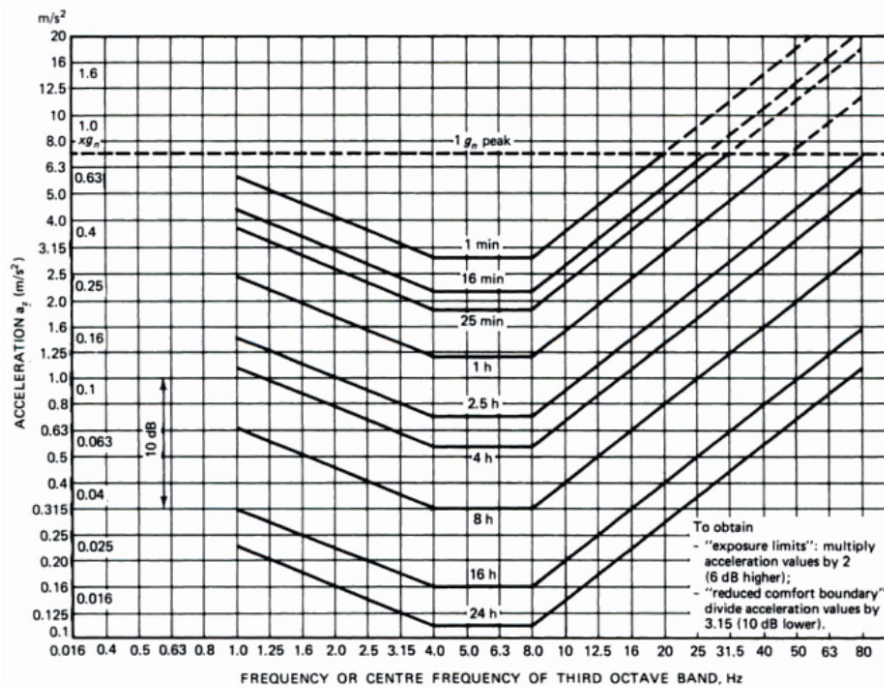
Figure 1.1: Iso-Fatigue Curves as defined by norm ISO2631

Alternatively, the same norm proposes some synthetic coefficients to evaluate the degree of comfort of a given railtrack section; one example is the following formula (1.1); which takes into account vibrational behaviour in all three directions, adequately windowed through frequency ponderation curves in order to give higher statistical weight to those disturbances falling within the 4-8 Hz interval, the one to which human body is most sensible.

$$a=\sqrt{\left(1.4\,a_{xw}\right)^2+\left(1.4\,a_{yw}\right)^2+a_{zw}^2} \qquad (1.1)$$

The third aspect is more or less a result of both the previous ones; in order to both increase average comfort, prevent derailments or smaller-scale incidents and regulate circulation velocity, maintenance must obviously be done on the tracks; large-scale periodic replacements of track sections, though, are very time-consuming and can paralyze the trains' normal circulation for days – the alternative being instead prompt prehemptive intervention only on those sections which feature anomalies to be addressed.

## 1.2. Irregularity Measurement

There are many ways to evaluate track geometry by employing adequately equipped monitoring vehicles. Among the various systems, a couple can be mentioned; for more information on the topic of railtrack diagnostics, refer to the comprehensive overview contained in the extensive work by Esveld [2]:

- Optical Measuring Systems employ lasers and mirrors enclosed in a track measuring beam; the traverse time of the laser from the source to the return of its reflection is measured and converted into a distance, obtaining a evaluation of the geometry. Usually, there are three such beams mounted on the vehicle, the front and rear one used as reference and the middle one as the one actually providing the measurement through the so called "Chord Measuring" as in Figure 1.2;



Figure 1.2: Chord Measurement Laser System - Image from Mermec Group (https://www.mermecgroup.com [3])

- Telescopic Measuring Systems instead employ pneumatic actuators which press a set of additional wheels into a forced contact with the rails, so that their movement is perfectly adherent to the profile of the track, both vertically through horizontal-axis measurement wheels (which is normally the case of the actual train wheels, due to the contact with the track being almost anelastic) and horizontally through vertical-axis ones (which is instead quite different from the real case, due to friction dynamics getting overwritten).

One or more of these devices can be mounted on dedicated vehicles employed for the railtrack monitoring, called "Diagnostic Trains"; due to the relatively complex technology, only a few manufacturers of such vehicles exist, and transport societies quite often have to rely on externally provided services for monitoring duties.

In Italy, a small fleet of Diagnostic Trains is part of the RFI, with the so called "Archimede" [4] being mostly employed for traditional lines and ETR500Y1 (Aiace) and ETR500Y2 (DiaManTe – Diagnostica Manutenzione Tecnologica) being dedicated to high-speed tracks. No such vehicles, though, are currently used for smaller-scale circulation monitoring, like urban railways or underground networks; this work's topic will in fact be focused on one possibility for monitoring the track geometry of one such line, namely the Milan Underground Network run by ATM. The chosen reference vehicle is the 900 Series electric train manufactured by AnsaldoBreda, also known "Meneghino" after a local way of saying "from Milan" but also doubling as a corruption of MNG, Metropolitana di Nuova Generazione (Next Generation Underground). This vehicle, pictured in Figure 1.3, currently operates on 3 out of 5 Milan Metro lines – the other two instead relying on autonomous-driving convoys – therefore its modelization can provide a valuable insight to be employed on all of the metropolitan network.



Figure 1.3: The 900 Series Meneghino electric train (photo provided by WikipediaCommons)

Switching from inter-urban lines to urban public transport, though, and in particular an underground line, presents some additional challenges with respect to the previously discussed cases. The employment of diagnostic vehicles on a local line is in fact hampered by a number of issues, for example the much reduced interval between trains (in the order of some minutes opposed to tenths of minutes to hours for inter-urban lines) and the relative absence of alternative paths for normal

circulation to keep flowing, effectively paralyzing the network. Even dedicating only part of a convoy for measurement is not a praticable option, since the average underground train is composed of just a few carts (seldom more than 3), and replacing even one of them with a purely diagnostic one (making it unusable for public transportation) would dramatically reduce the efficiency of the line.

All of these make for the necessity to provide measurements directly from trains during their service, through the employment of adequately positioned accelerometers and an algorithm for the reconstruction, through a simplified model of the train, of the track geometry which generated those very accelerations; again, though, even if many works have been published on the topic of such algorithms, mainly as a more economically affordable alternative to expensive Diagnostic Trains – especially if outsourced (one of particular relevance by De Rosa et al. [5]), they mostly deal with high-speed circulation, where some approximations can be done which are no longer valid when speaking of metropolitan transportation, such as constant velocity (due to the much closer distance of stations) or overall rectilinear trajectory. Hence the need of choosing the correct algorithm both in terms of practicability and robustness to varying boundary conditions regarding both velocity and trajectory.

Among the several possible algorithms, two broad categories can be discerned:

- Signal-based algorithms do not employ a model of the system, while instead relying exlusively on the signal itself which is variously elaborated to reconstruct the disturbance that generated it; among the simplest examples there is the double integration os such signal employed for the aforementioned inertial systems (for example discussed by Weston et al. [6] or Real et al. [7]); although simple, this method is actually quite problematic both in implementation and in the obtained results – integrating non-white noise will in fact generate a drift unless a high-pass filter is employed, hindering the analysis of long wavelengths;

- Model-based algorithms are instead usually preferred due to their flexibilty; they aim at reconstructing a simplified version of the vehicle and use quantities measured on various points of said vehicle (most likely of parts not directly affected by the track geometry) to reconstruct the exact behaviour of all of its organs.

In this work the second class will be the object of our study, but another distinction to be made is the domain in which said model is made to operate:

- Frequency-domain methods allow for the description of the analyzed section disturbance with a limited number of synthetic parameters; one example of their application in the track monitoring field is the analysis by S. Alfi and S. Bruni [8]. Although simpler and arguably more precise, they feature a number of issues, namely the impossibility of detecting a localized deformation and

the inapplicability of such systems on an online-kind of measurement gig (due to them relying on already having registered data in order to obtain a generalized spectrum);

- Time-domain methods are the ones analyzed in this paper, as they were deemed more interesting for several reasons; most importantly, though, for the aforementioned usage on online applications, and also because comfort-related considerations (which are mainly related to frequency of sollecitation) can still be made through post-processing of the signals (obtainment of spectra, PSDs, filtering, etc.).

The latter category features primarily two algorithms to evaluate an unknown input (what is generally defined as a random "disturbance" in the correct working of a linear system), both based upon algorithms generally used to evaluate the *state* of a system and thus obtaining its random input as a sort of by-product. The first and simplest is called Unknown Input Observer and is based on Luenberger Observer, while the second is a modification of a Kalman Filter; although, once again, the latter choice is the way to go to ensure almost perfect results (as demonstrated for example by Tsunashima et al. [9]), the comparison is imperfect due to not considering a fundamental detail: in order to work, Kalman Filter requires the previous knowledge of certain statistical data of the input we're trying to determine (in particular an estimation of its variance), making it less than optimal when compared with a less accurate algorithm which does not require additional data other than the accelerations of the train.

For these reasons, the following work will be centered around the possibilities and limitations of the U.I.O. algorithm in the railtrack disturbance estimation field, starting with a presentation of the algorithm from a mathematical point of view, and then with its in-field application.

# 2   Unknown Input Observer

The U.I.O. (acronym standing for Unknown Input Observer) is, at its core, a repurposed Luenberger Observer [10] combined with a second estimator for a to-be-determined input generically identified as a disturbance $d$. In the goal of this work, such disturbance is the misalignment of a rail track in terms of vertical irregularity, transversal irregularity and roll variation with respect to the nominal values; the state $x$, instead, is the combination of velocity and displacement of all the bodies employed to describe the model of a railcar, namely the carbody itself, two bogies and four wheelsets.

## 2.1.   U.I.O. Theoretical Outline

Given a generic mechanical system described in the canonical state-space form expressed in (2.1) and (2.2), where an unknown disturbance $d$ acts on the system (but does *not* directly influence the output dynamics, as will be furtherly stressed upon later on):

$$\begin{cases} \dot{x}=A\,x+B\,u+E\,d & (2.1) \\ y=C\,x & (2.2) \end{cases}$$

By multiplying (2.1) by matrix $C$, a direct correlation (2.3) can be derived between the derivative of output $y$ and the aforementioned disturbance $d$:

$$C\,\dot{x}=CA\,x+CB\,u+CE\,d=\dot{y} \qquad (2.3)$$

From this equation, the (2.4) can be easily obtained, that is, the desired formulation of the required observer – an estimate of disturbance $d$ whose error dynamics can be controlled through an appropriate tuning of gain matrix $L$ as will be demonstrated in a short while. From this moment on, for simplicity, the pseudoinverse of product matrix $CE$ will be identified as matrix $M$.

$$\hat{d}=\left(CE\right)^{+}\left(\dot{y}-CA\,x-CBu\right)=M\left(\dot{y}-CA\,x-CBu\right) \qquad (2.4)$$

Notice that, being the dimension of $CE$ equal to the number of analyzed signals by the number of to-be estimated inputs, this matrix is in general not square – since most likely more signals will be required to grant convergence on the estimation of a smaller number of random inputs – hence the pseudoinverse in place of a common

inverse matrix. There is, though, a limitation on this matrix (therefore on the choice of output matrix $C$, since $E$ is determined by the system itself), a necessary condition (2.5) for the applicability of the U.I.O. regarding its rank and that of matrix $E$:

$$rank(CE)=rank(E)$$ (2.5)

Which *de facto* means that the number of observed states have to be at least equal to that of unknown inputs to be estimated, but most likely higher in order to fulfill this condition.

Quite obviously, while in the (2.4) the state $x$ appears, that is not a known information; thus, the disturbance estimator must be combined with a Luenberger observer to generate a state estimation, obtaining the final result depicted in the (2.6):

$$\begin{cases} \dot{\hat{x}}=A\,\hat{x}+B\,u+E\,\hat{d}+L(y-C\,\hat{x}) \\ \hat{d}=(CE)^+(\dot{y}-CA\,\hat{x}-CB\,u)=M(\dot{y}-CA\,\hat{x}-CB\,u) \end{cases}$$ (2.6)

On an algorithm point of view, the estimation procedure can be schematized through the block diagram in Figure 2.1 below:
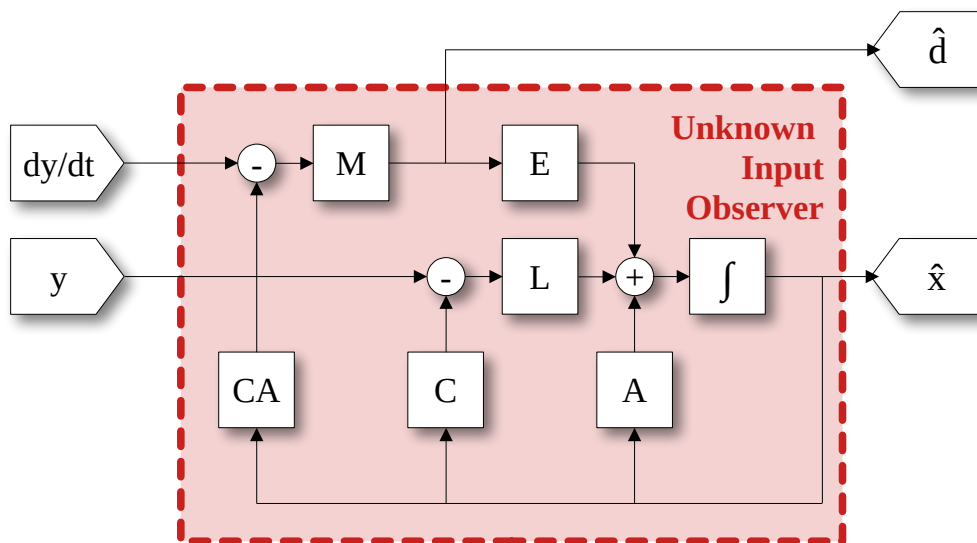


Figure 2.1: U.I.O. Algorithm Block Diagram

In order to obtain a formulation of the aforementioned state estimate that is independent from the measurements' derivative, an auxiliary variable $z$ is introduced. Said variable $z$ depends on both the state estimation and the output $x$ as per the (2.7):

$$z=\hat{x}-H\,y$$ (2.7)

By defining matrix $H$ in (2.7) as equal to the product of $E$ and $M$, the dynamics of $z$ and output $y$ described in (2.8) can be decoupled as seen in (2.9); notation can be furtherly simplified by introducing matrix $T$ in place of the expression $I - EMC$ (2.10) and matrix $F$ as the result of $TA - LC$ (2.11); this last matrix will be the one defining the dynamics of the estimator:

$$\dot{z} = A\hat{x} + Bu + EM\dot{y} - EMCA\hat{x} - EMCBu + Ly - LC\hat{x} - H\dot{y} \qquad (2.8)$$

$$\dot{z} = (A - EMCA)\hat{x} + (B - EMCB)u + Ly - LC\hat{x} \qquad (2.9)$$

$$\dot{z} = (TA - LC)\hat{x} + TBu + Ly = \dots$$
$$\dots = (TA - LC)z + (TA - LC)Hy + TBu + Ly \qquad (2.10)$$

$$\dot{z} = Fz + TBu + (FH + L)y = Fz + TBu + Ky \qquad (2.11)$$

The (2.11) is the final formulation of the auxiliary variable dynamics, and it is in fact independent from the derivative of output $y$.

Now, error dynamics must be introduced to demonstrate that the estimator that has just been constructed is, in fact, accurate; defining the error vector as in (2.12) and (2.13), a decomposition of matrix $K$ into two different matrices $K_1$ and $K_2$ can thus be introduced (2.14), reminding the relation expressed in (2.2):

$$\varepsilon = x - \hat{x} \qquad (2.12)$$

$$\dot{\varepsilon} = Ax + Bu + Ed - \dot{z} - H\dot{y} \qquad (2.13)$$

$$\dot{\varepsilon} = Ax + Bu + Ed - Fz$$
$$- TBu - K_1Cx - K_2y - HCAx - HCBu - HCEd \qquad (2.14)$$

From this point, reintroducing the relation expressed in (2.7) and summing and subtracting the same term $(A - HCA - K_1C)z$ as in (2.15), the (2.16) can be obtained:

$$\dot{\varepsilon} = (A - HCA - K_1C)x + (B - HCB - TB)u$$
$$+ (E - HCE)d - K_2y - Fz + (A - HCA - K_1C)z \qquad (2.15)$$
$$- (A - HCA - K_1C)\hat{x} + (A - HCA - K_1C)Hy$$

$$\dot{\varepsilon} = (A - HCA - K_1C)\varepsilon + (I - HC - T)Bu + (I - HC)Ed$$
$$+ ((A - HCA - K_1C) - F)z + ((A - HCA - K_1C)H - K_2)y \qquad (2.16)$$

In order for this demonstration to be completed, a pure dynamic relation between the error $\varepsilon$ and its derivative must be obtained, with no other inputs having any influence whatsoever; through some of the already introduced definitions and relations, (2.17) and (2.18) can be obtained. Notice that, from a theoretical standpoint, this passage is much more relevant than what initially appears, since it

allows to demonstrate that the apparently conflicting formulations by Chen/Patton [11] and Ding [12], despite taking opposite routes, are actually completely equivalent given the difference in notation, allowing to effectively provide a definition for the two matrices $K_1$ (2.19) and $K_2$ (2.20):

$$
\begin{cases}
I - HC - T = I - EMC - T = T - T = \begin{bmatrix} 0 \end{bmatrix} & (2.17) \\
(I - HC)E = (I - EMC)E = E - E(CE)^+ CE = E - E = \begin{bmatrix} 0 \end{bmatrix} & (2.18) \\
(A - HCA - K_1 C) - F = (TA - K_1 C) - (TA - LC) = \begin{bmatrix} 0 \end{bmatrix} \Leftrightarrow K_1 = L & (2.19) \\
(A - HCA - K_1 C)H - K_2 = FH - K_2 = \begin{bmatrix} 0 \end{bmatrix} \Leftrightarrow K_2 = FH & (2.20)
\end{cases}
$$

Moving from this assumptions, error dynamics can be obtained, as expressed in (2.21); since the relation matrix between the error and its derivative is only matrix $F$:

$$
\dot{\varepsilon} = (A - HCA - LC)\varepsilon = F\varepsilon \tag{2.21}
$$

As anticipated, through the placement of the poles of matrix $F$ it is possible to generate an adequate gain matrix $L$ to employ in a Luenberger observer that will be associated with the disturbance estimation equation described in the (2.4).

One point that should be reminded, though, is that although what the name might suggest, the original focus of U.I.O. method is not to determine the random input itself, while rather estimating the state of the system regardless of it being subject to said random input. This means that, for example, although the (2.11) allowed to decouple the *state* estimate dynamics from the output derivative, the same cannot be said for the true goal of the application, that is to estimate the *disturbance*. Hence, this *modus operandi* implies to have perfect knowledge not only of output $y$, but also of its derivative as seen in (2.4); while in ideal conditions this wouldn't really be a problem, any field application features non-neglibible measurement noise which severely hinders any attempt at derivation – i.e., the signal constantly changes its trend, resulting in the output derivative being mostly driven by its noise, rather than its "general" trend. Also, since signals are subject to discrete sampling, such derivative would also feature discontinuities – and hence singularities in the process of reconstructing the disturbance signal.

There are a number of possible solutions to the issue:

- The first and most "obvious" solution is to use said derivative as the actual output; to better explain, measurements of both velocity and acceleration can be carried out simultaneously, despite only actually treating the former as the output $y$ of the system (to be fed to the estimation algorithm, which will employ a selection of rows from an identity matrix as its matrix $C$ – further details in section 2.3.1) while the latter is only used as its derivative; this method is failproof on-paper, but it fails to factor in that measuring velocities is not a trivial task; furthermore, although possible, the costs associated with

measuring velocities, when compared to even an extensive use of accelerometers, would make any large-scale application unfeasible;

- The second way, which will be employed for the rest of this work, is a more "pragmatic" variation of the previous one: as it has been remarked, problems arise due to the possibility of incurring into discontinuities – whose derivative results in a singuarity; the opposite operation, though, can only result (at least for the interests of this study) in inherently continuous functions. Hence, while actual measurement is necessarily an acceleration, its integral (which is, disregarding noise for a while, an estimation of velocity) can work just as fine as the input of the algorithm;

- The third way is little more than an hypothesis, since no supporting evidence has been found in documentation regarding either practicability or actual advantages; most importantly, aside from a small selection of experimental results, it could very well be argued whether the inherent complexity of this method really outbalances the advantages it tries to bring – which is, to avoid further manipulation of the output signal. The method, tentatively named "Derivative Estimation Algorithm", will be discussed in section 2.2.

## 2.2. Derivative Estimation Algorithm

What follows is a tentative solution to the output derivative issue, not in itself without criticalities; please notice that this way of proceeding won't see application in this work aside from the first dummy systems employed to tune and refine the algorithm, after which more consolidated approaches will be preferred. However, it is deemed interesting to introduce such procedure in a perspective of further development, since its perks-to-issues balance seem to be heavily dependant on the study case, in particular becoming much more interesting the more complex the system becomes (both in terms of variables number and mutual interactions), not to mention any potential case in which output elaboration is not a viable option.

The main core of the reasoning is exceptionally simple, as it relies on inverting (2.7) in order to obtain (2.22), that is a relation linking $y$ (and hence its derivative) to the auxiliary variable $z$ and the state estimate; notice that $z$ is not actually utilized by the U.I.O. algorithm, as it was introduced more as a mathematical exploit in order to analyze error dynamics, meaning it has no physical meaning whatsoever:

$$z = \hat{x} - H \, y \Rightarrow \dot{y} = H^+(\dot{\hat{x}} - \dot{z}) = (EM)^+(\dot{\hat{x}} - \dot{z}) \tag{2.22}$$

This means that the following system can be obtained, a system of two differential equations – (2.23) and (2.24) – to be combined with the aforementioned estimation of output derivative (2.25) and the disturbance estimator (2.26), in a system that will be reported here as a resume:

$$\begin{cases} \dot{\hat{x}} = A\,\hat{x} + B\,u & (2.23) \\ \dot{z} = (TA - LC)\,\hat{x} + TBu + L\,y & (2.24) \\ \dot{y} = (EM)^+(\dot{\hat{x}} - \dot{z}) & (2.25) \\ \hat{d} = (CE)^+(\dot{y} - CA\,\hat{x} - CBu) & (2.26) \end{cases}$$

This theoretical architecture, although somewhat fascinating, has several glaring issues: the main red flag is the pseudoinverse of matrix $H$, which there are no guarantees actually exists; in fact, this will quite often be the case, not allowing to proceed in the first place.

With the most crippling issue out of the way, there still are some imperfections to be taken into account; assuming $H$ doesn't have a null determinant (or to have been able to ignore the problem), a second differential equation has still been introduced, resulting in a second dynamic (generally at a much higher frequency) superimposed over the original correct result (then again, easily disposable of through the employment of a low-pass filter, most likely a device in any case featured by the system). The same considerations will be explored in more detail in Section 2.3.1.

The final problem is mainly related to the requirement of using a *previous* state in order to determine the subsequent value of the derivative of output *y*. This is unavoidable, as if such delay wasn't introduced, we would incur in an "algebraic loop", a numerical issue which is the request by the system of an input which is itself part of the output of said system requiring it: in layman's terms, it means that the system is asking for a value (in this case the state estimation derivative – (2.23)) that it cannot obtain, since in order to do that the same system – in particular the (2.24) – should *work* to begin with. Hence the memory block featured in the upper part of Figure 2.2, which has the undesirable consequence of making the system time-discrete and, most importantly, its results heavily dependent on the solver step-size:
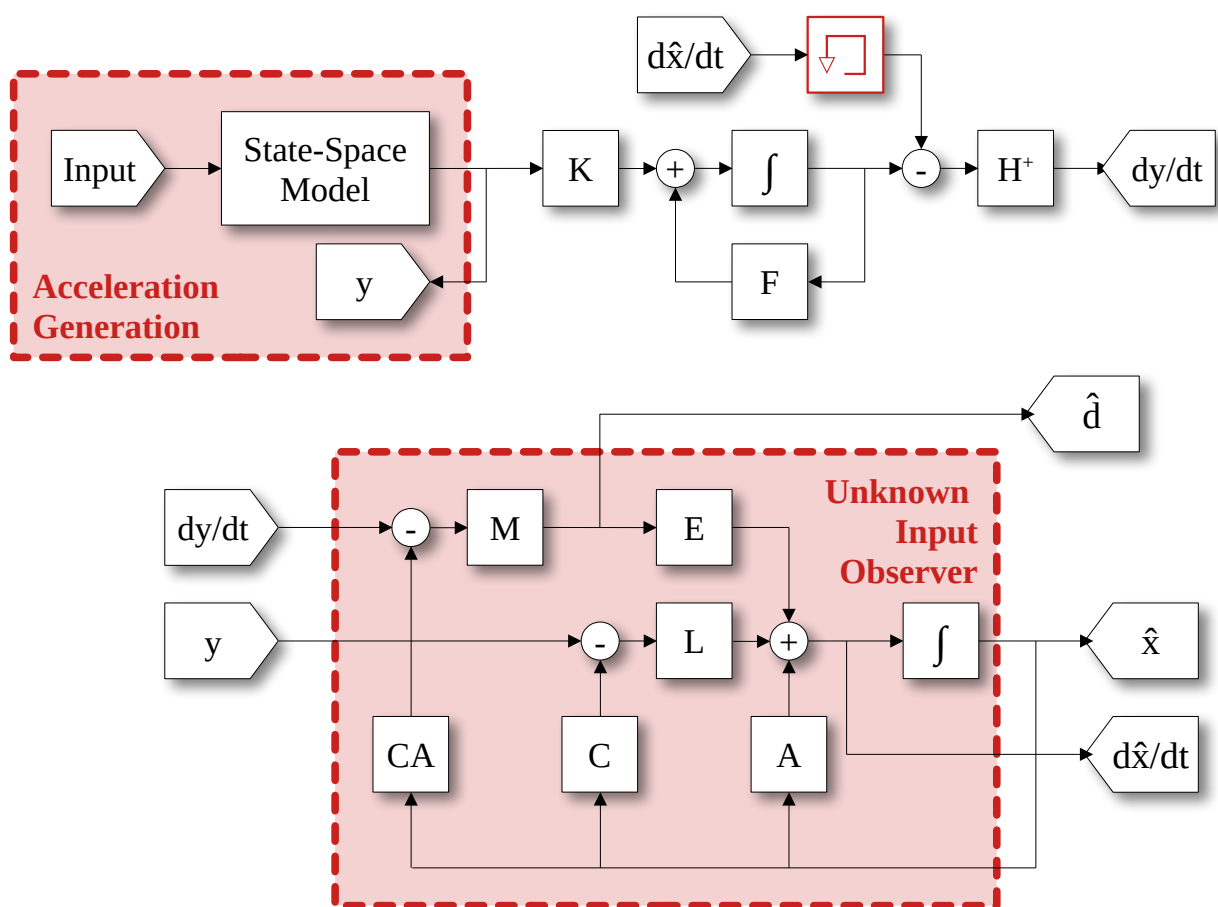


Figure 2.2: Derivative Estimation Algorithm Block Diagram (above) and corresponding U.I.O. Algorithm (below) - notice the red memory block in the upper part

## 2.3.  2 D.o.F. Trial System

In order to verify the functionality and potential of the U.I.O. algorithm, it was decided to implement it on the simplest possible trial system: an harmonic oscillator composed by a 2 and subsequently 3 bodies of equal mass connected by springs and dampers, thus featuring respectively 2 and 3 degrees of freedom. Disturbance, for simplicity, is rendered as an unknown force applied to mass 1, specifically the result of multiple sinusoidal actions with mutually unrelated amplitude, frequency and phase.

This simple system is pictured in Figure 2.3 below, and its data are listed in Table 2.1:

Table 2.1: 2 / 3 D.o.F. Trial System Data

| Parameter | Value |
|-----------|-------|
| **Mass** | 1000 kg |
| **Damping** | 80 Ns/m |
| **Stiffness** | 1100 N/m |
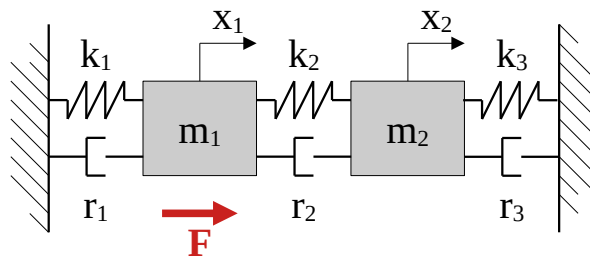


Figure 2.3: 2 D.o.F. Linear Oscillator

On the topic of data, it must be reminded that this section assume as valid the premise of complete and perfect knowledge of the system, since the same model will be used to obtain an output to be processed; in turn, the result will be compared with the input it received. In a real application, the first part of the sequence is not a work of synthesis, but rather the result of measurements from an existing mechanical system from which is our job to derive a comprehensive (if reasonably approximated) modelization; furthermore, an additional measurement-related noise could be featured in the data fed to the algorithm. In simpler terms, in a real case only measurement data to be fed to an algorithm will be available, either generated real-time by the vehicle or previously recorded and stored to be separately analyzed. The algorithm' parameters will be built upon the (linear) synthetic model employed to describe the (generally *not* linear) physical system behaviour; since no "real value" will be available to be compared with our estimations, particular attention will be

devoted to the selection of said parameters, as a relatively minor variation could translate in large scale errors in the disturbance estimation, but there would be no way to actually notice.

To run the 2 D.o.F. trial system, a number of choices can be made on three different options:

- Type of Output: as output of the mechanical system and input of the disturbance estimation algorithm either acceleration or its integral can be employed as reference; the other theoretical option described at 2.1, that is to directly use velocity as a secondary output and not as a result of post-processing, won't be addressed, both for physical unfeasibility and an overlapping of results with the integrated acceleration method (at least as long as the signal is not affected by noise); from this moment on, the two considered options will be referred to as "Acceleration" and "Velocity Model", respectively;

- Derivation Method: a sub-choice of previous parameter, since in the velocity case the derivative of the output is the original acceleration measurement itself. In the case of acceleration, though, the possibility of employing the Derivative Estimation Algorithm will be explored, instead of relying on its "true" derivative – which could be used, but only as long as the measurement doesn't feature noise-induced discontinuities;

- Number of Considered Outputs: being this a 2 D.o.F. system, the choice of how many state variables to employ as input for the algorithm is limited to either 1 or 2; that being said, despite the former choice might suggest that either of the two masses' motion is valid as observed state, it'll be shown in depth that this is not the case, as both methods require one precise choice of input (the only difference being exclusivity in the case of acceleration, not so in the case of velocity);

Many combinations of these three options will be analysed in order to infer considerations of general validity to be applied to more complex systems, both in terms of input type, system geometry and number of D.o.F.; it should be remarked, though, that since these choices are not entirely independent one with the other, the actual number of possible configurations is very limited.

## 2.3.1. Acceleration Model

If acceleration is used as an output, the choice of state variables to be considered is obligated, both in number and in identity. Since we are interested in acceleration, which is *not* a part of state formulation (velocity + displacement) we need to use a selection of rows of matrix $A$ and $E$ as our matrix $C$ and the other one relating $y$ with $d$ – from now on it will be referred to as $G$. The problem is easily noticed, though; a direct relation between disturbance $d$ (to be determined) and output $y$ is not featured

in the original premise of the U.I.O. (2.2), as it would result in an output equation in the form of (2.27) below (notice the appearance of said matrix $G$ in the (2.28)):

$$\begin{cases} \dot{x}=A\,x+B\,u+E\,d & (2.27) \\ y=C\,x+G\,d & (2.28) \end{cases}$$

In the specfic case that has been discussed until now, the matrices $A$ and $E$ have the form depicted in the (2.29), thus if the entire selection of acceleration was employed for the estimation, the matrices $C$ and $G$ would result as in the (2.30):

$$A=\begin{bmatrix} -2\dfrac{r}{m} & +\dfrac{r}{m} & -2\dfrac{k}{m} & +\dfrac{k}{m} \\ +\dfrac{r}{m} & -2\dfrac{r}{m} & +\dfrac{k}{m}m & -2\dfrac{k}{m} \\ 1 & 0 & 0 & 0 \\ 0 & 1 & 0 & 0 \end{bmatrix}; E=\begin{bmatrix} +\dfrac{1}{m} \\ 0 \\ 0 \\ 0 \end{bmatrix} \qquad (2.29)$$

$$C=\begin{bmatrix} -2\dfrac{r}{m} & +\dfrac{r}{m} & -2\dfrac{k}{m} & +\dfrac{k}{m} \\ +\dfrac{r}{m} & -2\dfrac{r}{m} & +\dfrac{k}{m}m & -2\dfrac{k}{m} \end{bmatrix}; G=\begin{bmatrix} +\dfrac{1}{m} \\ 0 \end{bmatrix} \qquad (2.30)$$

As it is now clear, utilizing the first acceleration (the one of the mass directly affected by the input force) determines the appearance of a non-null term in matrix $G$.

Notice that this is something that *could* theoretically be dealt with: output equation can be transformed, or in other terms the reference systems could be changed (for example measuring *different* degrees of freedom, like the relative distance between the masses) in order to neglect the matrix $G$. This operator is called "Null-Space", and in mathematical terms it equates to multiply all terms of output equation (2.28) by a transformation matrix $N_S$ (as per (2.31)) so that the product between said matrix and the problem matrix $G$ is equal to a null matrix (hence the name "Null Space", meaning to project the system on an axis set where $d$ has no direct relation with $y$):

$$y=C\,x+G\,d \Rightarrow N_S\,y=N_S\,C\,x+N_S\,G\,d$$
$$being\ N_S\neq[0]:N_S\,G=[0] \qquad (2.31)$$

Problem is, for such a system the null-space method does nothing but reaffirm what has been previously stated: the corresponding null-space to any $G$ matrix of the form $[a\ 0]$, being $a$ any non-null value, would be a matrix of the form $[0;\ b]$, again proving that the indirect input is, once again, the one required to determine the disturbance.

Regarding gains, one possible choice is to proceed with a pole-placement, but before doing that the fixed poles (related to the system itself, and hence not modifiable) and the modifiable ones (related to the actual choice of gain matrix *L*, and thus the only one that can be influenced and whose desired position we can employ for its determination) must be separated. This can be done through the transformation of the system itself into its "Observability Staircase Form" (through a transformation matrix *X*), allowing us to graphically separate its unobservable (fixed poles) and observable part, as seen in (2.32) and (2.33):

$$TA \Rightarrow XTA = \begin{bmatrix} TA_{not\,obs} & W \\ [0] & TA_{obs} \end{bmatrix} \tag{2.32}$$

$$TA_{not\,obs} = \begin{bmatrix} \lambda_{1\,not\,obs} & 0 & \dots & 0 \\ 0 & \lambda_{2\,not\,obs} & \dots & 0 \\ \vdots & \vdots & \ddots & \vdots \\ 0 & 0 & \dots & \lambda_{N\,not\,obs} \end{bmatrix} \tag{2.33}$$

For the poles to be arbitrarily placed, it was decided to use real negative numbers, so to ensure maximum stability (and prevent undesirable dynamic effects) and most importantly to more easily monitor the placement algorithm correct functioning (through comparison of the actual obtained poles of matrix *F* and the aforementioned poles employed in placement).

Thus we obtain that for a 2 D.o.F. the only input that can be employed is the acceleration of undisturbed mass (mass 2), leaving just the choice of derivative algorithm to be made:

- When utilizing the "true" derivative, highly accurate results can be observed (Figure 2.4 and Figure 2.5); then again, this result is relatively uninteresting, since it reduces to invert a known system (which, as already explained, is in itself an idealization) with little-to-no actual elaboration.
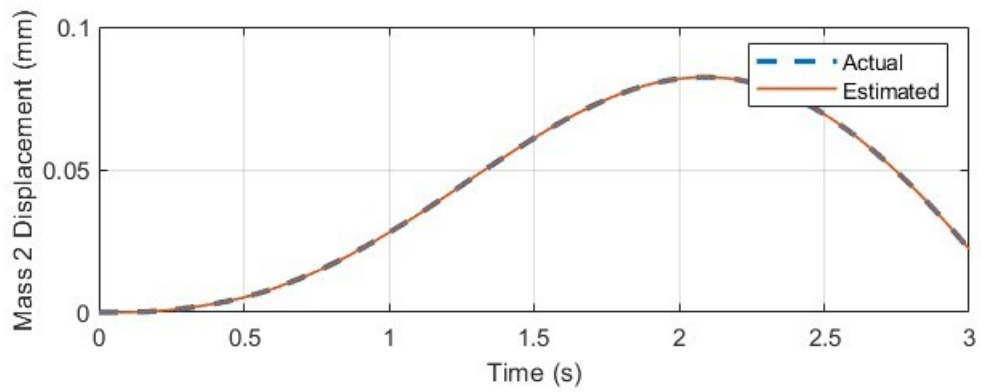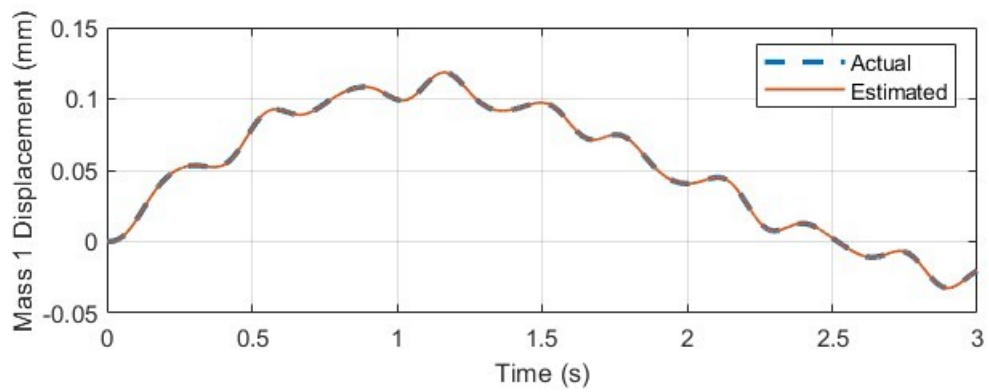
Figure 2.4: Acceleration Model - 2 D.o.F. State Estimation
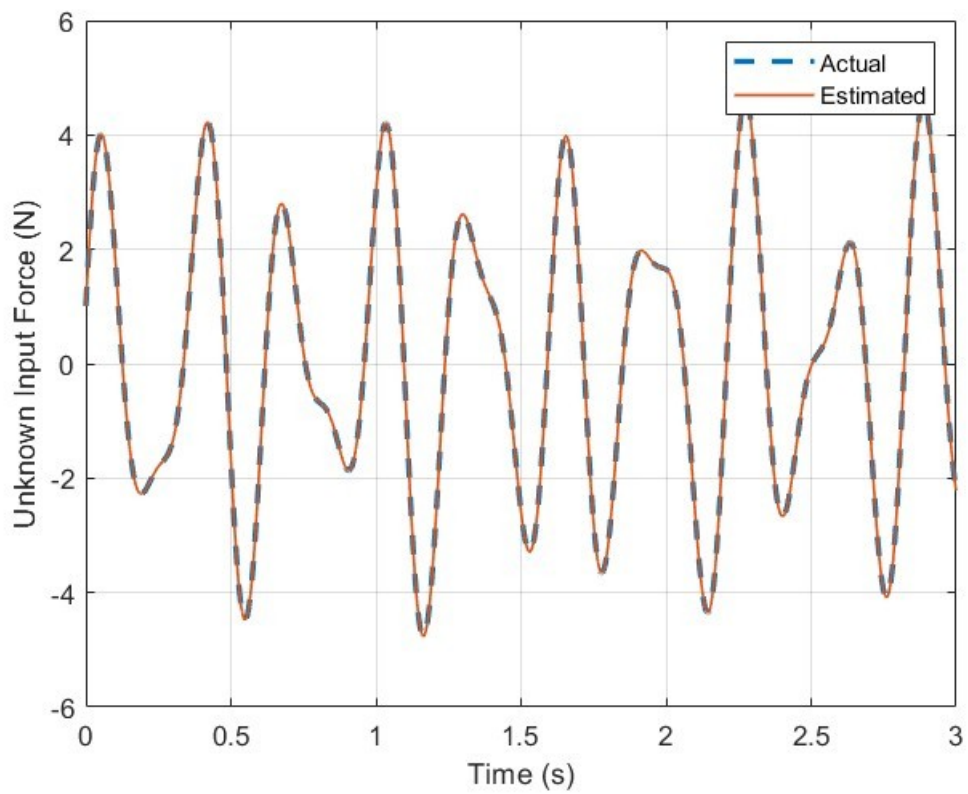


Figure 2.5: Acceleration Model - 2 D.o.F. Force Estimation

- If Derivative Estimation is employed, an interesting effect can be observed which was previously mentioned: as per (2.24) and (2.25), yet *another* equation has been introduced into the system, over which we have very limited control; a differential equation results, quite obviously, in a dynamics law, hence an higher frequency harmonic superimposed on the correct estimation (Figure 2.6) can be observed;
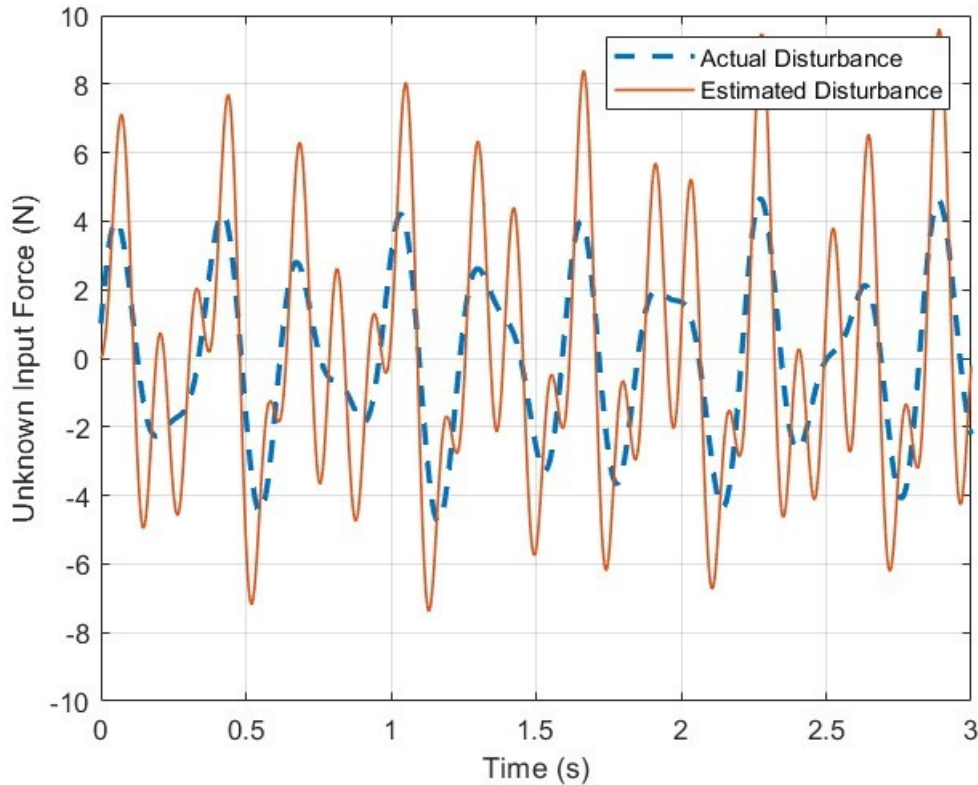


Figure 2.6: Acceleration Model - 2 D.o.F. Force Estimation through Derivative Estimation (0,005s timestep)

The properties of said harmonic seem to be directly connected to the solver step-size which can be now considered as an additional tuning parameter to improve estimation: in particular, a lower step-size results in not one, but *two* beneficial effects. First, an higher frequency in said overlaying dynamics: if the end result dynamic behaviour is expected to fall within a certain range of frequency, it will also be possible to tune the timestep in order to leave this additional harmonic outside of that range, and thus what cutoff frequency a low-pass filter should work with in order to delete it along with natural-source noise. Second, one of the main issues with Derivative Estimation appears to be a tendency to overshoot and hence overestimate actual disturbance; it can be observed that decreasing step-size has a very positive relation with reduction of said overshoot (Figure 2.7 and Figure 2.8).
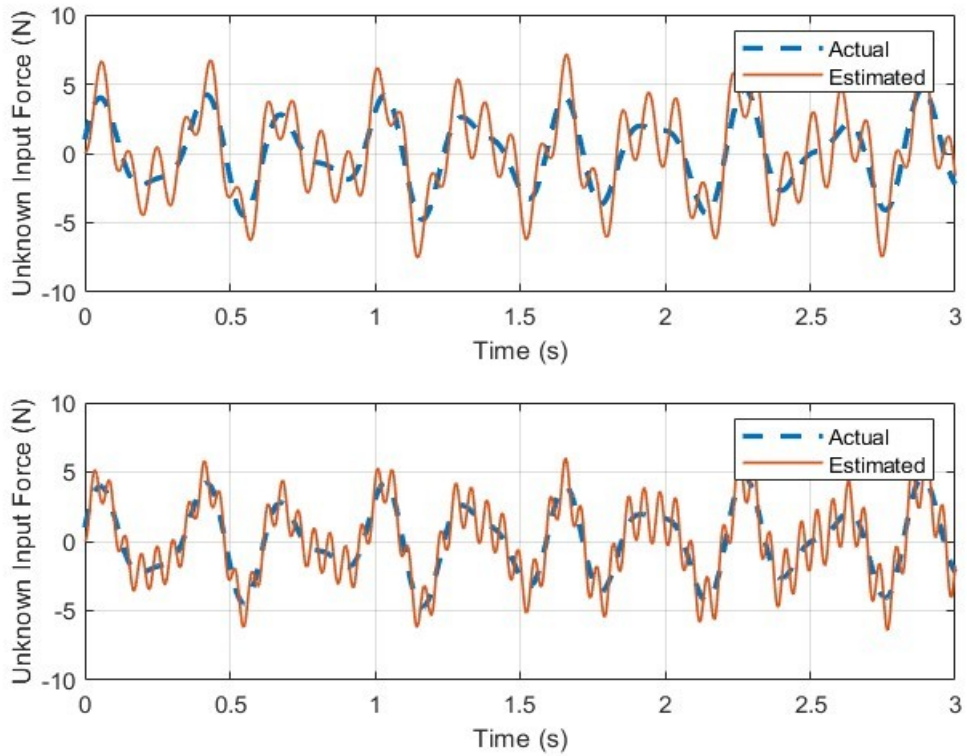
Figure 2.7: Comparison of Overshoot and interferencing dynamics between a 0,003s (above) and a 0,001s (below) timestep
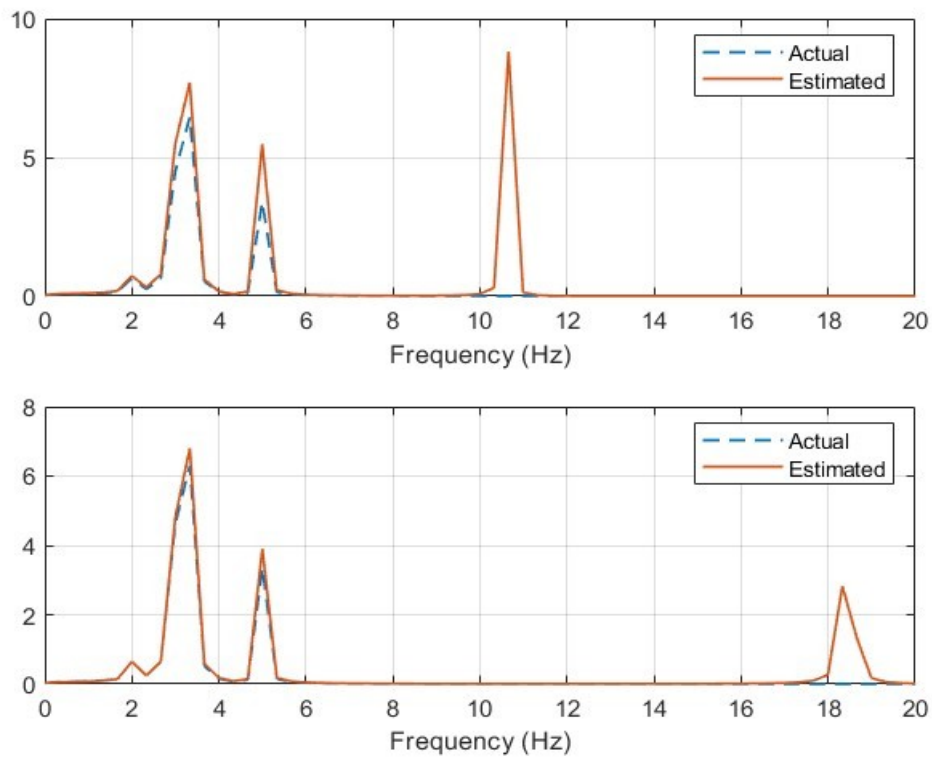


Figure 2.8: Comparison of the Power Spectral Density of actual and estimated force between a 0,003s (above) and a 0,001s (below) timestep

## 2.3.2. Velocity Model

On the opposite side, if velocity is utilized as input of the estimation algorithm, we are obligated to choose as target *exactly* the one mass our disturbance is applied to; were we not to oblige to this condition, the fundamental condition of U.I.O. ((2.5), which will be reported here as a reminder) would not be fulfilled:

$$rank(CE) = rank(E) \tag{2.5}$$

In this case matrix $C$ is a selection of rows from an identity matrix with size equal to matrix $A$; as depicted in the (2.34), the previously mentioned matrix $G$ is now null, due to having considered the lower half of the system (2.29) instead of the upper one:

$$C = \begin{bmatrix} 1 & 0 & 0 & 0 \\ 0 & 1 & 0 & 0 \end{bmatrix}; G = \begin{bmatrix} 0 \\ 0 \end{bmatrix} \tag{2.34}$$

As per the definition of an identity matrix, this means that all values on the same row are equal to zero, except for the value in the column corresponding to its row – i.e., $C_{ab} \neq 0$ if and only if $a = b$. This means, though, that if only rows relative to undisturbed motions are selected, those will be rows for which the only non-null term is in a different position than in the column matrix $E$: this results in a null matrix product $CE$, which doesn't allow to proceed with the algorithm as the inverse – specifically the *pseudo*inverse – of a null matrix (matrix $M$) does not exist.

Unlike acceleration case, though, it is not forbidden to use additional outputs, although in this specific case the employment of additional outputs does not significally contribute to the accuracy of the result. However, using only one input (at least in such a simple case) occasionally results in the impossibility to proceed with the Pole Placement, due to the MatLab$^{\text{TM}}$ Algorithm flagging the system as "nearly uncontrollable", which would mean that almost infinite gains are necessary in order to grant stability to the system: this is simply not correct, though, most likely a result of the algorithm's inadequacy – it was actually demonstrated that the desired poles for the system could be obtained by manually setting the gain matrix with a mere trial-and-error approach, disproving the uncontrollability denounced by the program. Anyway, using two inputs avoids such unpleasant problems, as it allows for the complete controllability of the estimator dynamics, save for an unvaried pole in the origin.

Regarding results, high compatibility can be observed between estimated and actual disturbance (Figure 2.9 - in this case employing 2 inputs to avoid algorithm-related problems), again a widely expected result:
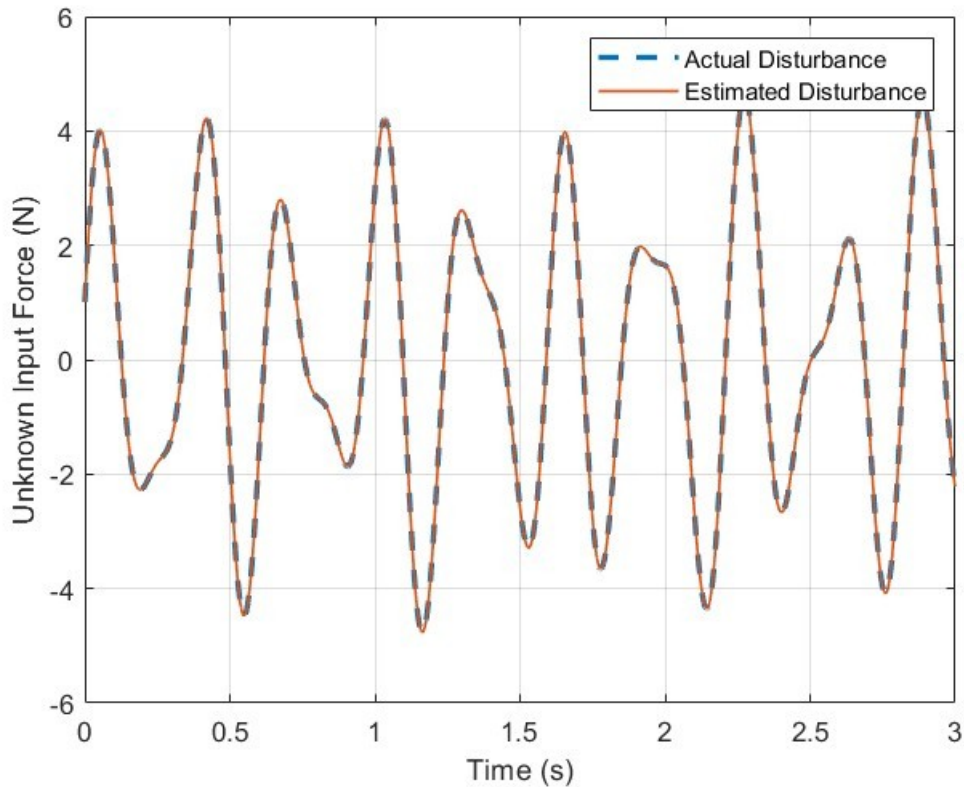
Figure 2.9: Velocity Model - 2 D.o.F. Force Estimation

## 2.4.  3 D.o.F. Trial System

The exact same procedure was therefore applied to an extended version of the previous system, this time composed of three masses separated by springs and dampers, again subject to a to-be-determined force F applied to mass 1, as presented in Figure 2.10 below. Notice that this system, although rudimentary, is starting to resemble the target application; at its core, in fact, the train model we'll employ in the next sections can be reduced to three bodies (or more accurately, three *series* of bodies) variously connected by springs and dampers; these results will therefore be much more useful to also suggest which Degrees of Freedom will be actually needed in the real field situation as well.
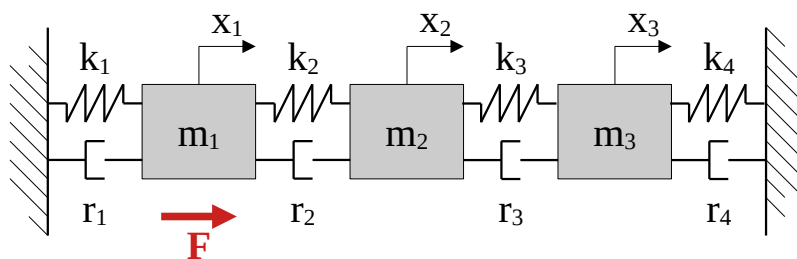


Figure 2.10: 3 D.o.F. Linear Oscillator

Since it would be useless to once again list down all possible situations, a simple resume of collected data and considerations will follow:

- Regarding Acceleration Model, the use of both uninfluenced degrees of freedom as outputs seems not to provide benefits whatsoever: if we decide to stick with the "classical" derivative, it is found that, in Figure 2.11, the results get quite distrbed, superimposing to the correct values another harmonic, signaling a bad correlation between the inputs;
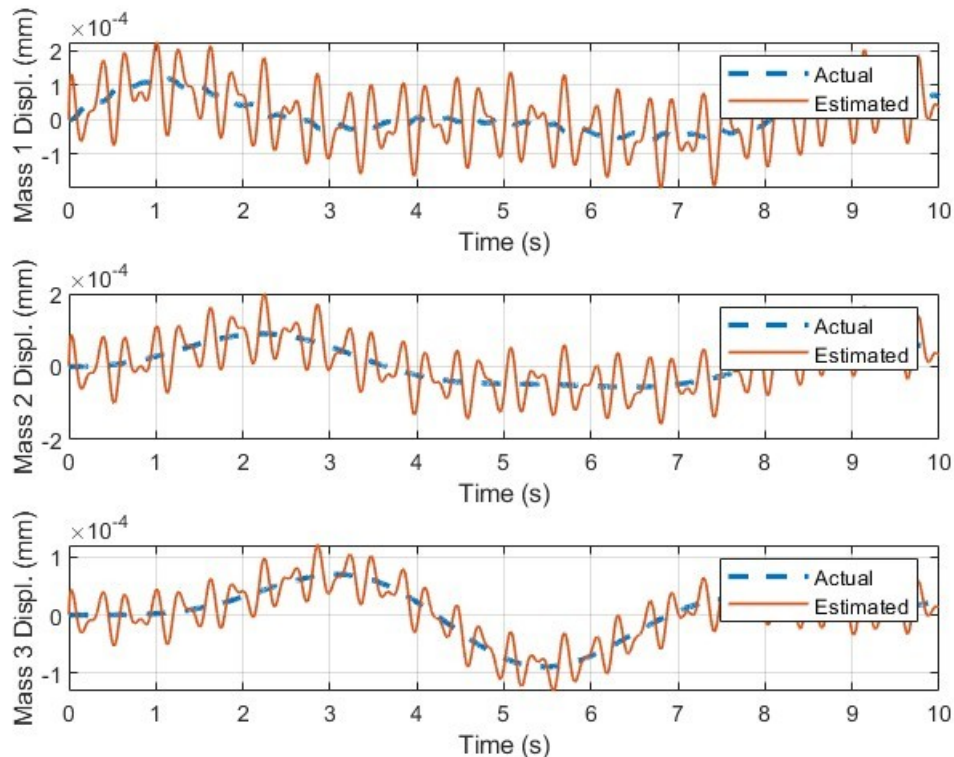


Figure 2.11: Acceleration Model - 3 D.o.F. State Estimation through the use of both Mass 2 and 3 Accelerations as input (0,001s timestep)

Were we to still try and apply the Derivative Estimation Algorithm, we would be stuck immediately, since the procedure seems unable to provide useful results with multiple outputs (resulting in a not-pseudoinvertible matrix *H*). This marks the last instance this experimental algorithm will be employed in this paper, leaving space for further examination.

- If instead only one acceleration is used (the one from mass 2, the closest to the affected one), an adequate estimation of the correct trajectory can be observed for both the classical derivative and the estimated one, again the latter featuring the issue of being heavily influenced by step size – an optimal compromise between processing time and precision being around 0,0001 s.

- If integrated velocities are employed, instead, the highly accurate results pictured in Figure 2.12 (this time without any problem regarding single-input pole placement) can be obtained, except that the less inputs are analyzed, the more the measure seems to start diverging from the correct value as the simulation time goes on – hence the choice to employ both the velocities of Mass 1 and 2 as inputs:
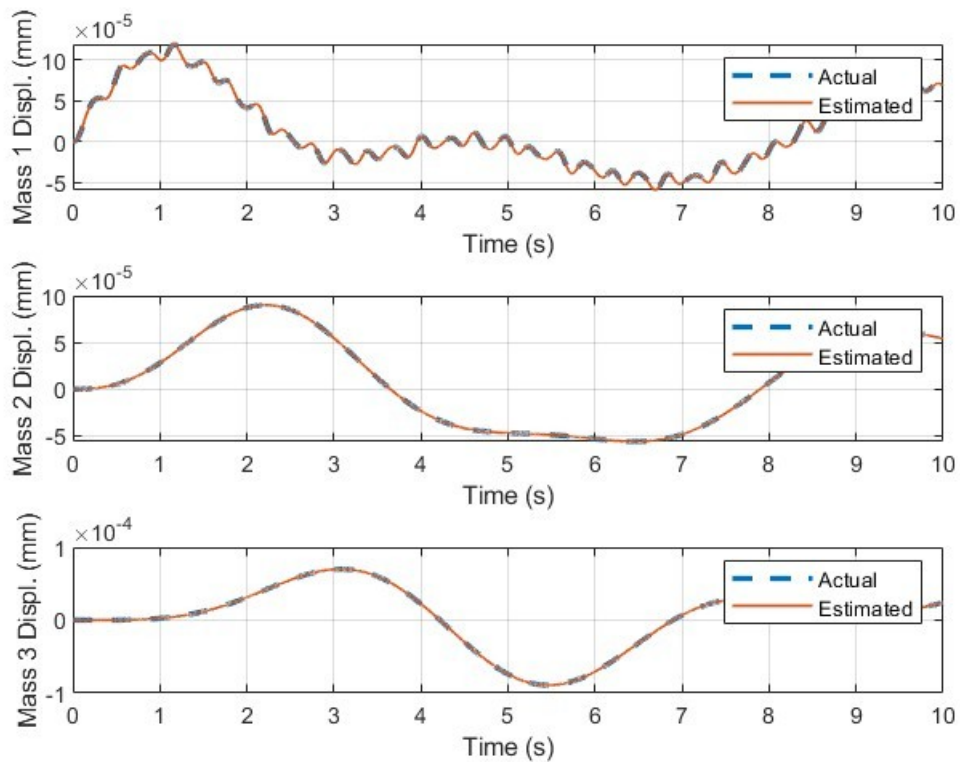


Figure 2.12: Velocity Model - 3 D.o.F. State Estimation

The reason for this behaviour might be that the more rows are considered within matrix $C$, the less poles of $A$ are left uncontrollable: for comparison, for single output model there is only 1 modifiable pole, while for both 2 and 3 outputs we have 5 (the maximum number, as the origin pole is by default fixed). This doesn't only mean that the immediately adjacent Degrees of Freedom (so to speak, in terms of moving masses) have a beneficial effect on driving the estimator, but also that the further we go from the disturbance we are to measure, the less it seems to make a difference on the overall result. In our study case, this translates into a relative uselessness of the carbody acceleration values for the analysis of an input entering the system from the wheelset side, which is already a notable reduction of possible input sets to be tested.

## 2.5.   General Considerations

All these consideration made on both the 2 and the 3 D.o.F. systems give a fairly good first impression of the optimal setup for the first true application on a real case: firstly, the use of direct acceleration is not a real option, as it is already too unreliable of a model on simple systems such as the ones presented before; it should be noted, anyway, that the Derivative Estimation seems to provide fairly good results for single output systems (despite clearly not being the most optimal path). Second point: the most optimal output set to be analyzed in order to reconstruct a random input force has been determined: the one mass on which such force is applied is required in both 2 and 3 D.o.F. cases, while the immediately adjacent one only contributes to a certain degree to the general accuracy of the estimation.

All of this might seem trivial and/or uninteresting – since these systems are only that good of a simplification of the railcar one – but is in fact the core of the algorithm itself: which of the infinite combinations of possible system outputs are required in order to extract a valid estimation? The above considerations actually provide a fairly accurate answer to an otherwise impervious task. It could be argued, in fact, that what was done until now is a *force* estimation, while the required result is a *displacement* one which is indeed a very different problem; through an admittedly very rough reasoning, though, it can be shown that this difference is actually much less marked than expected – and that our choice of these particular pair of trial systems was much less simplistic or detached from the real application than it could initially seem.

In the vertical case, since contact between the railtrack and the wheelset is supposed to happen in a perfectly rigid, anelastic way, displacement of said wheelset coincides with the vertical geometry of the track, and is thus the desired estimation target. This means that while that is *not* a force, it actually behaves as such with respect to the immediately adjacent mass – i.e., the bogies; this makes the system much more similar to the 2 D.o.F. case analyzed in the Section 2.3, just as pictured in Figure 2.13:
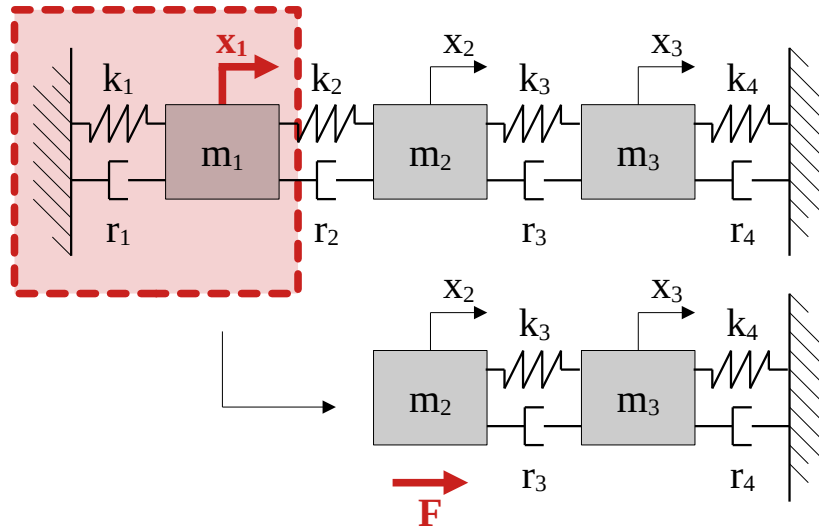
Figure 2.13: Conversion of a Displacement-subjected 3 D.o.F.
system to a Force-subjected 2 D.o.F. one

As it can be easily observed, imposing a displacement on mass 1 is effectively the same as applying a force to mass 2, since the two are connected through a spring-damper parallel; this reduces the system to a 2 D.o.F. one, and will result in a significant reduction in the matrices size.

In the lateral case, things are not that simple, and the 3 D.o.F. pictured in Figure 2.14 system becomes much more correct to describe what's happening: lateral displacement and yaw rotation are in fact *not* geometrically imposed, but instead the result of contact forces that act on those D.o.F.; this means that the system will, albeit indirectly, try to actually estimate a *force* value, but this time applied on the wheelset instead of directly to the bogies.
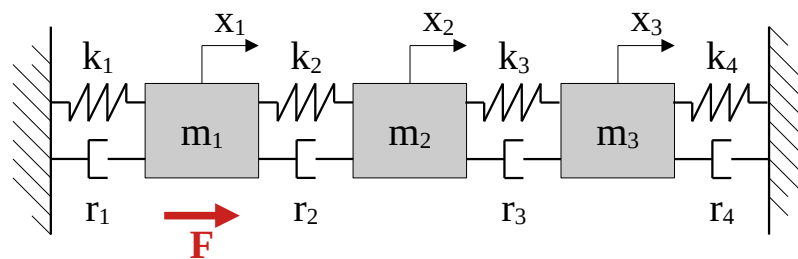


Figure 2.14: 3 D.o.F. Linear Oscillator

On the algorithm side of things, this means that the "mass 1" – the wheelset – will be required to estimate such forces, thus decoupling vertical and horizontal evaluation of the railcar system. It is also noteworthy to anticipate, though, that wheelset accelerations won't be sufficient to determine the full set of unknown inputs; while yaw rotation and lateral displacement are, once again, the result of contact forces, roll

rotation will be approximated as an externally imposed variable not different from vertical displacement, *de facto* once again redirecting to the reasoning exposed at previous point and making the "immediately adjacent body" measurement – the bogie – required for the estimation. The approximation keeping into account both constrained motion and contact force is represented by Figure 2.15:
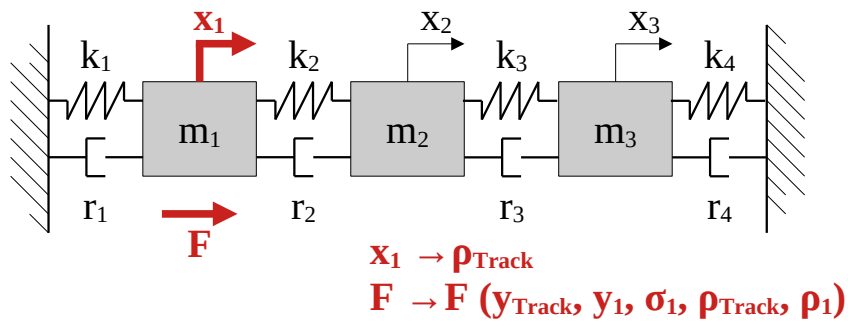


Figure 2.15: Linear Oscillator-like representation of the lateral train system; on the first mass (wheelset) act both a force and a fixed displacement.

Having said all of that, it's time for the first true application, this time much more closely representing the object of our studies both in shape and in operating conditions: a 10 D.o.F. model accounting for the vertical and rotational motion of the frontward bogie, the backward bogie and the cart itself, with the vertical motion of the four axles as the determined motion – the aforementioned "Vertical Model". But since this case differs from the previous ones also regarding the nature of the disturbance itself (again, being not a force, but rather a motion which is translated into a force through the elongation of the primary suspension spring-damper couple), some further adjustments will be made on the system and the matrix representing it.

# 3 Vertical Irregularity Estimation

As a first application of the U.I.O. method to estimate track irregularities, in this chapter the vertical irregularity will be analyzed. For this problem, it is possible to fully decouple the lateral and roll dynamics of the vehicle, therefore a much simpler 10 Degrees of Freedom model to be used (namely the vertical displacement of the wheelsets, the bogies and the carbody and pitch rotation of the latter two). The aforementioned model is pictured in the Figure 3.1 below:
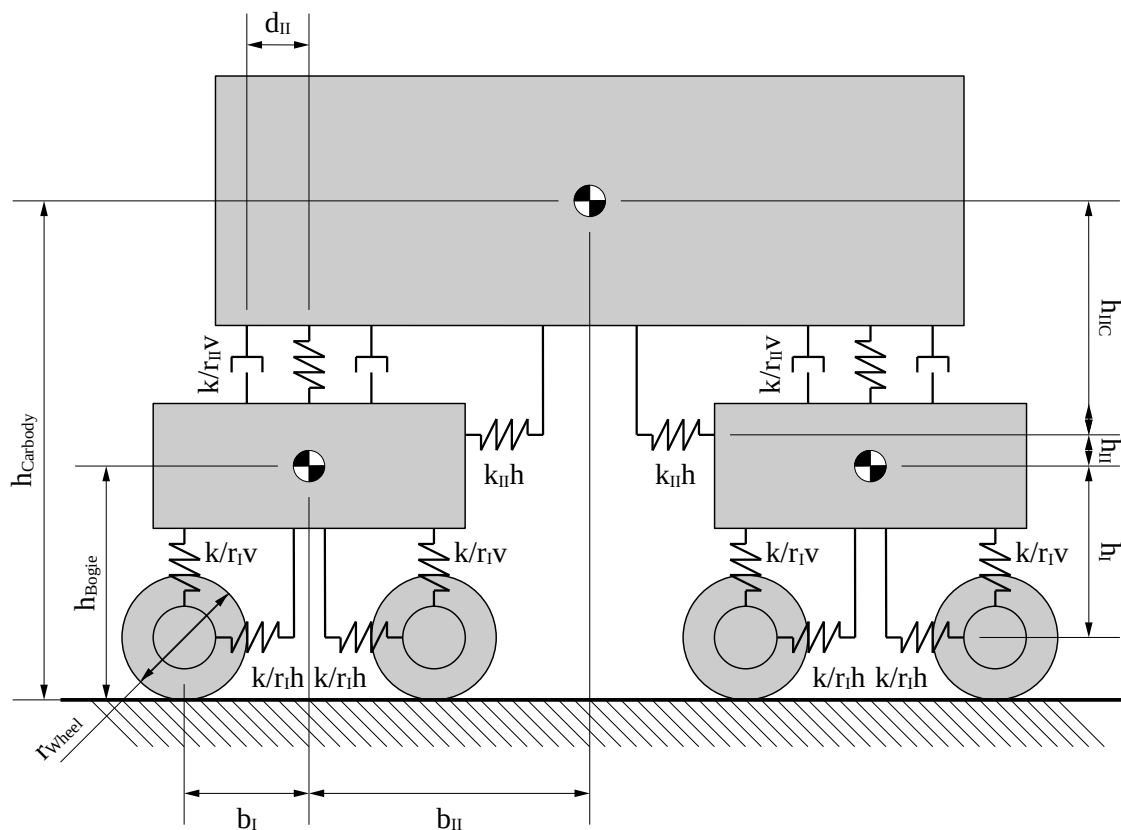


Figure 3.1: 10 D.o.F. Vertical Train Model Scheme

## 3.1. Model Data

In the following pages the data relative to the Meneghino Model employed on the Milan Underground System will be presented, as well as the Jacobian matrices (Table 3.3 to Table 3.7) obtained from the elaboration of such data with regards to the vertical dynamics.

Table 3.1: 10 D.o.F. Vertical Train Model Data

| Parameter | Symbol | Value |
|---|---|---|
| Carbody Mass | $m_C$ | 17817 kg |
| Carbody Pitch Inertia | $J_{C\beta}$ | 435000 kg/m$^2$ |
| Bogie Mass | $m_B$ | 2100 kg |
| Bogie Pitch Inertia | $J_{B\beta}$ | 2600 kg/m$^2$ |
| Wheelset Mass | $m_W$ | 1050 kg |
| Primary Vertical Damping | $r_{Iv}$ | 44000 Ns/m |
| Primary Vertical Stiffness | $k_{Iv}$ | 2000000 N/m |
| Primary Longitudinal Damping | $r_{Ih}$ | 340000 Ns/m |
| Primary Longitudinal Stiffness | $k_{Ih}$ | 16600000 N/m |
| Secondary Vertical Damping | $r_{IIv}$ | 37500 Ns/m |
| Secondary Vertical Stiffness | $k_{IIv}$ | 1020200 N/m |
| Secondary Longitudinal Stiffness | $k_{IIh}$ | 250000 N/m |

Table 3.2: 10 D.o.F. Vertical Train Geometrical Data

| Parameter | Symbol | Value |
|---|---|---|
| Gauge | $S$ | 0,75 m |
| Carbody Baricentre Height | $h_C$ | 1,59 m |
| Bogie Baricentre Height | $h_B$ | 0,46 m |
| Wheel Radius | $r_w$ | 0,41 m |
| Primary Susp. Longitudinal Distance | $b_I$ | 1,075 m |
| Secondary Susp. Longitudinal Distance | $b_{II}$ | 5,55 m |
| Secondary Springs/Dampers Longitudinal Dist. | $d_{II}$ | 0,32 m |
| Primary Susp. - Bogie Vertical Distance | $h_I$ | 0,05 m |
| Secondary Susp. - Bogie Vertical Distance | $h_{II}$ | 0,24 m |
| Secondary Susp. - Carbody Vertical Distance | $h_{IIC}$ | 0,89 m |
| Secondary Outer Damper Longitudinal Distance | $x_{ext}$ | $b_{II} + d_{II}$ |
| Secondary Inner Damper Longitudinal Distance | $x_{int}$ | $b_{II} - d_{II}$ |

Table 3.3: Jacobian of Primary Vertical Springs and Dampers

|  | $x_C$ | $\beta_C$ | $x_{B1}$ | $\beta_{B1}$ | $x_{B2}$ | $\beta_{B2}$ | $x_{W1}$ | $x_{W2}$ | $x_{W3}$ | $x_{W4}$ |
|---|---|---|---|---|---|---|---|---|---|---|
| $\mathbf{k_{Iv1}}$ | 0 | 0 | -1 | $-b_I$ | 0 | 0 | +1 | 0 | 0 | 0 |
| $\mathbf{k_{Iv2}}$ | 0 | 0 | -1 | $+b_I$ | 0 | 0 | 0 | +1 | 0 | 0 |
| $\mathbf{k_{Iv3}}$ | 0 | 0 | 0 | 0 | -1 | $-b_I$ | 0 | 0 | +1 | 0 |
| $\mathbf{k_{Iv4}}$ | 0 | 0 | 0 | 0 | -1 | $+b_I$ | 0 | 0 | 0 | +1 |

Table 3.4: Jacobian of Primary Longitudinal Springs and Dampers

|  | $x_C$ | $\beta_C$ | $x_{B1}$ | $\beta_{B1}$ | $x_{B2}$ | $\beta_{B2}$ | $x_{W1}$ | $x_{W2}$ | $x_{W3}$ | $x_{W4}$ |
|---|---|---|---|---|---|---|---|---|---|---|
| $\mathbf{k_{Ih1}}$ | 0 | 0 | 0 | $-h_I$ | 0 | 0 | 0 | 0 | 0 | 0 |
| $\mathbf{k_{Ih2}}$ | 0 | 0 | 0 | 0 | 0 | $+h_I$ | 0 | 0 | 0 | 0 |
| $\mathbf{k_{Ih3}}$ | 0 | 0 | 0 | $-h_I$ | 0 | 0 | 0 | 0 | 0 | 0 |
| $\mathbf{k_{Ih4}}$ | 0 | 0 | 0 | 0 | 0 | $+h_I$ | 0 | 0 | 0 | 0 |

Table 3.5: Jacobian of Secondary Vertical Dampers

|  | $x_C$ | $\beta_C$ | $x_{B1}$ | $\beta_{B1}$ | $x_{B2}$ | $\beta_{B2}$ | $x_{W1}$ | $x_{W2}$ | $x_{W3}$ | $x_{W4}$ |
|---|---|---|---|---|---|---|---|---|---|---|
| $\mathbf{r_{IIvFR}}$ | -1 | $-x_{ext}$ | +1 | $+d_{II}$ | 0 | 0 | 0 | 0 | 0 | 0 |
| $\mathbf{r_{IIvFL}}$ | -1 | $-x_{int}$ | +1 | $-d_{II}$ | 0 | 0 | 0 | 0 | 0 | 0 |
| $\mathbf{r_{IIvRR}}$ | -1 | $+x_{int}$ | 0 | 0 | +1 | $+d_{II}$ | 0 | 0 | 0 | 0 |
| $\mathbf{r_{IIvRL}}$ | -1 | $+x_{ext}$ | 0 | 0 | +1 | $-d_{II}$ | 0 | 0 | 0 | 0 |

Table 3.6: Jacobian of Secondary Vertical Springs

|  | $x_C$ | $\beta_C$ | $x_{B1}$ | $\beta_{B1}$ | $x_{B2}$ | $\beta_{B2}$ | $x_{W1}$ | $x_{W2}$ | $x_{W3}$ | $x_{W4}$ |
|---|---|---|---|---|---|---|---|---|---|---|
| $\mathbf{k_{IIvF}}$ | -1 | $-b_{II}$ | +1 | 0 | 0 | 0 | 0 | 0 | 0 | 0 |
| $\mathbf{k_{IIvR}}$ | -1 | $+b_{II}$ | 0 | 0 | +1 | 0 | 0 | 0 | 0 | 0 |

Table 3.7: Jacobian of Secondary Longitudinal Springs

|  | $x_C$ | $\beta_C$ | $x_{B1}$ | $\beta_{B1}$ | $x_{B2}$ | $\beta_{B2}$ | $x_{W1}$ | $x_{W2}$ | $x_{W3}$ | $x_{W4}$ |
|---|---|---|---|---|---|---|---|---|---|---|
| $\mathbf{k_{IIhF}}$ | 0 | $+h_{IIC}$ | 0 | $+h_{II}$ | 0 | 0 | 0 | 0 | 0 | 0 |
| $\mathbf{k_{IIhR}}$ | 0 | $-h_{IIC}$ | 0 | 0 | 0 | $-h_{II}$ | 0 | 0 | 0 | 0 |

It must be taken into account that, since roll motion is being knowingly ignored in such model, we are *de facto* considering the *average* vertical alignment of the track; in order to obtain a separate full reconstruction of the vertical profile of the rails, we'd need to integrate the results with an estimation of the difference between the two tracks' vertical geometry, which directly translates into the roll motion of the wheelsets (a problem that will be addressed in Section 4).

## 3.2. State-Space Model Construction

Since elastic interaction between wheels and tracks can be neglected, the vertical motion of a single wheel exactly corresponds to the vertical alignment of the rail it rolls upon; in the same way, the average vertical alignment of the tracks will be the same as the vertical motion of the wheelset centre. Said movement is also one of the freedom degrees – albeit an externally determined one – thus the system must be decomposed as in (3.1) and (3.2) into two different sections in order to obtain (3.3), the classical state-space formulation:

$$
\begin{bmatrix} M_{FF} & M_{FC} \\ M_{CF} & M_{CC} \end{bmatrix} \begin{Bmatrix} \ddot{x}_F \\ \ddot{x}_C \end{Bmatrix} + \begin{bmatrix} R_{FF} & R_{FC} \\ R_{CF} & R_{CC} \end{bmatrix} \begin{Bmatrix} \dot{x}_F \\ \dot{x}_C \end{Bmatrix} + \dots
$$
$$
\dots + \begin{bmatrix} K_{FF} & K_{FC} \\ K_{CF} & K_{CC} \end{bmatrix} \begin{Bmatrix} x_F \\ x_C \end{Bmatrix} = \bar{0}
$$

(3.1)

$$
M_{FF}\ddot{x}_F + R_{FF}\dot{x}_F + K_{FF}x_F = \dots
$$
$$
\dots = -M_{FC}\ddot{x}_C - R_{FC}\dot{x}_C - K_{FC}x_C
$$

(3.2)

$$
\begin{Bmatrix} \ddot{x}_F \\ \dot{x}_F \end{Bmatrix} = \begin{bmatrix} -M_{FF}^{-1}R_{FF} & -M_{FF}^{-1}K_{FF} \\ I & [0] \end{bmatrix} \begin{Bmatrix} \dot{x}_F \\ x_F \end{Bmatrix}
$$
$$
+ \begin{bmatrix} -M_{FF}^{-1}R_{FC} & -M_{FF}^{-1}K_{FC} \\ [0] & [0] \end{bmatrix} \begin{Bmatrix} \dot{x}_C \\ x_C \end{Bmatrix}
$$

(3.3)

For simplicity, the terms will be expressed in a more synthetic form as per the definitions at (3.4), so that the complete system can be written as in the (3.5):

$$
\begin{Bmatrix} \dot{x}_F \\ x_F \end{Bmatrix} = x
$$
$$
\begin{bmatrix} -M_{FF}^{-1}R_{FF} & -M_{FF}^{-1}K_{FF} \\ I & [0] \end{bmatrix} = A
$$
$$
\begin{bmatrix} -M_{FF}^{-1}R_{FC} & -M_{FF}^{-1}K_{FC} \\ [0] & [0] \end{bmatrix} = E
$$
$$
x_C = d
$$

(3.4)

$$
\dot{x} = Ax + E \begin{Bmatrix} \dot{d} \\ d \end{Bmatrix}
$$

(3.5)

The system building is not yet complete, though. The 12$^{th}$ order state vector accounts for all required motions of bogies and carbody both in displacement and velocity, but so does the disturbance vector itself, since it affects the system in both position

(through the primary spring) and velocity (through the primary damper); this would mean the need to estimate two different disturbances, one for the actual displacement and one for its derivative, without applying the knowledge of their mutual relation, resulting in an underconstrained system. In order to take said piece of information into account, the input matrix $E$ must be divided into two submatrices $E_1$ and $E_2$, referring respectively to the disturbance and its derivative (3.6):

$$E \begin{Bmatrix} d \\ \dot{d} \end{Bmatrix} d = \begin{bmatrix} E_1 E_2 \end{bmatrix} \begin{Bmatrix} d \\ \dot{d} \end{Bmatrix} = E_1 d + E_2 \dot{d} \qquad (3.6)$$

This allows us to employ an extended state as in the (3.7), converting the system into a 16$^{th}$ grade one; through the definitions in the (3.8), the (3.9) can be obtained:

$$\begin{Bmatrix} \dot{x} \\ \dot{d} \end{Bmatrix} = \begin{bmatrix} A & E_1 \\ [0] & [0] \end{bmatrix} \begin{Bmatrix} x \\ d \end{Bmatrix} + \begin{bmatrix} E_2 \\ I \end{bmatrix} \dot{d} \qquad (3.7)$$

$$\begin{Bmatrix} \dot{x} \\ \dot{d} \end{Bmatrix} = x_{extended}; \begin{bmatrix} A & E_1 \\ [0] & [0] \end{bmatrix} = A_{extended}; \begin{bmatrix} E_2 \\ I \end{bmatrix} = E_{extended}; \dot{d} = \tilde{d} \qquad (3.8)$$

$$\dot{x}_{extended} = A_{extended} x_{extended} + E_{extended} \tilde{d} \qquad (3.9)$$

It should be noted, though, that due to this particular formulation of the problem, the result of the algorithm (and as long as a simulated system will be employed, the input of the linear model) won't be the irregularity itself, but its derivative. As long as noise is absent, this won't have any consequence; when noise is featured, even in a simulated environment, though, it could happen that the disturbance derivative does not feature a null average value, resulting in a linear trend superimposed over its integral (the displacement itself). This will be addressed through a highpass filter, with a cutoff frequency such that relevant information will be left untouched.

Next step towards a complete modelization is taking into account that the desired result is not the motion of all four wheelsets, but just one – from now on, we'll consider the frontmost one – the other three being simply the first one delayed of a value $\tau$ (as per the functions (3.10) to (3.13)) dependant on the mutual inputs distance $\delta$ and the velocity $v$ of the train itself, through the transfer function (3.14):

$$\begin{cases} d_1(t) = d(t) & (3.10) \\ d_2(t) = d(t - \tau_2) & (3.11) \\ d_3(t) = d(t - \tau_3) & (3.12) \\ d_4(t) = d(t - \tau_4) & (3.13) \end{cases}$$

$$\tau_k = \frac{\delta_k}{v}; G(s) = e^{-s\tau}; \qquad (3.14)$$

Problem is, this formulation is not a linear one, and hence cannot be directly inserted into the model; in order to do that, an approximation known as Padé Approximation must be separately discussed.

### 3.2.1. Padé Approximation

In order to discuss the approximation as an independent instrument, the hypothetical (3.15) system, subject to 2 equal inputs, one featuring a $\tau$ time delay with respect to the other, will be taken into account.

$$\dot{x} = A x + E d = A x + \begin{bmatrix} E_1 & E_2 \end{bmatrix} \begin{Bmatrix} d_1 \\ d_2 \end{Bmatrix} \tag{3.15}$$

Since the algorithm of the U.I.O. is directly dependant on the employed model, the latter shall be modified accordingly by reducing the variables constituting the disturbance vector to just one, and implementing the relationship with the others inside the state matrix.

One way of dealing with the issue could actually accepting more separate values employing them as a way to cancel out measurement noise, through averaging of the results (adequately translated of the correct delay value); nonetheless, an alternative method to deal with the issue does exist, that allows to obtain one single estimate through an aptly modified series of matrices, thus bypassing the need for output postprocessing (something this entire method tries to avoid).

This method is known as Padé Approximation and is a way to modelize a series of 2 or more consecutive delayed signals by approximating the exponential formulation of the delay with a linear one, compatible with the state-space structure; the simplest way to sum up the procedure is to simply apply a Taylor Expansion to the delay formulation as in (3.16);

$$e^{-s\tau} \simeq 1 - \frac{\tau s}{1!} + \frac{(\tau s)^2}{2!} - \frac{(\tau s)^3}{3!} + ... \simeq \frac{P(s)}{Q(s)} \tag{3.16}$$

Then, the (3.17) and the (3.18) can be used to obtain a polynomial equation in Laplace variable $s$; the order of such equation only depends on the choice of parameters $m$ and $n$ – in this case, since a quadratic formulation is desired, it has been chosen $m=n=2$, resulting in the (3.19):

$$P(s) = a_n (\tau s)^n + a_{n-1} (\tau s)^{n-1} + ... + a_0 = \sum_{k=0}^{n} a_k (\tau s)^k \tag{3.17}$$

$$Q(s) = b_m (\tau s)^m + b_{m-1} (\tau s)^{m-1} + ... + b_0 = \sum_{k=0}^{m} b_k (\tau s)^k \tag{3.18}$$

$$e^{-s\tau} \simeq \frac{12 - 6\,\tau\,s + (\tau\,s)^2}{12 + 6\,\tau\,s + (\tau\,s)^2} \tag{3.19}$$

This can be employed to create the (3.20), which is another dynamic subsystem which takes into account the separate dynamics of the delayed input as a function of the previous one. The obtained transfer function can then be converted into the (3.21) matrix form and thus conjugated with the original state equation in the same way as the disturbance derivative extended state to obtain the (3.22):

$$\begin{cases} \dot{x}_P = A_P\,x_P + B_P\,d_1 \\ d_2 = C_P\,x_P + D_P\,d_1 \end{cases} \tag{3.20}$$

$$A_P = \begin{bmatrix} 0 & 1 \\ -12/\tau^2 & -6/\tau \end{bmatrix}; B_P = \begin{bmatrix} 0 \\ 1 \end{bmatrix}; C_P = \begin{bmatrix} 0 & -12/\tau \end{bmatrix}; D_P = 1 \tag{3.21}$$

$$\begin{Bmatrix} \dot{x} \\ \dot{x}_P \end{Bmatrix} = \begin{bmatrix} A & [0] \\ [0] & A_P \end{bmatrix} \begin{Bmatrix} x \\ x_P \end{Bmatrix} + \begin{bmatrix} E_1 \\ B_P \end{bmatrix} d_1 + \begin{bmatrix} E_2 \\ [0] \end{bmatrix} (C_P\,x_P + E_2\,D_P\,d_1)$$

$$\begin{Bmatrix} \dot{x} \\ \dot{x}_P \end{Bmatrix} = \begin{bmatrix} A & E_2\,C_P \\ [0] & A_P \end{bmatrix} \begin{Bmatrix} x \\ x_P \end{Bmatrix} + \begin{bmatrix} E_1 + E_2\,D_P \\ B_P \end{bmatrix} d_1 \tag{3.22}$$

### 3.2.2. Complete State-Space Model with delayed inputs

In the study case that is being dealt with, the inputs are one "original" input and a series of 3 equal ones with progressively increasing time delays. This results in the (3.23) matrix formulation:

$$\begin{Bmatrix} \dot{x} \\ \dot{x}_{P2} \\ \dot{x}_{P3} \\ \dot{x}_{P4} \end{Bmatrix} = \begin{bmatrix} A & E_2\,C_{P2} & E_3\,C_{P3} & E_4\,C_{P4} \\ [0] & A_{P2} & [0] & [0] \\ [0] & [0] & A_{P3} & [0] \\ [0] & [0] & [0] & A_{P4} \end{bmatrix} \begin{Bmatrix} x \\ x_{P2} \\ x_{P3} \\ x_{P4} \end{Bmatrix} + \dots$$

$$\dots + \begin{bmatrix} E_1 + E_2\,D_{P2} + E_3\,D_{P3} + E_4\,D_{P4} \\ B_P \\ B_P \\ B_P \end{bmatrix} d_1 \tag{3.23}$$

It must be reminded, though, that this is but an approximation and the application limits of an approximation are not infinite. In fact, since the formulation of matrices $A_P$ and $C_P$ depends on the value of time delay $\tau$, it is relatively obvious that this method grants the best results if such delay is limited.

Since the vehicle taken into consideration in this work is a generally low-speed urban public transport (considering a velocity interval of 10-100 km/h), its low velocity results in a higher time delay for the same space interval; furthermore, the spatial distance between the two wheelsets sharing the same bogie is almost an order of magnitude lower than the one separating the bogies themselves. This means that applying the Padé Approximation could result in heavily compromised results, thus it could be decided to limit its application to the rear axle of each bogie, maintaining two separate outputs for the two front ones, to be averaged in a second phase.

If this last choice is selected, the (3.24) system requires two separate inputs to obtain all the required accelerations, and in turn will result in two estimations differing in the initial delay between the signals:

$$
\begin{Bmatrix} \dot{x} \\ \dot{x}_{P2} \\ \dot{x}_{P4} \end{Bmatrix} = \begin{bmatrix} A & E_2 C_P & E_4 C_P \\ [0] & A_P & [0] \\ [0] & [0] & A_P \end{bmatrix} \begin{Bmatrix} x \\ x_{P2} \\ x_{P4} \end{Bmatrix} + \ldots
$$
$$
\ldots + \begin{bmatrix} E_1 + E_2 D_P & E_3 + E_4 D_P \\ B_P & [0] \\ [0] & B_P \end{bmatrix} \begin{Bmatrix} d_1 \\ d_3 \end{Bmatrix}
$$

(3.24)

## 3.3.   Model Validation

Once its general structure has been defined, some tests have been conducted to evaluate if the simplified system is an adequate approximation of the real train behaviour. To this end, the accelerations resulting from the actual misalignment of the track (Figure 3.2) being fed to the 10 D.o.F. model were compared with those obtained by a more accurate multibody model provided by PoliMi; this model takes into account non-linear effects, and any potential coupling between vertical and lateral dynamics (which were instead ignored in the linear model). Both simulation outputs were obtained for the velocity profile reported in Figure 3.3.
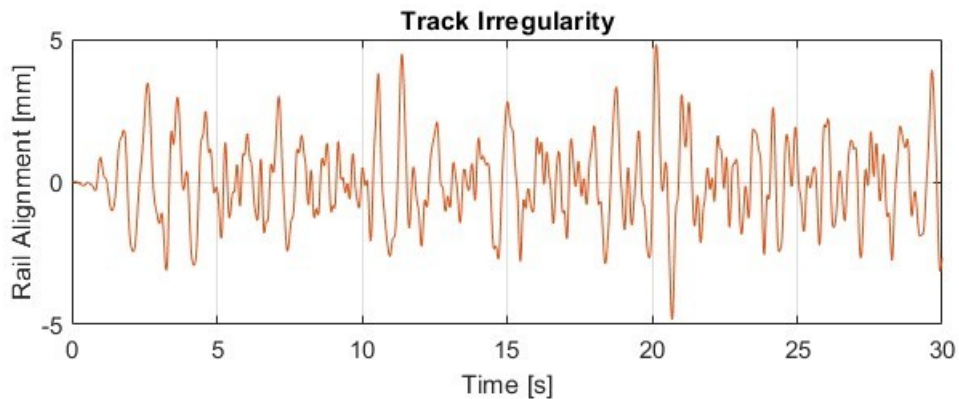


Figure 3.2: Track Irregularity
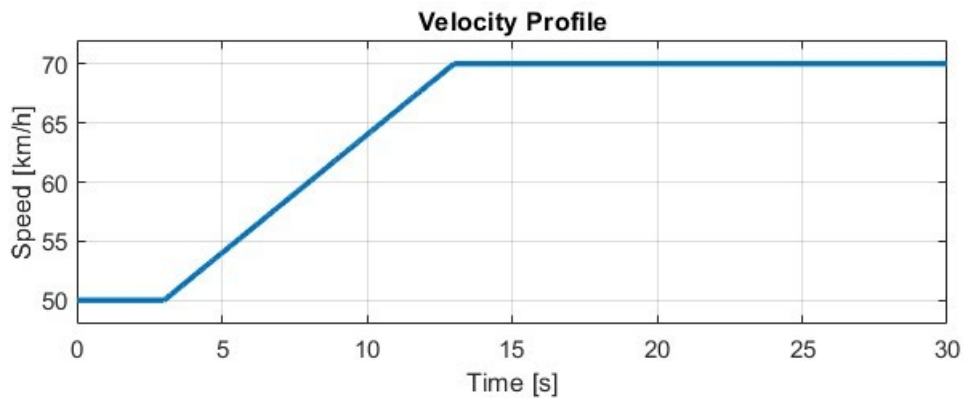
Figure 3.3: Velocity Profile

As seen in Figure 3.4, though, the employment of this approximation seems to provide uncorrect results for the rear bogie:
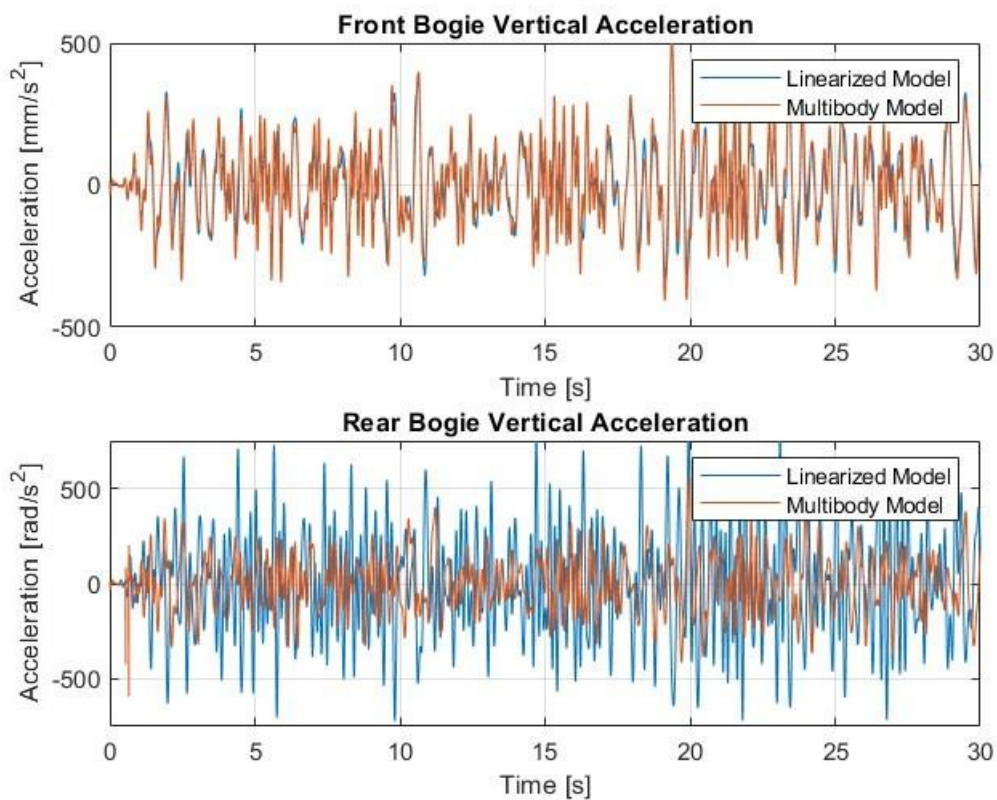


Figure 3.4: Comparison of Bogie virtual vertical acceleration with the one obtained through a single-input linear system (variable speed 50-70km/h simulation)

It can be observed, though, that while the rear bogie (the one featuring the larger distance and thus the harsher delay approximation) features conflicting results, the front one is, by comparison, much closer to the actual values; this means that the

aforementioned hypothesis of Padé Approximation not being adequate to modelize the comparatively huge distance between the front and the rear wheels (in particular at the fairly low velocity at which the measurations were made) was correct all along, but also that the same Approximation performs exceptionally well for limited intervals like the one between the first and second axle. Hence, the second option of limited employment of the Approximation for the two axles of the same bogie can be chosen (Figure 3.5) with little to no negative effect on results:
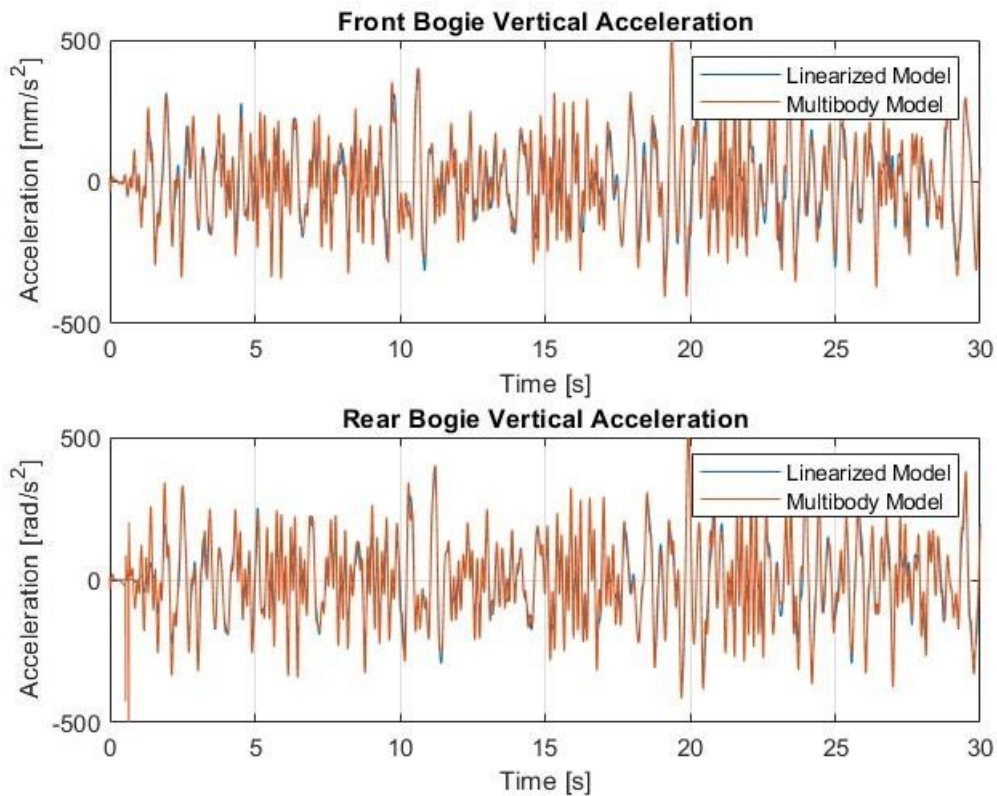


Figure 3.5: Comparison of Bogie virtual vertical acceleration with the one obtained through a double-input linear system (variable speed 50-70km/h simulation)

## 3.4.  Gain Matrix Calculation

Now that the system has been validated, next step is to elaborate the optimal poles' positioning of observer matrix $F$, and thus the correct gain matrix $L$. First, though, it must be decided which acceleration to actually use for the estimation.

From the multibody simulation mimicking the real train any set of "measurement data" can be freely extracted, mirroring the infinite choices of positioning of accelerometers; as foreshadowed in 2.4, though, there's already a very good approximation on what to look for. Since the results we are interested in are relative to an externally imposed displacement on a mass 1 connected with a mass 2 through a certain geometry of springs and dampers, that is almost equivalent to the application of the force generated by such displacement (by elastic and dampening

effect) on said mass 2, and hence makes it clear which body is required to be monitored, that is the mass 2 or, as it is called in a railcar, the bogies. Moreover, had we decided to employ the measurement of the *wheelsets* for the estimation, two flagrant problems would have arised:

- Physical installation of vertical accelerometers on a fast-rotating structure such as a train axle is not an easy task; in particular, it would make almost impossible to run the system without a low-pass filtering of some sort, due to the intrinsic vibrational behaviour of the wheelset (which could as well affect the measurement due to partial overlapping with the relevant frequency range);

- On a logical point of view, if measuring acceleration on the wheelset was required, then neither the bogie measurement nor the entirety of the U.I.O. would be needed, since due to supposed anelasticity in the wheel-track contact it would equate to measuring the double derivative of the vertical geometry itself, hence reducing the whole issue of "estimating" to a double integration and potentially a filter.

Notice that both points will be subverted in the second half of this study, when lateral dynamics will be discussed. It is quite relevant to notice, however, that the second case features much more complex modelization issues and hence – while the first one will remain an issue (although overlapping becomes less of a problem due to different frequency spectrums between vertical and lateral irregularity) – the second problem will be rendered null due to the contradiction of its premise (i.e., horizontal displacement is NOT anelastically imposed by the track).

Back to pole placement, the same procedure exposed in Section 2 and based on the staircase form will be employed. In this particular case, it can be observed that out of all the poles of matrix *TA*, there is none which is truly "non-observable", but some of them can be defined as *almost* unobservable, just like trying to excite a vibration mode of a system by acting in the very proximity of one of that mode's nodes. In order to discern observable poles from these aforementioned quasi-unobservable ones (since there is no real null submatrix to be used as a reference) it was arbitrarily decided to set $10^{-5}$ as the threshold value for any entry to be considered null, resulting in 5 out of 22 being of the latter category and being left untouched by the placement. As per the remaining 17, it can be observed by their position that trying once again to bring them down to the real axis would be an unsustainable task in terms of gain matrix; in order to generalize the procedure, it was decided to simply double the negative real part of each observable pole and then subtract another tentative value equal to double the module of its imaginary part as pictured in Figure 3.6, so that even purely imaginary poles achieve an adequate damping ratio:
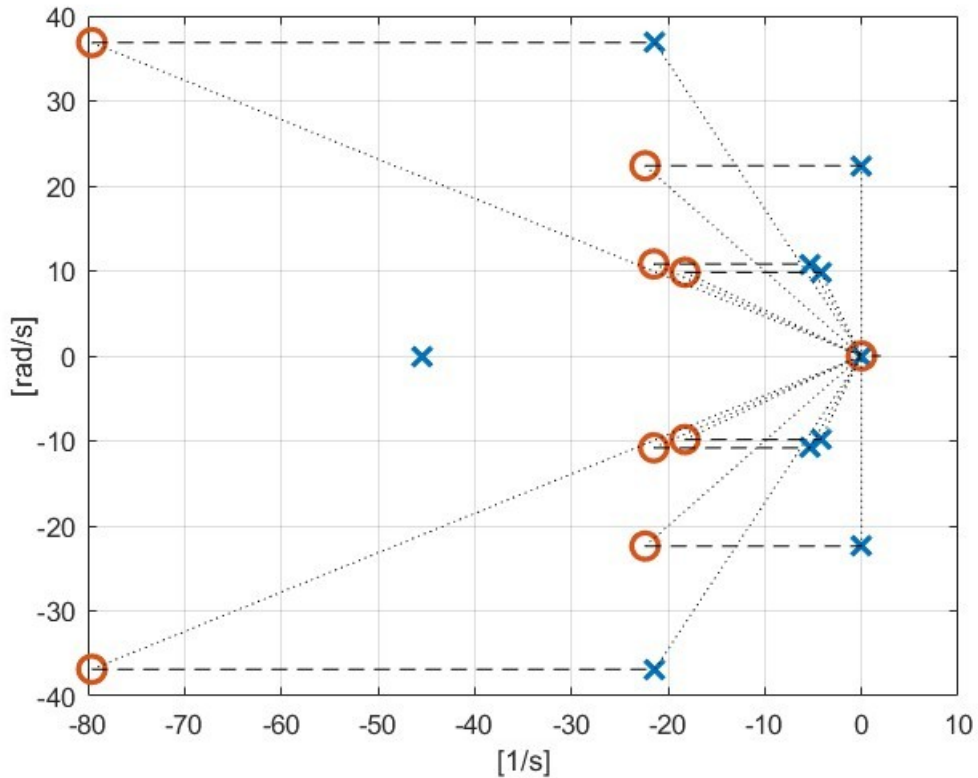
Figure 3.6: Example of Pole Placement for V = 50km/h. Notice the one non-zero non-observable pole at around -45.

In the perspective of allowing speed to actually change during the analysis (instead of arbitrarily fixing it at the start and maintaining it constant for the entire duration of the simulation), it shouldn't go unnoticed that introducing the Padé Approximation made the system (in particular state matrix *A*) dependant on velocity. This means that if the entire U.I.O. procedure is repeated from the start once the velocity is fixed, the gain matrix *L* obtained through the pole-placement on said matrix *A* will be, in turn, dependant on speed; the interesting question is: can the same matrix *L*, calculated for a certain velocity, be employed for a *different* value of speed without losing in general accuracy?

The importance of this hypothesis is paramount and cannot be overstated: if this wasn't the case, in order to apply the U.I.O. estimator in a variable velocity environment, the system would require to not only update the system matrices used in the U.I.O. model while the speed changes (which is necessary, but ultimately not overly heaving on computational power), but it should also constantly recalculate the optimal gain matrix, an operation which would needlessly slow down the algorithm; most importantly, the actual updating cannot physically be continuous, and it would ultimately depend on the precision with whom speed is measured – i.e. what actually counts as a "different velocity"? A 1 km/h delta or a 0,001 km/h one? -

making the following consideration natural: if in any case velocity trend must be discretized in a series of intervals, however small, it would be much more practical to reduce them in number by creating a series of intervals – for example, 10 km/h ones – for which an adequate gain matrix has been predetermined and can be directly applied with no need for recalculation. Even better, if this number of intervals could be reduced to *one* (i.e. the same gain matrix *L* being employed at *any* speed in the considered interval), potential problems related to maintaining continuity in the estimation would be bypassed. As easily predictable, this last condition won't be the case, but some degree of elasticity in velocity between observer and real system can be found and exploited.

In order to verify this last criterion, the analysis of how the eigenvalues of the control matrix *F* are modified when considering a system matrix *A* at a different velocity than the one employed to calculate *L*; Figure 3.7, Figure 3.8 and Figure 3.9 are a collection of results for different fixed *L* matrices:
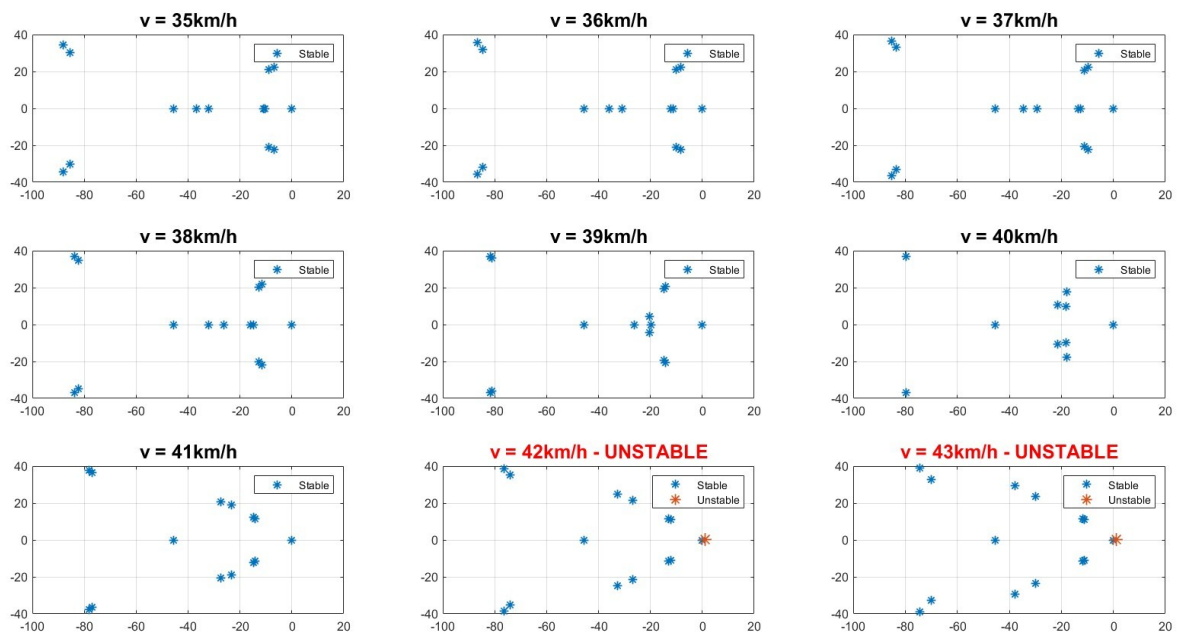


Figure 3.7: Pole Placement for a fixed V = 40km/h within a -5 to +3km/h interval
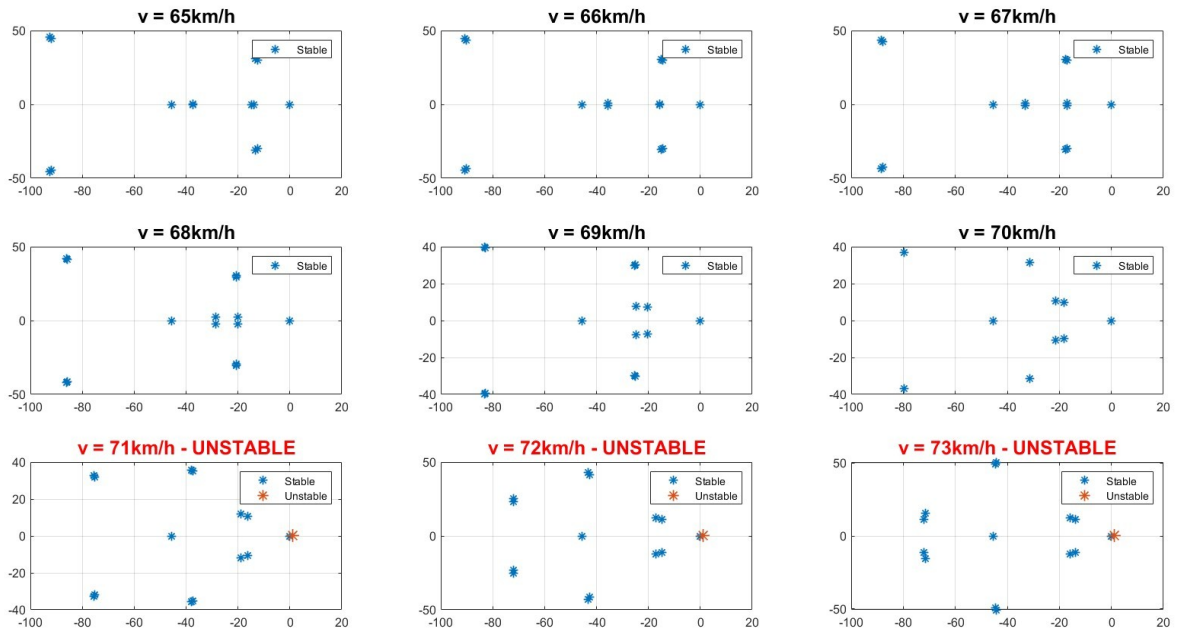
Figure 3.8: Pole Placement for a fixed V = 70km/h within a -5 to +3km/h interval
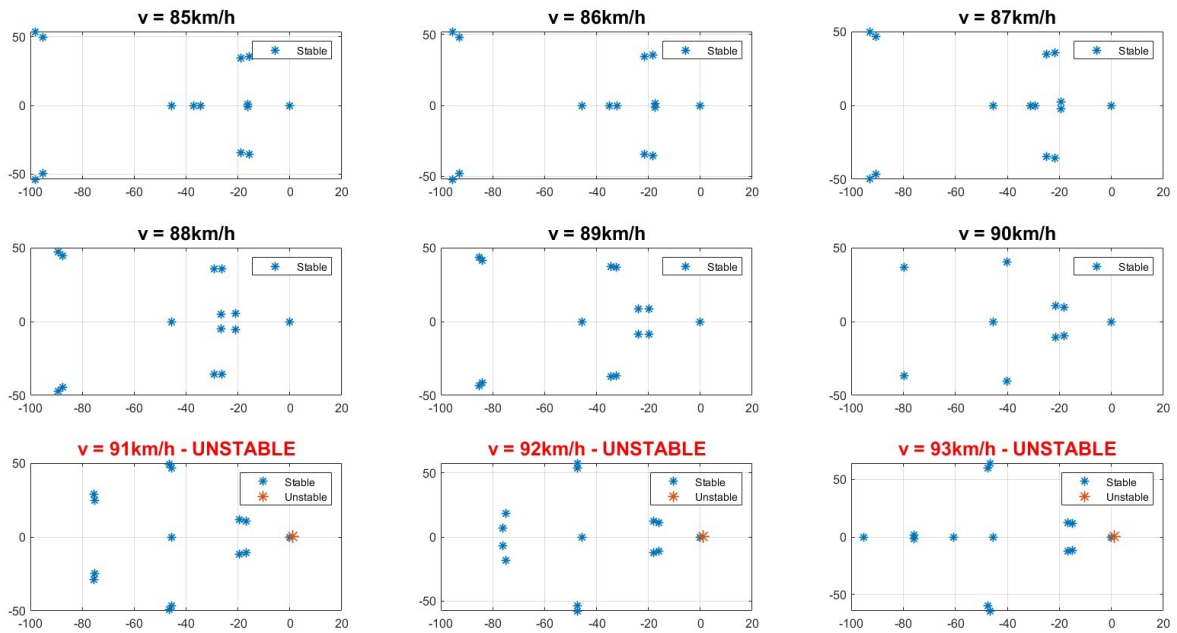


Figure 3.9: Pole Placement for a fixed V = 90km/h within a -5 to +3km/h interval

It can hence be deduced that, for every speed considered for the matrix *L*, stability can be granted for the observer for any real speed which is lower than the former down to 5 km/h (i.e., a gain matrix obtained for 40 km/h can be applied for a vehicle moving from 35 to 40 km/h with no potential instability) with a eigenvalues' real part

positivity tolerance of 0,001 (within numerical uncertainty). It should also be noticed, though, that the particular speeds for which the opposite direction (real speed higher than observer one) is not admissible feature seem to suggest that for lower speeds our approach results in an overly precautional scheduling.

Once this data have been extracted, it means that only $L$ matrices for fixed intervals of 5 km/h need to be calculated and can then be utilized for all the velocity interval from that particular value down to 5 km/h lower, as pictured in the block diagram in Figure 3.10; in order to apply this knowledge, the time history of the velocity (in this case, the graph in Figure 3.3) must be registered and approximated to the higher multiple of 5 km/h, thus programming the scheduling for the gain matrices which have been previously calculated and can be stored as known data.
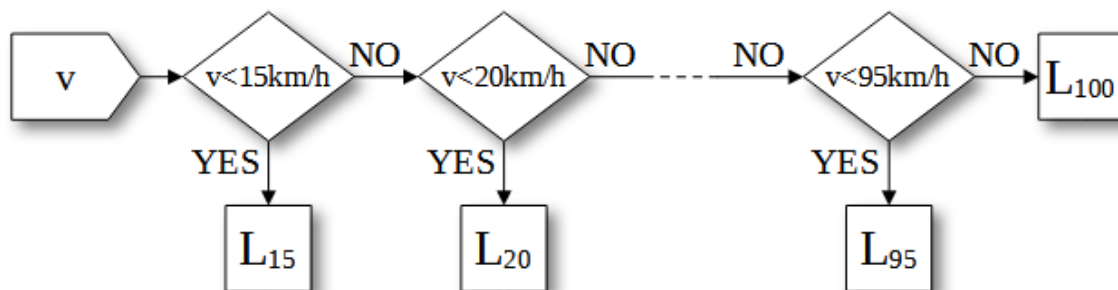


Figure 3.10: Gain Scheduling for the selection of matrix L

## 3.5.  Results

Now that the observer has been set up entirely, it was tested on the study case; a to-be-determined vertical disturbance has thus been applied on a vertical multibody system which for the interests of this study will be virtually the same as the real vehicle, since it approximates it in a much more detailed fashion than the simplified linear model applied here.

The results will be separated between the straight track case (which will feature the very same irregularity as described in Figure 3.2) and one example of curved track (namely a 135m radius turn) featuring a different irregularity profile.

### 3.5.1.  Straight Track Case

The first obtained results are relative to the simplest straight track case, and as it can be seen in Figure 3.11 in the next page they can be described as generally very accurate:
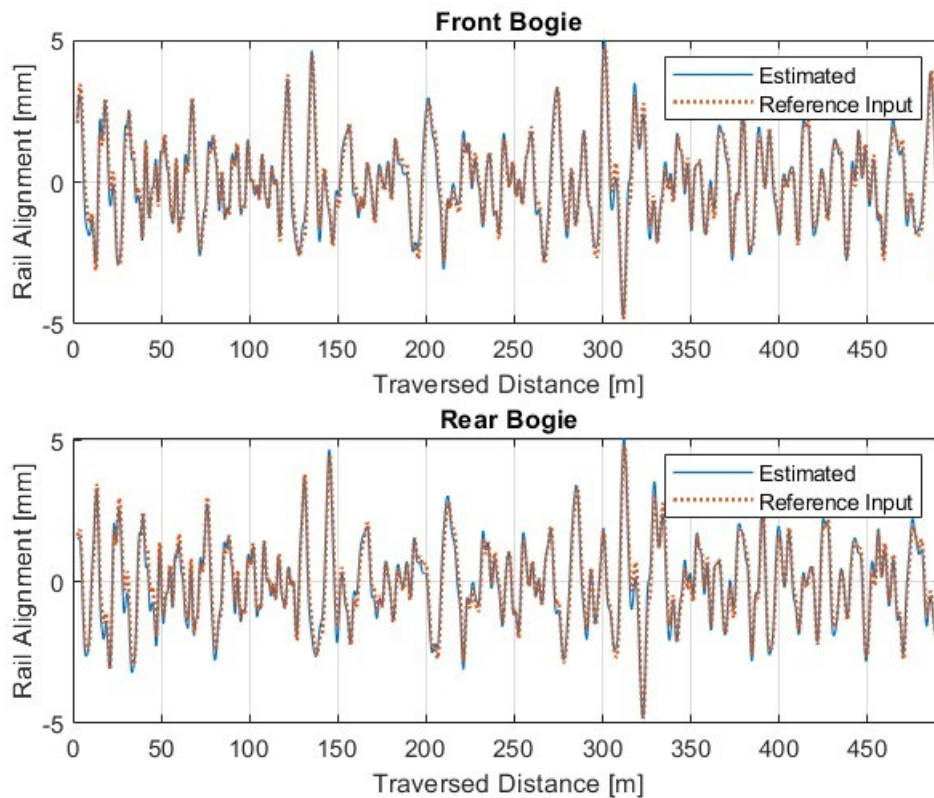
Figure 3.11: 10 D.o.F. Model - U.I.O. results for a straight track at variable velocity
(time history)

Although the results relative to the straight track can be seen as almost perfect through a qualitative evaluation, this preliminary examination is best confirmed by the employment of some more rational criteria such as the actual error in estimation pictured in the graph in Figure 3.12 (absolute value), which never exceeds 1mm (average absolute value: 0,2406mm for the front, 0,2533mm for the rear) and to a more accurate analysis is mostly to be imputed to a slight x-axis misalignment of the estimation and the real value – whose reason must in turn be researched into the numerical error due to timestep discretization. In order to verify this, it is possible to switch to a frequency domain analysis and observe even more coherent outputs.

In fact, as can be observed when analyzing the PSD of both real and estimated disturbance pictured in Figure 3.13 for both front and rear bogie, the real only difference (and arguably a very marginal one) is relative to the lowest frequencies, but those data can be easily explained (and potentially discarded, since the real values PSD confirms that there is no relevant input at such high wavelength) as the effect of the previously discussed highpass filter required to neglect non-white noise integration drifting.
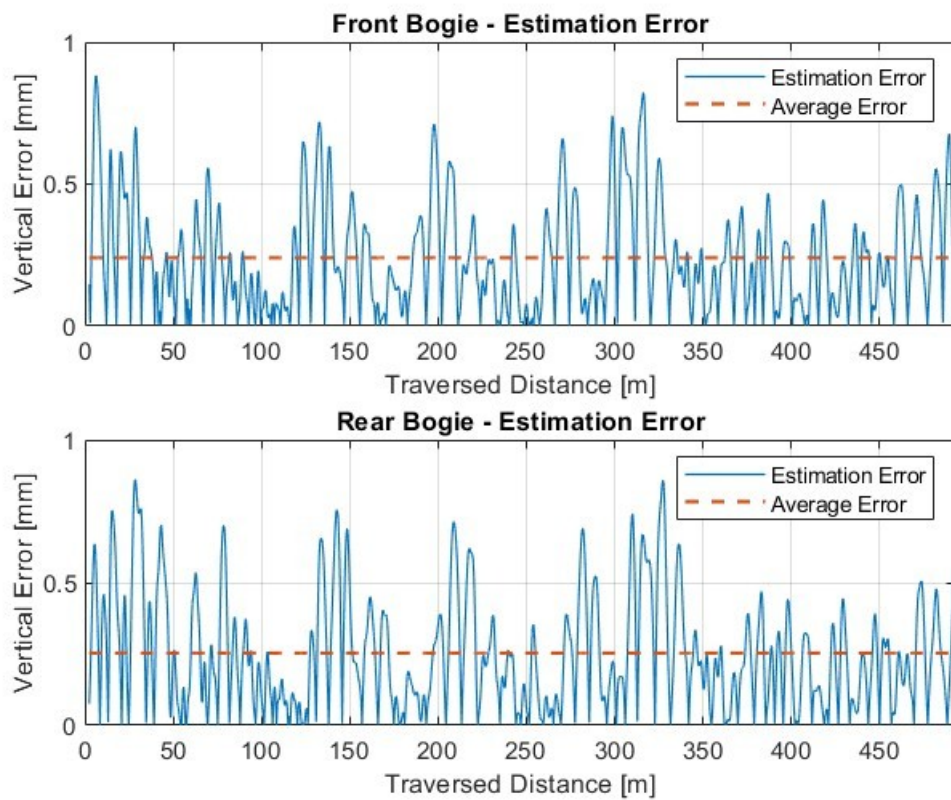
Figure 3.12: 10 D.o.F. Model – Estimation Error
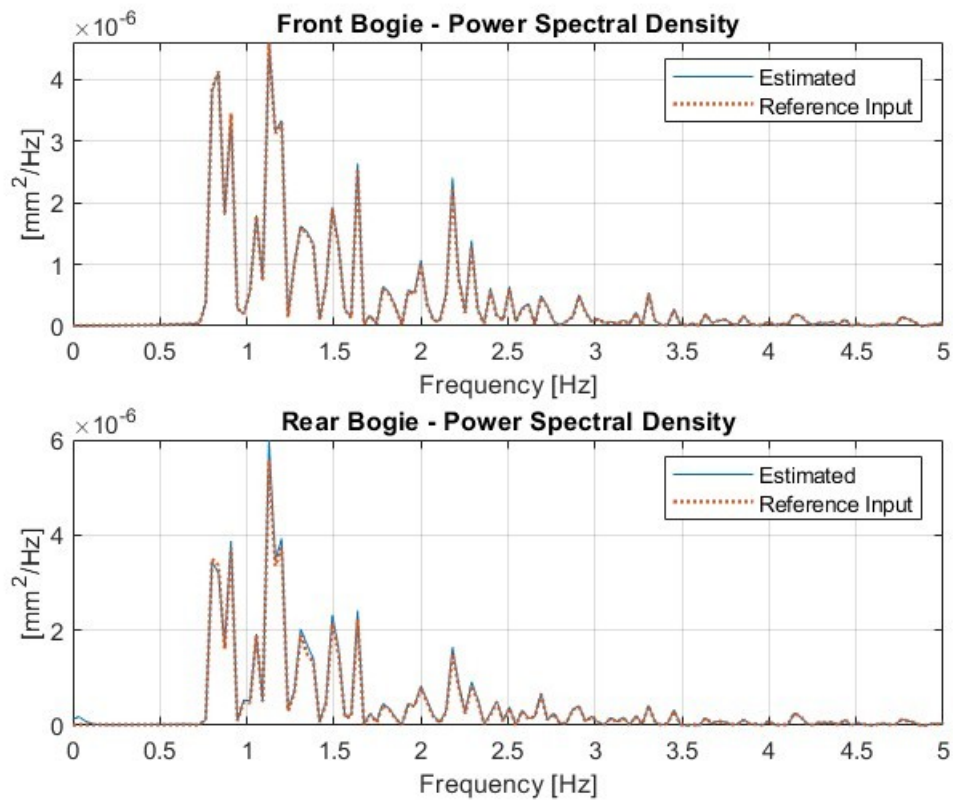


Figure 3.13: 10 D.o.F. Model – Straight Track estimation PSD

### 3.5.2. 135m Radius Turn Case

Mostly the exact same considerations can be made when dealing with a curved track; the following graphs (Figure 3.14 to Figure 3.17) refer to a 135m radius curve (among the tightest ones the considered vehicle can go through while still providing relevant data for the disturbance estimation – i.e., at a high enough speed to solicit sufficient accelerations):
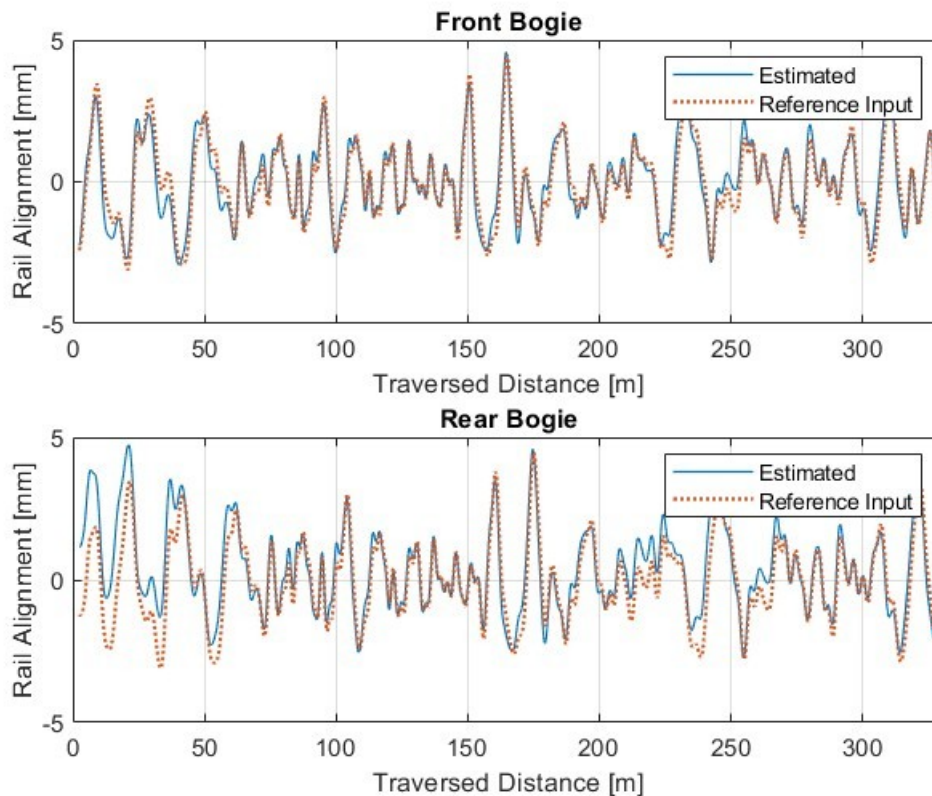


Figure 3.14: 10 D.o.F. Model –  U.I.O. results for a 135m radius - Curved Track at variable velocity (time history)

As it can be easily observed, the results are less precise (especially at the start of the analysis – but that is mostly related to some differences in the multibody simulation way of dealing with delayed inputs) but still highly promising. Regarding average error, the value is arguably quite higher than the straight case (0,3547mm in the front, 0,5488mm in the rear) but again, the 65% difference in favour of the front bogie estimation not only clarifies the merely simulative nature of this displacement, but confirms that the front bogie can indeed provide a perfectly serviceable estimation; furthermore, if the actual error trend in Figure 3.15 is analyzed, it can be observed that the difference between real and is actually well below the 1mm threshold save for a couple phases, respectively the starting one and another one around 250m – where a quite abrupt speed change is taking place.
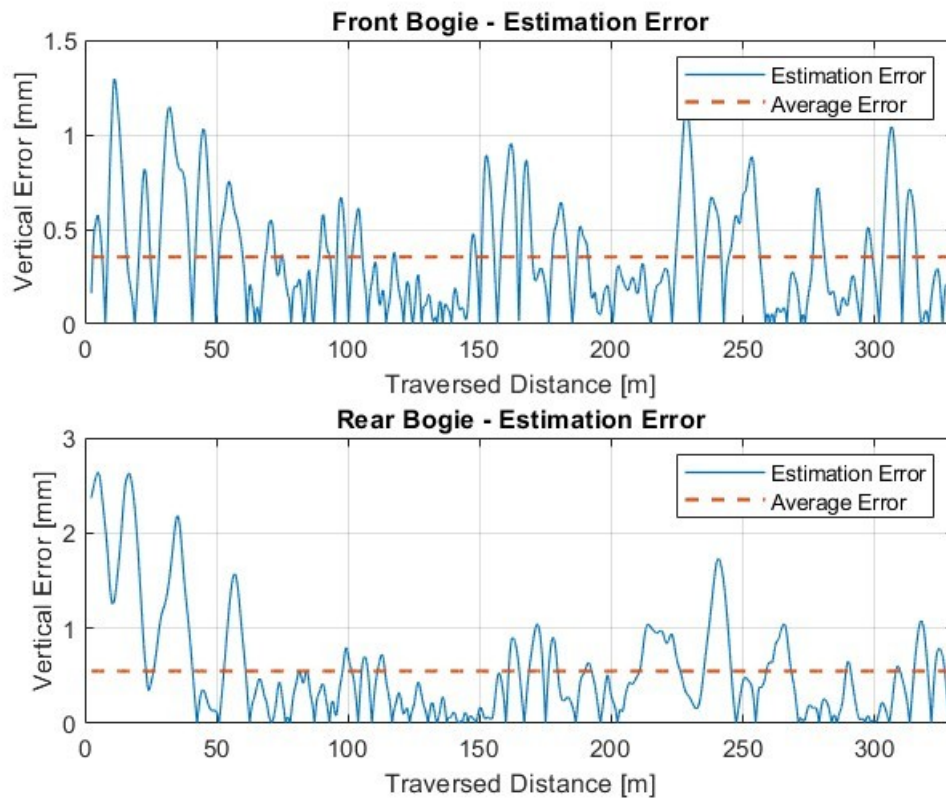
Figure 3.15: 10 D.o.F. Model – Estimation Error (135m radius curve)

The PSD graph of Figure 3.16, in the same way, confirms the suspected behaviours: the only sensitive difference between real and estimated power values is featured at low frequencies, which validates the perceived nature of the error in the time history – a very high wavelenght superimposing over the estimated disturbance, causing a sort of "translation" of certain tracts of such time history towards slightly higher values (i.e. the starting phase of the rear bogie time history being almost perfect in shape, except for a circa 2mm upwards shift) – a detail highlighted in Figure 3.17; this issue could be easily addressed with the employment of a better low-pass filter, but it has been decided to not change the one used in the previous case to highlight the differences and the possibilities of the method.

In conclusion, it can be argued that, given the correct parameters to model the train behaviour, the U.I.O. can provide an accurate estimation of vertical geometry of the track through this simplified 10 D.o.F. model, if anything through the employment of the front bogie measurements, and in any case further refinement of results (through filtering of output and potentially accelerational inputs, too) can greatly improve consistency.
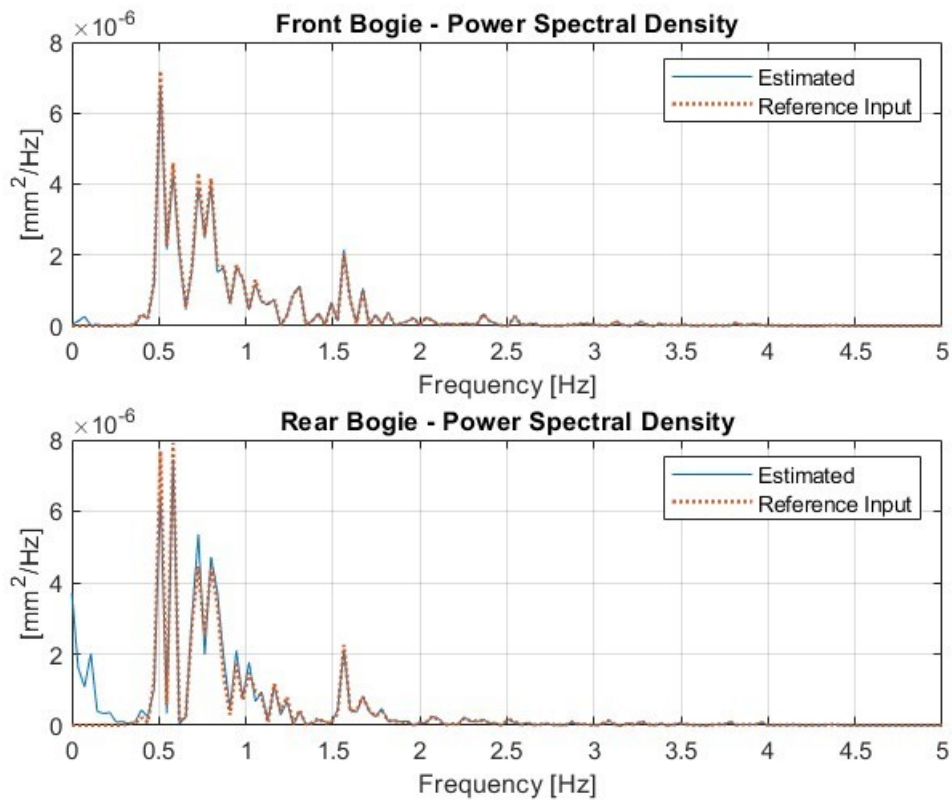
Figure 3.16: 10 D.o.F. Model – 135m radius curve estimation PSD
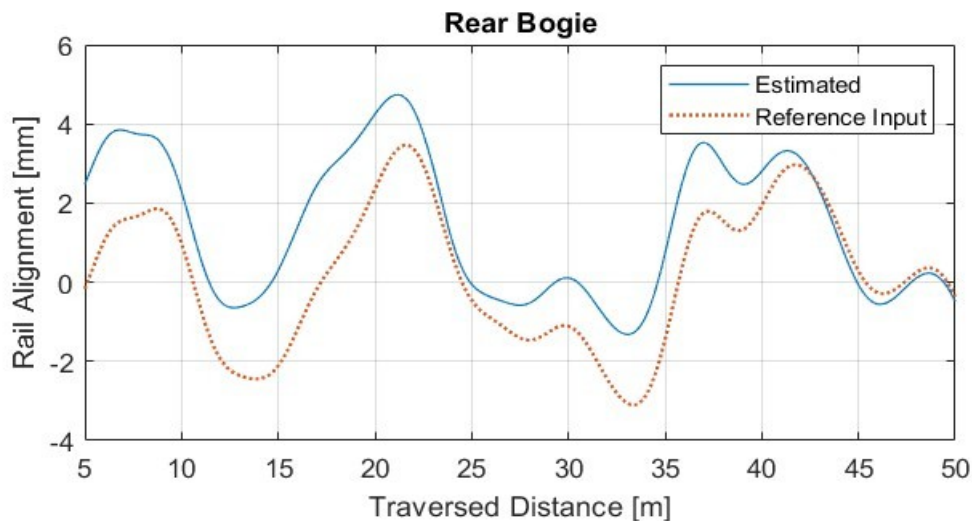


Figure 3.17: Upwards shift detail in the rear bogie time history - 135m radius curve

On the negative sides, it must be recognized that the system struggles more the more distant it gets from a straigh track, which is something not entirely unexpected, being the model a linearized one taking the straight configuration as the standard geometry.

In order to furtherly confirm these qualitatively deduced considerations, a couple indices were created to derive a general valutation of consistency for both the time

and the frequency domain. For the time domain, it was decided to employ the normalized squared error defined as in the (3.25); for the frequency domain, it was instead utilized the same definition but using the difference of spectral intensity as the error (3.26):

$$\alpha = \frac{\sum_{t=0}^{T} \left( x_{irr}(t) - x_{estimated}(t) \right)^2}{\sum_{t=0}^{T} x_{irr}^2(t)} \tag{3.25}$$

$$\beta = \frac{\sum_{f=0}^{f_{NYQ}} \left( \left| FFT_{irr}(f) \right| - \left| FFT_{estimated}(f) \right| \right)^2}{\sum_{f=0}^{f_{NYQ}} \left| FFT_{irr}(f) \right|^2} \tag{3.26}$$

The actual values obtained in both cases for these indices, reported in Table 3.8 below, seem to perfectly confirm the previously described deductions:

Table 3.8: Values of indices for the straight and curved negotiation

| Index | Value (Straight Track) | Value (135m Rad. Turn) |
|---|---|---|
| $\alpha_{FRONT}$ | 0,043 | 0,106 |
| $\alpha_{REAR}$ | 0,050 | 0,308 |
| $\beta_{FRONT}$ | $4,9 \times 10^{-4}$ | $9,6 \times 10^{-3}$ |
| $\beta_{REAR}$ | $6,4 \times 10^{-3}$ | 0,237 |

This data confirm that the estimation is much more effective when operated along a straight track (especially if evaluated in the frequency domain), and that the front wheel estimation is the one that should be considered as the most reliable output, but also that the main reason for time history discrepancies has to be found in slight time misalignments between the estimated and the real value (in turn mostly dependent from the algorithm timestep) – exception made for the initial shift for the 135m radius turn.

# 4 Lateral Irregularity Estimation

The second application for the U.I.O. is the reconstruction of transversal irregularity; in this case, lateral dynamics are coupled with roll motion, therefore the estimation of the two must be conducted simultaneously. To this end, an adequate model must be built to represent lateral dynamics; the selected version is a 21 D.o.F. model (pictured in Figure 4.1) with lateral displacement, yaw and roll of carbody, bogies and wheelsets as independent variables.

To deal with lateral dynamics, however, is a much more intricate issue than the vertical irregularity one, mostly due to the higher complexity of the contact dynamics which this time must factor in aspects such as friction and elastic normal contact. These relations between track geometry and the behaviour of the model will be explored in Section 4.2.
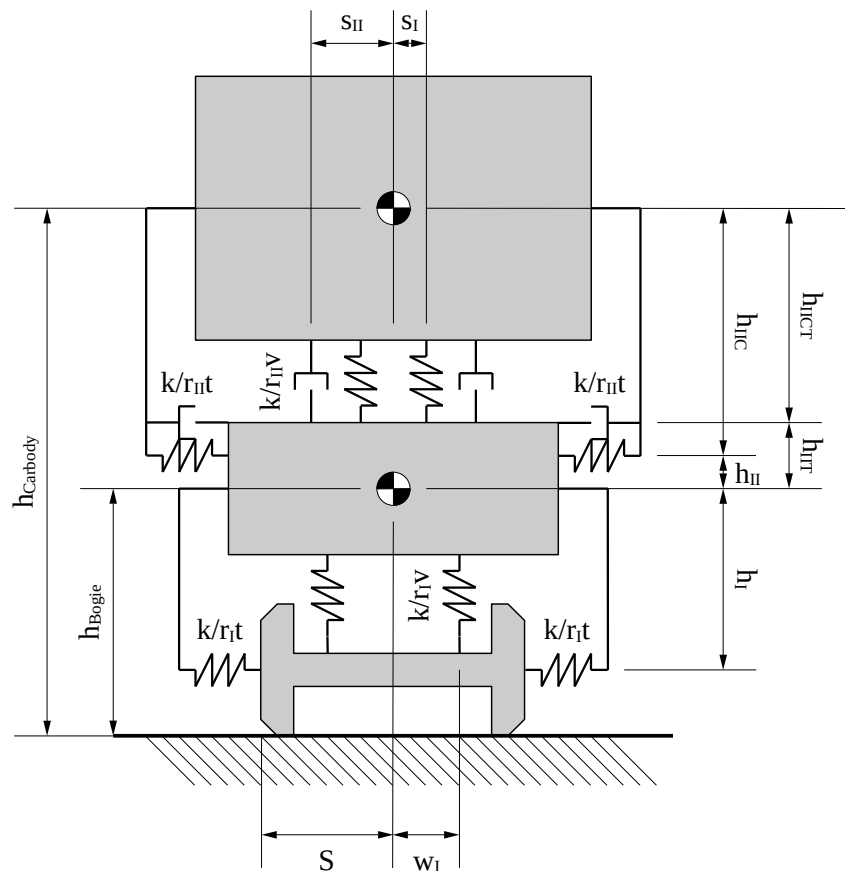


Figure 4.1: 21 D.o.F. Lateral Train Model Scheme

## 4.1. Model Data

Just as in the vertical case, the relevant data referring to the lateral model (Table 4.1 and Table 4.2) will be featured in the next pages, as well as the Jacobian matrices (Table 4.3 to Table 4.10) obtained by their manipulation; notice that in order to simplify notation, only the relevant (i.e. non-null) matrix blocks will be featured, meaning that primary suspensions' Jacobians won't feature the terms relative to the carbody (since they would just be zeros due to primary suspensions not being affected by the motion of the carbody), while in the secondary suspensions' ones the wheelset terms will be neglected. This means the primary Jacobians must be preceded by 3 columns of zeros, while secondary Jacobians must be followed by 12 columns of zeros:

Table 4.1: 21 D.o.F. Lateral Train Model Data

| Parameter | Symbol | Value |
|---|---|---|
| Carbody Mass | $\mathbf{m_C}$ | 17817 kg |
| Carbody Yaw Inertia | $\mathbf{J_{C\sigma}}$ | 427000 kg/m$^2$ |
| Carbody Roll Inertia | $\mathbf{J_{C\varrho}}$ | 52200 kg/m$^2$ |
| Bogie Mass | $\mathbf{m_B}$ | 2100 kg |
| Bogie Yaw Inertia | $\mathbf{J_{B\beta}}$ | 3750 kg/m$^2$ |
| Bogie Roll Inertia | $\mathbf{J_{B\varrho}}$ | 1200 kg/m$^2$ |
| Wheelset Mass | $\mathbf{m_W}$ | 1050 kg |
| Wheelset Yaw Inertia | $\mathbf{J_{W\beta}}$ | 540 kg/m$^2$ |
| Wheelset Roll Inertia | $\mathbf{J_{W\varrho}}$ | 540 kg/m$^2$ |
| Primary Vertical Damping | $\mathbf{r_{Iv}}$ | 44000 Ns/m |
| Primary Vertical Stiffness | $\mathbf{k_{Iv}}$ | 2000000 N/m |
| Primary Longitudinal Damping | $\mathbf{r_{Ih}}$ | 340000 Ns/m |
| Primary Longitudinal Stiffness | $\mathbf{k_{Ih}}$ | 16600000 N/m |
| Primary Transversal Damping | $\mathbf{r_{It}}$ | 200000 Ns/m |
| Primary Transversal Stiffness | $\mathbf{k_{It}}$ | 8360000 N/m |
| Secondary Vertical Damping | $\mathbf{r_{IIv}}$ | 37500 Ns/m |
| Secondary Vertical Stiffness | $\mathbf{k_{IIv}}$ | 1020200 N/m |
| Secondary Longitudinal Stiffness | $\mathbf{k_{IIh}}$ | 250000 N/m |
| Secondary Transversal Damping | $\mathbf{r_{IIt}}$ | 20000 Ns/m |
| Secondary Transversal Stiffness | $\mathbf{k_{IIt}}$ | 250000 N/m |

Table 4.2: 21 D.o.F. Lateral Train Geometrical Data

| Parameter | Symbol | Value |
|---|---|---|
| Gauge | $\mathbf{S}$ | 0,75 m |
| Carbody Baricentre Height | $\mathbf{h_C}$ | 1,59 m |
| Bogie Baricentre Height | $\mathbf{h_B}$ | 0,46 m |
| Wheel Radius | $\mathbf{r_w}$ | 0,41 m |
| Primary Susp. Longitudinal Distance | $\mathbf{b_I}$ | 1,075 m |
| Secondary Susp. Longitudinal Distance | $\mathbf{b_{II}}$ | 5,55 m |
| Primary Suspension Lateral Distance | $\mathbf{w_I}$ | 0,95 m |
| Secondary Longitudinal/Vertical Springs Lateral Distance | $\mathbf{s_I}$ | 0,95 m |
| Secondary Vertical Dampers Lateral Distance | $\mathbf{s_{II}}$ | 1,17 m |
| Secondary Transversal Dampers Longitudinal Dist. | $\mathbf{e_{II}}$ | 0,35 m |
| Primary Susp. - Bogie Vertical Distance | $\mathbf{h_I}$ | 0,05 m |
| Secondary Susp. - Bogie Vertical Distance | $\mathbf{h_{II}}$ | 0,24 m |
| Secondary Susp. - Carbody Vertical Distance | $\mathbf{h_{IIC}}$ | 0,89 m |
| Secondary Transversal Damper - Bogie Vertical Distance | $\mathbf{h_{IIT}}$ | 0,355 m |
| Secondary Transversal Damper - Carbody Vertical Distance | $\mathbf{h_{IICT}}$ | 0,775 m |
| Secondary Transversal Outer Damper Longitudinal Distance | $\mathbf{x_{ext}}$ | $b_{II} + e_{II}$ |
| Secondary Transversal Inner Damper Longitudinal Distance | $\mathbf{x_{int}}$ | $b_{II} - e_{II}$ |

Table 4.3: Jacobian of Primary Vertical Springs and Dampers (Bogies + Wheelsets)

| | $y_{B1}$ | $\sigma_{B1}$ | $\rho_{B1}$ | $y_{B2}$ | $\sigma_{B2}$ | $\rho_{B2}$ | $y_{W1}$ | $\sigma_{CW1}$ | $\rho_{W1}$ |
|---|---|---|---|---|---|---|---|---|---|
| $\mathbf{k_{Iv1}}$ | 0 | 0 | $-w_I$ | 0 | 0 | 0 | 0 | 0 | $+w_I$ |
| $\mathbf{k_{Iv2}}$ | 0 | 0 | $-w_I$ | 0 | 0 | 0 | 0 | 0 | 0 |
| $\mathbf{k_{Iv3}}$ | 0 | 0 | 0 | 0 | 0 | $-w_I$ | 0 | 0 | 0 |
| $\mathbf{k_{Iv4}}$ | 0 | 0 | 0 | 0 | 0 | $-w_I$ | 0 | 0 | 0 |
| | $y_{W2}$ | $\sigma_{CW2}$ | $\rho_{W2}$ | $y_{W3}$ | $\sigma_{CW3}$ | $\rho_{W3}$ | $y_{W4}$ | $\sigma_{CW4}$ | $\rho_{W4}$ |
| $\mathbf{k_{Iv1}}$ | 0 | 0 | 0 | 0 | 0 | 0 | 0 | 0 | 0 |
| $\mathbf{k_{Iv2}}$ | 0 | 0 | $+w_I$ | 0 | 0 | 0 | 0 | 0 | 0 |
| $\mathbf{k_{Iv3}}$ | 0 | 0 | 0 | 0 | 0 | $+w_I$ | 0 | 0 | 0 |
| $\mathbf{k_{Iv4}}$ | 0 | 0 | 0 | 0 | 0 | 0 | 0 | 0 | $+w_I$ |

### Table 4.4: Jacobian of Primary Longitudinal Springs and Dampers (Bogies + Wheelsets)

| | $y_{B1}$ | $\sigma_{B1}$ | $\rho_{B1}$ | $y_{B2}$ | $\sigma_{B2}$ | $\rho_{B2}$ | $y_{W1}$ | $\sigma_{CW1}$ | $\rho_{W1}$ |
|---|---|---|---|---|---|---|---|---|---|
| $k_{Ih1}$ | 0 | $-w_I$ | 0 | 0 | 0 | 0 | 0 | $+w_I$ | 0 |
| $k_{Ih2}$ | 0 | $-w_I$ | 0 | 0 | 0 | 0 | 0 | 0 | 0 |
| $k_{Ih3}$ | 0 | 0 | 0 | 0 | $-w_I$ | 0 | 0 | 0 | 0 |
| $k_{Ih4}$ | 0 | 0 | 0 | 0 | $-w_I$ | 0 | 0 | 0 | 0 |
| | $y_{W2}$ | $\sigma_{CW2}$ | $\rho_{W2}$ | $y_{W3}$ | $\sigma_{CW3}$ | $\rho_{W3}$ | $y_{W4}$ | $\sigma_{CW4}$ | $\rho_{W4}$ |
| $k_{Ih1}$ | 0 | 0 | 0 | 0 | 0 | 0 | 0 | 0 | 0 |
| $k_{Ih2}$ | 0 | $+w_I$ | 0 | 0 | 0 | 0 | 0 | 0 | 0 |
| $k_{Ih3}$ | 0 | 0 | 0 | 0 | $+w_I$ | 0 | 0 | 0 | 0 |
| $k_{Ih4}$ | 0 | 0 | 0 | 0 | 0 | 0 | 0 | $+w_I$ | 0 |

### Table 4.5: Jacobian of Primary Transversal Springs and Dampers (Bogies + Wheelsets)

| | $y_{B1}$ | $\sigma_{B1}$ | $\rho_{B1}$ | $y_{B2}$ | $\sigma_{B2}$ | $\rho_{B2}$ | $y_{W1}$ | $\sigma_{CW1}$ | $\rho_{W1}$ |
|---|---|---|---|---|---|---|---|---|---|
| $k_{It1}$ | $-1$ | $+b_I$ | $+h_I$ | 0 | 0 | 0 | $+1$ | 0 | 0 |
| $k_{It2}$ | $-1$ | $-b_I$ | $+h_I$ | 0 | 0 | 0 | 0 | 0 | 0 |
| $k_{It3}$ | 0 | 0 | 0 | $-1$ | $+b_I$ | $+h_I$ | 0 | 0 | 0 |
| $k_{It4}$ | 0 | 0 | 0 | $-1$ | $-b_I$ | $+h_I$ | 0 | 0 | 0 |
| | $y_{W2}$ | $\sigma_{CW2}$ | $\rho_{W2}$ | $y_{W3}$ | $\sigma_{CW3}$ | $\rho_{W3}$ | $y_{W4}$ | $\sigma_{CW4}$ | $\rho_{W4}$ |
| $k_{It1}$ | 0 | 0 | 0 | 0 | 0 | 0 | 0 | 0 | 0 |
| $k_{It2}$ | $+1$ | 0 | 0 | 0 | 0 | 0 | 0 | 0 | 0 |
| $k_{It3}$ | 0 | 0 | 0 | $+1$ | 0 | 0 | 0 | 0 | 0 |
| $k_{It4}$ | 0 | 0 | 0 | 0 | 0 | 0 | $+1$ | 0 | 0 |

### Table 4.6: Jacobian of Secondary Vertical Dampers (Carbody + Bogies)

| | $y_C$ | $\sigma_C$ | $\rho_C$ | $y_{B1}$ | $\sigma_{B1}$ | $\rho_{B1}$ | $y_{B2}$ | $\sigma_{B2}$ | $\rho_{B2}$ |
|---|---|---|---|---|---|---|---|---|---|
| $r_{IIvFR}$ | 0 | 0 | $-s_{II}$ | 0 | 0 | $+s_{II}$ | 0 | 0 | 0 |
| $r_{IIvFL}$ | 0 | 0 | $+s_{II}$ | 0 | 0 | $-s_{II}$ | 0 | 0 | 0 |
| $r_{IIvRR}$ | 0 | 0 | $-s_{II}$ | 0 | 0 | 0 | 0 | 0 | $+s_{II}$ |
| $r_{IIvRL}$ | 0 | 0 | $+s_{II}$ | 0 | 0 | 0 | 0 | 0 | $-s_{II}$ |

### Table 4.7: Jacobian of Secondary Vertical Springs (Carbody + Bogies)

| | $y_C$ | $\sigma_C$ | $\rho_C$ | $y_{B1}$ | $\sigma_{B1}$ | $\rho_{B1}$ | $y_{B2}$ | $\sigma_{B2}$ | $\rho_{B2}$ |
|---|---|---|---|---|---|---|---|---|---|
| $k_{IIvF}$ | 0 | 0 | $-s_I$ | 0 | 0 | $+s_I$ | 0 | 0 | 0 |
| $k_{IIvR}$ | 0 | 0 | $-s_I$ | 0 | 0 | 0 | 0 | 0 | $+s_I$ |

Table 4.8: Jacobian of Secondary Longitudinal Springs (Carbody + Bogies)

|  | $y_C$ | $\sigma_C$ | $\rho_C$ | $y_{B1}$ | $\sigma_{B1}$ | $\rho_{B1}$ | $y_{B2}$ | $\sigma_{B2}$ | $\rho_{B2}$ |
|---|---|---|---|---|---|---|---|---|---|
| $k_{IIhF}$ | 0 | $-s_I$ | 0 | 0 | $+s_I$ | 0 | 0 | 0 | 0 |
| $k_{IIhR}$ | 0 | $-s_I$ | 0 | 0 | 0 | 0 | 0 | $+s_I$ | 0 |

Table 4.9: Jacobian of Secondary Transversal Dampers (Carbody + Bogies)

|  | $y_C$ | $\sigma_C$ | $\rho_C$ | $y_{B1}$ | $\sigma_{B1}$ | $\rho_{B1}$ | $y_{B2}$ | $\sigma_{B2}$ | $\rho_{B2}$ |
|---|---|---|---|---|---|---|---|---|---|
| $r_{IItFR}$ | -1 | $+x_{ext}$ | $+h_{IICT}$ | +1 | $-e_{II}$ | $+h_{IIT}$ | 0 | 0 | 0 |
| $r_{IItFL}$ | +1 | $-x_{int}$ | $-h_{IICT}$ | -1 | $-e_{II}$ | $-h_{IIT}$ | 0 | 0 | 0 |
| $r_{IItRR}$ | -1 | $-x_{int}$ | $+h_{IICT}$ | 0 | 0 | 0 | +1 | $-e_{II}$ | $+h_{IIT}$ |
| $r_{IItRL}$ | +1 | $+x_{ext}$ | $-h_{IICT}$ | 0 | 0 | 0 | -1 | $-e_{II}$ | $-h_{IIT}$ |

Table 4.10: Jacobian of Secondary Transversal Springs (Carbody + Bogies)

|  | $y_C$ | $\sigma_C$ | $\rho_C$ | $y_{B1}$ | $\sigma_{B1}$ | $\rho_{B1}$ | $y_{B2}$ | $\sigma_{B2}$ | $\rho_{B2}$ |
|---|---|---|---|---|---|---|---|---|---|
| $k_{IItF}$ | -1 | $+b_{II}$ | $+h_{IIC}$ | +1 | 0 | $+h_{II}$ | 0 | 0 | 0 |
| $k_{IItR}$ | -1 | $-b_{II}$ | $+h_{IIC}$ | 0 | 0 | 0 | +1 | -1 | $+h_{II}$ |

Notice that the vertical and lateral model are de facto not coherent one with the other, since in the vertical one the secondary dampers featured a longitudinal distance from the middle plane between the wheelsets of the same bogie; considering both dampers on the same middle plane – thus nullifying the aforementioned distance – was in fact a deliberate choice so to decouple vertical and lateral model. In the real case, such dampers are disposed along a rectangle, but only on two opposing angles, as pictured in the Figure 4.2 below, creating a mutual relation between the bogie roll and pitch:
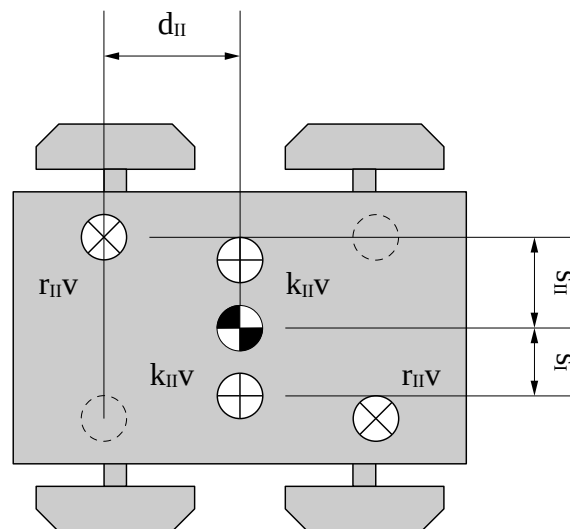


Figure 4.2: Vertical Secondary Suspension Disposition Scheme

## 4.2.  Wheel-Rail Contact Dynamics

In order to describe the lateral and yaw rotation of the vehicle, the acting forces and torques must be derived, in particular the lateral forces acting on the wheelset due to frictional contact with the rails, and the longitudinal forces (also originated from friction) which generate a yaw rotation due to the interaction between the wheel profile and the track geometry.

To obtain these forces, and to make it possible to describe them in a linear fashion (which is compatible with the U.I.O. superstructure), it is necessary to relate them (through a series of linearized coefficients as in (4.2)) with the so-called "creepages", which are the values of transversal (*T*) and longitudinal (*L*) speeds of both wheels normalized by the value of the vehicle advancement speed, as described in the (4.1) (for a more comprehensive discussion on the creepages theory, refer to the work on the topic by G. Diana and F. Cheli [13]):

$$\varepsilon_{L\text{left}} = \frac{V_{L\text{left}}}{V} \; ; \varepsilon_{L\text{right}} = \frac{V_{L\text{right}}}{V} \; ; \varepsilon_{T\text{left}} = \frac{V_{T\text{left}}}{V} \; ; \varepsilon_{T\text{right}} = \frac{V_{T\text{right}}}{V} \; ; \qquad (4.1)$$

$$\begin{cases} F_L = f_{LL} \varepsilon_L + f_{LT} \varepsilon_T \\ F_T = f_{TL} \varepsilon_L + f_{TT} \varepsilon_T \end{cases} \qquad (4.2)$$

(notice: the correlation coefficients are negative numbers, since friction force is as expected opposite to the direction of relative motion)

The problem is thus divided in two subsections; the former, that is, extracting the coefficients featured in (4.1) required to linearly correlate these creepages $\varepsilon$ with forces, will be dealt later on by employing some externally supplied resources; the latter, instead, will be dealt immediately – how to determine the velocities of the contact points between wheels and tracks in a constantly changing contact situation?

While the problem is relatively simple when the vehicle is travelling in a straight track, it gets much harder to solve in a closed form when this is not the case, even more so when trying to convert it to a linearized formulation; hence, some fundamental simplifications will be required right from the start. The first and foremost one is to simplify the contact kinematics:

- Speed will be calculated for a fixed point in on the middle plane of the wheel (and not the *actual* contact point, which changes during motion);

- Roll rotation will be considered as geometrically constrained by the track plane angle, redirecting this section of the problem to the longitudinal dynamics case; this  approximation, admissible due to the relatively low value of relative wheelset-track roll, allows to bypass the otherwise tremendously complex geometric relation between roll and lateral displacement;

- Third and last one, the contact between the wheel profile and the track will be simplified, reducing the latter to a geometrical line with no dimension except length; thus the contact point won't move relatively to the track (except for its lateral alignment $y_T$, which is exactly what the algorithm will try to determine).

Starting with the kinematics, the system will be based upon a reference frame placed in the middle plane of the track itself and parallel to the track – and hence to the advancing speed of the vehicle; as it can be seen in Figure 4.3, in such a reference system, the lateral displacement of the centre of mass of the wheelset will be identified as $y$ and will be orthogonal to the vehicle speed. The other considered velocity is yaw rotation, which does not only include the wheelset own rotation with respect to the bogies ($\sigma$), but also that of the system itself, identified as $\vartheta$, which takes into account the fact that the vehicle is following a curving track:
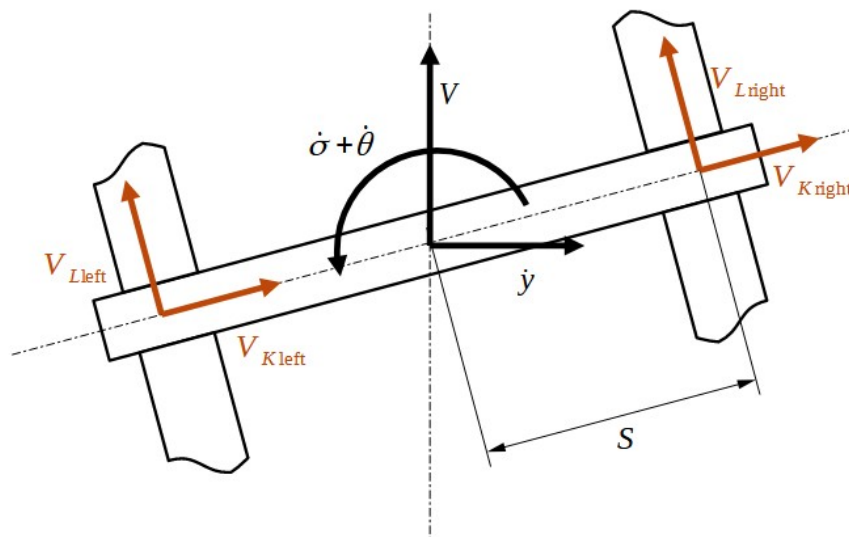


Figure 4.3: Reference frame and conventions of the contact point velocities

Since creepages relate both components of the relative wheel-track speed with contact forces, the contact point velocity must be decomposed into a longitudinal and transversal components, along perpendicular directions which together define the tangency plane of the wheel on the rail.

The first thing to determine is the longitudinal velocity of the contact points; due to the Angle of Attack, this value is not only a function of advancement speed itself, but the lateral speed as well due to the aforementioned Angle of Attack. The other term is due to yaw rotation (again including the system own rotation $\vartheta$ as well), which determines a longitudinal contribution through the gauge (identified as $S$ in Figure 4.3). All of these terms must be added to the angular velocity $\Omega$ of the wheelset itself,

which must be multiplied by the (potentially different in curves) rolling radii of the two wheels into account, obtaining (4.3):

$$\begin{cases} V_{L\,\text{left}} = V\cos\sigma - \dot{y}\sin\sigma - S(\dot{\sigma}+\dot{\vartheta}) - \Omega R_{\text{left}} \\ V_{L\,\text{right}} = V\cos\sigma - \dot{y}\sin\sigma + S(\dot{\sigma}+\dot{\vartheta}) - \Omega R_{\text{right}} \end{cases} \tag{4.3}$$

The same can be done for lateral velocity as well, still using Figure 4.3 as a reference: in this case, the main term is related to the lateral displacement $y$ of the wheelset, projected on its axis' direction (identified as $K$ and not $T$ for reasons which will become clear in a while); vehicular speed as well provides a contribution, although minimal due to Angle of Attack being likely very low. Another contribution which must not be ignored, though, (Figure 4.4) is rolling rotation, since the point we're considering is *not* at the centre of the wheel, but on the wheel external surface:
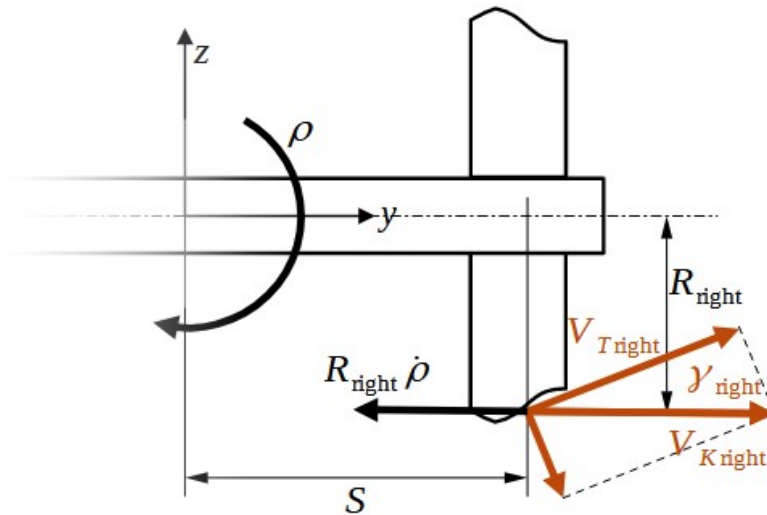


Figure 4.4: Roll contribution to wheel contact point lateral velocity

The final result of all these contributions can be summed up in the (4.4):

$$\begin{cases} V_{K\,\text{left}} = V\sin\sigma + \dot{y}\cos\sigma - R_{\text{left}}\,\dot{\rho} \\ V_{K\,\text{right}} = V\sin\sigma + \dot{y}\cos\sigma - R_{\text{right}}\,\dot{\rho} \end{cases} \tag{4.4}$$

In order to determine these radii, though, not only the wheel and rail profiles must be known, but also the equilibrium value of relative lateral displacement (as formulated in (4.6)) around which the rolling radius can be simplified as a linearly incremental value as per the (4.5):

$$R_{\text{left/right}} = R_{\text{left/right}\,eq} + \frac{\partial \Delta R_{\text{left/right}}}{\partial y_{rel}} y_{rel} \tag{4.5}$$

$$y_{rel} = y - y_T - R_{\text{left/right}\,eq} - y_{eq} \tag{4.6}$$

Going back to lateral kinematics, the value found with the (4.4) is along direction $K$ (that is, along the wheelset axis). The final objective of this analysis, though, is to determine a velocity (and thus a force) along the wheel-rail tangency plane (direction $T$ in Figure 4.4), which is inclined of an angle $\gamma$ with respect to the $yz$ plane of the reference system ($z$ being the advancement direction). This means that only one of the components of the value found for "lateral velocity" determines a relative displacement and hence a friction effect, the other being a normal one which determines an elastic compression term. The transversal component has a value obtained from (4.7) and (4.8):

$$\begin{cases} V_{T\,\text{left}} = V_{K\,\text{left}} \cos \gamma_{\text{left}} \\ V_{T\,\text{right}} = V_{K\,\text{right}} \cos \gamma_{\text{right}} \end{cases} \tag{4.7}$$

$$\begin{aligned} V_{T\,\text{left/right}} = {}& \dot{y} \cos \sigma \cos \gamma_{\text{left/right}} + V \sin \sigma \cos \gamma_{\text{left/right}} - \dots \\ & - \dot{\rho} R_{\text{left/right}\,eq} \cos \gamma_{\text{left/right}} - \dots \\ & - \frac{\partial \Delta R_{\text{left/right}}}{\partial y_{rel}} \left( y - y_T - R_{\text{left/right}\,eq} \rho - y_{eq} \right) \dot{\rho} \cos \gamma_{\text{left/right}} \end{aligned} \tag{4.8}$$

Once all the non-linear equations have been obtained, they can be linearized around a series of steady-state values, such as the Angle of Attack, which need to be externally determined as a function of speed and the track geometry (i.e. its curvature radius); some of the values, though, are fixed – for example, both $\rho$ and its derivative are null at the equilibrium (since the train is considered to be parallel to the track plane in steady-state regime), as well as the lateral displacement $y$ (due to the train not moving on that direction while in a stationary condition). The static values of both longitudinal and transversal velocity can be obtained as in (4.9). Most importantly, though, the linear coefficients relating velocities to state variables can be derived, allowing to proceed with the linearization of velocities as in the (4.10):

$$\begin{cases} V_{L\,\text{left/right}\,eq} = V \cos \sigma_{eq} \mp \dot{\vartheta} S - \Omega R_{\text{left/right}\,eq} \\ V_{T\,\text{left/right}\,eq} = V \sin \sigma_{eq} \cos \gamma_{\text{left/right}\,eq} \end{cases} \tag{4.9}$$

$$V_{L/T} \simeq V_{L/T} + \left. \frac{\partial V_{L/T}}{\partial \Delta y} \right|_{eq} (y - y_{eq}) + \left. \frac{\partial V_{L/T}}{\partial \Delta \sigma} \right|_{eq} (\sigma - \sigma_{eq}) + \dots \tag{4.10}$$

Said coefficients are expressed in the equations (4.11) to (4.19) (notice that equations are untouched if switching from the left to the right side, except for equation (4.14) whose sign is inverted when changing sides – thus both have been reported for clarity):

$$\left.\frac{\partial V_L}{\partial y}\right|_{eq}=-\Omega\left.\frac{\partial \Delta R}{\partial y_{rel}}\right|_{eq} \tag{4.11}$$

$$\left.\frac{\partial V_L}{\partial \dot{y}}\right|_{eq}=-\sin\sigma_{eq} \tag{4.12}$$

$$\left.\frac{\partial V_L}{\partial \sigma}\right|_{eq}=-V\sin\sigma_{eq} \tag{4.13}$$

$$\left.\frac{\partial V_{L\,left}}{\partial \dot{\sigma}}\right|_{eq}=-S \qquad \left.\frac{\partial V_{L\,right}}{\partial \dot{\sigma}}\right|_{eq}=+S \tag{4.14}$$

$$\left.\frac{\partial V_L}{\partial \rho}\right|_{eq}=+\Omega\left.\frac{\partial \Delta R}{\partial y_{rel}}\right|_{eq}R_{eq} \tag{4.15}$$

$$\left.\frac{\partial V_L}{\partial y_T}\right|_{eq}=+\Omega\left.\frac{\partial \Delta R}{\partial y_{rel}}\right|_{eq} \tag{4.16}$$

$$\left.\frac{\partial V_T}{\partial \dot{y}}\right|_{eq}=+\frac{\cos\sigma_{eq}}{\cos\gamma_{eq}} \tag{4.17}$$

$$\left.\frac{\partial V_T}{\partial \sigma}\right|_{eq}=+V\frac{\cos\sigma_{eq}}{\cos\gamma_{eq}} \tag{4.18}$$

$$\left.\frac{\partial V_T}{\partial \dot{\rho}}\right|_{eq}=-\frac{R_{eq}}{\cos\gamma_{eq}} \tag{4.19}$$

Switching from velocities to forces, another action that must be taken into account is the elastic effect due to normal contact and deformation; this acts as an additional spring of which the elastic coefficient is obtained through the linearization of the (4.20) to obtain (4.21).

$$F_n=C_H\delta^{1,5}\simeq F_{neq}+\left.\frac{\partial F_n}{\partial \delta}\right|_{eq}(\delta-\delta_{eq})=F_{neq}+K_H(\delta-\delta_{eq}) \tag{4.20}$$

$$K_H=1,5\,C_H\delta^{0,5} \tag{4.21}$$

In these formulae, δ refers to the contact spring compression; since this fictional spring acts in the normal direction to the wheel-rail tangency plane, the relative wheel-rail displacement must be projected along said normal direction in order to obtain the aforementioned value δ.

In turn, when dealing with lateral forces, all resulting actions on the wheel-rail tangency surface (direction $K$) must be projected along the wheelset axial direction ($T$), so that they are coherent with the reference system used to evaluate the degrees of freedom. Thus, both friction forces (Figure 4.5), and elastic ones (Figure 4.6) must be projected again along direction $K$:
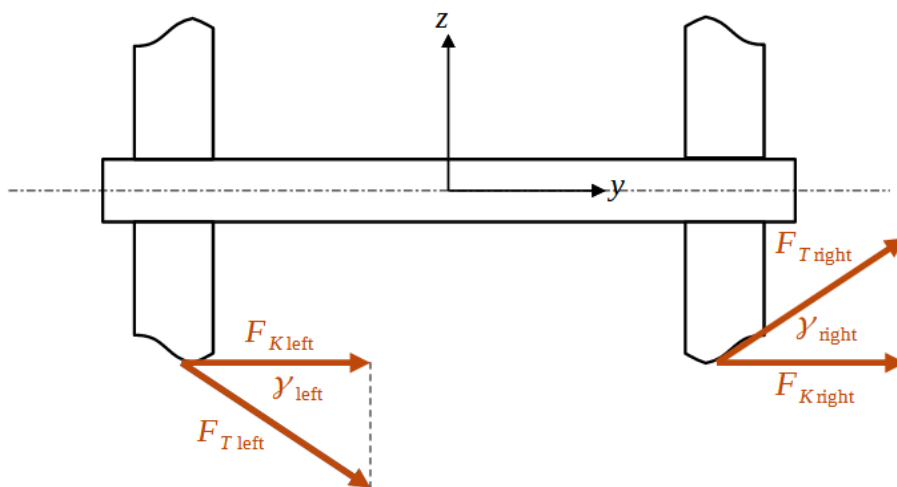


Figure 4.5: Projection of tangential contact forces along transversal direction
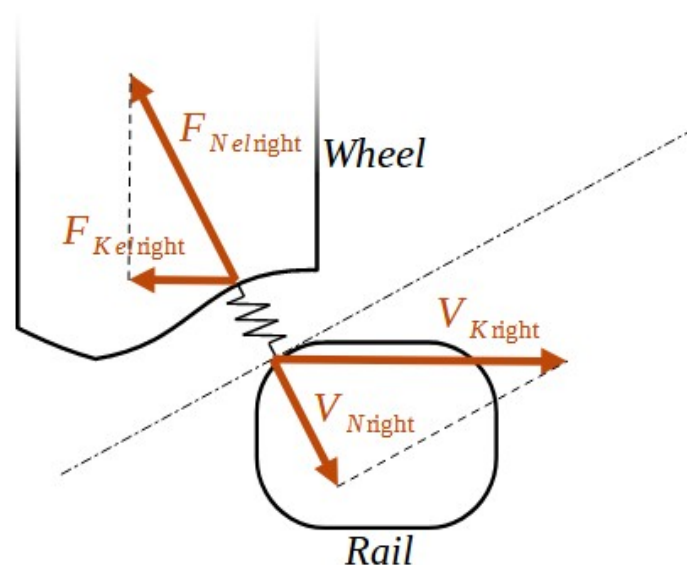


Figure 4.6: Railtrack-Wheel Elastic Contact Dynamics

All of this allows to express a linearized form of transversal and longitudinal force, following the general formulae (4.22) and (4.23) (notice that, being direction $K$ and $T$ not required anymore, from now on transversal force will be identified as $F_T$ to ensure a more intuitive notation):

$$F_L \simeq F_{Leq} + \frac{\partial F_L}{\partial \varepsilon_L}\bigg|_{eq} (\varepsilon_L - \varepsilon_{Leq}) + \frac{\partial F_L}{\partial \varepsilon_T}\bigg|_{eq} (\varepsilon_T - \varepsilon_{Teq}) = \ldots$$
$$\ldots = F_{Leq} + f_{LL}\Delta\varepsilon_L + f_{LT}\Delta\varepsilon_T \qquad (4.22)$$

$$F_T \simeq F_{Teq} + \frac{\partial F_T}{\partial \varepsilon_L}\bigg|_{eq} (\varepsilon_L - \varepsilon_{Leq}) + \frac{\partial F_T}{\partial \varepsilon_T}\bigg|_{eq} (\varepsilon_T - \varepsilon_{Teq}) = \ldots$$
$$\ldots = F_{Teq} + f_{TL}\Delta\varepsilon_L + f_{TT}\Delta\varepsilon_T \qquad (4.23)$$

Being the creepages $\varepsilon$ in turn linearized functions of the degrees of freedom (as per the (4.10), it is possible to derive a linearized function of said degrees of freedom to express the transversal and longitudinal force, and thus the yaw torque.

After some calculations which won't be reported here for brevity, the following coefficients (4.24) to (4.37) relating the state variables with lateral force and yaw torque can be obtained:

$$\frac{\partial F_T}{\partial \Delta y} = -f_{TL}\frac{\Omega}{V}\sin\sigma_{eq}\frac{\partial \Delta R_{\text{left}}}{\partial y_{rel}}\bigg|_{eq}\cos\gamma_{\text{left}eq} - K_{\text{left}}\sin^2\gamma_{\text{left}eq} - \ldots$$
$$-f_{TL}\frac{\Omega}{V}\sin\sigma_{eq}\frac{\partial \Delta R_{\text{right}}}{\partial y_{rel}}\bigg|_{eq}\cos\gamma_{\text{right}eq} - K_{\text{right}}\sin^2\gamma_{\text{right}eq} \qquad (4.24)$$

$$\frac{\partial F_T}{\partial \dot{y}} = -f_{TL}\frac{1}{V}\sin\sigma_{eq}\left(\cos\gamma_{\text{left}eq} + \cos\gamma_{\text{right}eq}\right) + \ldots$$
$$+f_{TT}\frac{1}{V}\cos\sigma_{eq}\left(\cos^2\gamma_{\text{left}eq} + \cos^2\gamma_{\text{right}eq}\right) \qquad (4.25)$$

$$\frac{\partial F_T}{\partial \Delta\sigma} = -f_{TL}\sin\sigma_{eq}\left(\cos\gamma_{\text{left}eq} + \cos\gamma_{\text{right}eq}\right) + \ldots$$
$$+f_{TT}1\cos\sigma_{eq}\left(\cos^2\gamma_{\text{left}eq} + \cos^2\gamma_{\text{right}eq}\right) \qquad (4.26)$$

$$\frac{\partial F_T}{\partial \dot{\sigma}} = -f_{TL}\frac{S}{V}\left(\cos\gamma_{\text{left}eq} - \cos\gamma_{\text{right}eq}\right) \qquad (4.27)$$

$$\frac{\partial F_T}{\partial \rho} = + f_{TL} \frac{\Omega}{V} \left. \frac{\partial \Delta R_{\text{left}}}{\partial y_{rel}} \right|_{eq} R_{\text{left}\,eq} \cos \gamma_{\text{left}\,eq} + \ldots$$

$$+ f_{TL} \frac{\Omega}{V} \left. \frac{\partial \Delta R_{\text{right}}}{\partial y_{rel}} \right|_{eq} R_{\text{right}\,eq} \cos \gamma_{\text{right}\,eq} \tag{4.28}$$

$$\frac{\partial F_T}{\partial \dot{\rho}} = - f_{TT} \frac{1}{V} \left( R_{\text{left}\,eq} \cos^2 \gamma_{\text{left}\,eq} + R_{\text{right}\,eq} \cos^2 \gamma_{\text{right}\,eq} \right) \tag{4.29}$$

$$\frac{\partial F_T}{\partial y_T} = + f_{TL} \frac{\Omega}{V} \sin \sigma_{eq} \left. \frac{\partial \Delta R_{\text{left}}}{\partial y_{rel}} \right|_{eq} \cos \gamma_{\text{left}\,eq} + K_{\text{left}} \sin^2 \gamma_{\text{left}\,eq} - \ldots$$

$$+ f_{TL} \frac{\Omega}{V} \sin \sigma_{eq} \left. \frac{\partial \Delta R_{\text{right}}}{\partial y_{rel}} \right|_{eq} \cos \gamma_{\text{right}\,eq} + K_{\text{right}} \sin^2 \gamma_{\text{right}\,eq} \tag{4.30}$$

$$\frac{\partial M_\sigma}{\partial \Delta y} = + f_{LL} \frac{\Omega}{V} S \left( \left. \frac{\partial \Delta R_{\text{left}}}{\partial y_{rel}} \right|_{eq} - \left. \frac{\partial \Delta R_{\text{right}}}{\partial y_{rel}} \right|_{eq} \right) \tag{4.31}$$

$$\frac{\partial M_\sigma}{\partial \dot{y}} = - f_{LT} \frac{S}{V} \cos \sigma_{eq} \left( \cos \gamma_{\text{left}\,eq} - \cos \gamma_{\text{right}\,eq} \right) \tag{4.32}$$

$$\frac{\partial M_\sigma}{\partial \Delta \sigma} = - f_{LT} S \cos \sigma_{eq} \left( \cos \gamma_{\text{left}\,eq} - \cos \gamma_{\text{right}\,eq} \right) \tag{4.33}$$

$$\frac{\partial M_\sigma}{\partial \dot{\sigma}} = + 2 f_{LL} \frac{S^2}{V} \tag{4.34}$$

$$\frac{\partial M_\sigma}{\partial \rho} = - f_{LL} \frac{\Omega}{V} S \left( \left. \frac{\partial \Delta R_{\text{left}}}{\partial y_{rel}} \right|_{eq} R_{\text{left}\,eq} - \left. \frac{\partial \Delta R_{\text{right}}}{\partial y_{rel}} \right|_{eq} R_{\text{right}\,eq} \right) \tag{4.35}$$

$$\frac{\partial M_\sigma}{\partial \dot{\rho}} = + f_{LT} \frac{S}{V} \left( R_{\text{left}\,eq} \cos \gamma_{\text{left}\,eq} - R_{\text{right}\,eq} \cos \gamma_{\text{right}\,eq} \right) \tag{4.36}$$

$$\frac{\partial M_\sigma}{\partial y_T} = - f_{LL} \frac{\Omega}{V} S \left( \left. \frac{\partial \Delta R_{\text{left}}}{\partial y_{rel}} \right|_{eq} - \left. \frac{\partial \Delta R_{\text{right}}}{\partial y_{rel}} \right|_{eq} \right) \tag{4.37}$$

### 4.2.1.  Straight Track Simplification

In this study case, a straight track will be considered; this greatly simplifies the previously discussed coefficients and nullifies a number of them, due to 3 conditions being simultaneously fulfilled:

- First, creepages being very low, so-called Kalker Theory holds true, which means that cross-coefficients $f_{LT}$ and $f_{TL}$ are null; furthermore, Angle of Attack is equal to 0 as well;

- Second, no difference is present anymore between the two sides of the vehicle (it being symmetric and in a perfectly symmetric contact condition with the two rails); this allows for example to employ a direct correlation between advancement speed $V$ and rotation velocity $\Omega$;

- Third and arguably most important, condition is unvaried between one axle and the next one, an hypothesis which wouldn't be valid any longer if trying to solve the much more complex problem of curved track.

The aforementioned simplifications reduce the displacement-force coefficients to the following (4.38) to (4.46):

$$\frac{\partial F_T}{\partial \dot{y}} = +2 f_{TT} \frac{1}{V} \tag{4.38}$$

$$\frac{\partial F_T}{\partial \dot{\rho}} = -2 f_{TT} \frac{1}{V} R_{eq} \tag{4.39}$$

$$\frac{\partial F_T}{\partial \Delta y} = -2 K \sin^2 \gamma_{eq} \tag{4.40}$$

$$\frac{\partial F_T}{\partial \Delta \sigma} = +2 f_{TT} \tag{4.41}$$

$$\frac{\partial F_T}{\partial y_T} = +2 K \sin^2 \gamma_{eq} \tag{4.42}$$

$$\frac{\partial M_\sigma}{\partial \Delta y} = +f_{LL} \frac{S}{R_{eq}} \left( \frac{\partial \Delta R_{\text{left}}}{\partial y_{rel}} \bigg|_{eq} - \frac{\partial \Delta R_{\text{right}}}{\partial y_{rel}} \bigg|_{eq} \right) \tag{4.43}$$

$$\frac{\partial M_\sigma}{\partial \dot{\sigma}} = +2 f_{LL} \frac{S^2}{V} \tag{4.44}$$

$$\frac{\partial M_\sigma}{\partial \rho} = -f_{LL} S \left( \frac{\partial \Delta R_{\text{left}}}{\partial y_{rel}} \bigg|_{eq} - \frac{\partial \Delta R_{\text{right}}}{\partial y_{rel}} \bigg|_{eq} \right) \tag{4.45}$$

$$\frac{\partial M_\sigma}{\partial y_T} = -f_{LL} \frac{S}{R_{eq}} \left( \frac{\partial \Delta R_{\text{left}}}{\partial y_{rel}} \bigg|_{eq} - \frac{\partial \Delta R_{\text{right}}}{\partial y_{rel}} \bigg|_{eq} \right) \tag{4.46}$$

## 4.3.   State-Space Model Construction

The coefficients that have been defined in the (4.38) to (4.46) relate either one of the state variables or the externally constrained parameter $y_T$ with either $F_T$ or $M_\sigma$; this means that they must be inserted on the right side of the equilibrium equation (4.47), but can be easily moved to the left side through some operations, resulting in the (4.48). The following equations (4.49) to (4.51) are simplified by taking into consideration only one wheelset as part of the system (thus comprising only the three variables $y$, $\sigma$, and $\rho$), omitting any other body composing the model:

$$M \ddot{x} + R \dot{x} + K x = \frac{\partial F}{\partial \dot{x}} \dot{x} + \frac{\partial F}{\partial x} x + \frac{\partial F}{\partial y_T} y_T \tag{4.47}$$

$$M \ddot{x} + \left( R - \frac{\partial F}{\partial \dot{x}} \right) \dot{x} + \left( K - \frac{\partial F}{\partial x} \right) x = \frac{\partial F}{\partial y_T} y_T \tag{4.48}$$

$$\frac{\partial F}{\partial \dot{x}} = \begin{bmatrix} \dfrac{\partial F_T}{\partial \dot{y}} & \dfrac{\partial F_T}{\partial \dot{\sigma}} & \dfrac{\partial F_T}{\partial \dot{\rho}} \\[2mm] \dfrac{\partial M_\sigma}{\partial \dot{y}} & \dfrac{\partial M_\sigma}{\partial \dot{\sigma}} & \dfrac{\partial M_\sigma}{\partial \dot{\rho}} \\[2mm] 0 & 0 & 0 \end{bmatrix} \tag{4.49}$$

$$\frac{\partial F}{\partial x} = \begin{bmatrix} \dfrac{\partial F_T}{\partial y} & \dfrac{\partial F_T}{\partial \sigma} & \dfrac{\partial F_T}{\partial \rho} \\[2mm] \dfrac{\partial M_\sigma}{\partial y} & \dfrac{\partial M_\sigma}{\partial \sigma} & \dfrac{\partial M_\sigma}{\partial \rho} \\[2mm] 0 & 0 & 0 \end{bmatrix} \tag{4.50}$$

$$\frac{\partial F}{\partial y_T} = \begin{bmatrix} \dfrac{\partial F_T}{\partial y_T} \\[2mm] \dfrac{\partial M_\sigma}{\partial y_T} \\[2mm] 0 \end{bmatrix} \tag{4.51}$$

(Notice that removing cross-correlations between transversal and longitudinal contact dynamics results in a number of Force-D.o.F. relations being null. This means some of the terms of the matrices (4.49), (4.50) and (4.51) get nullified as well)

This formulation, however, does not take into account the fact that also $\rho$, despite being formally part of the state, is externally constrained due to the previously exposed approximation; this means that it must be treated just like the vertical displacement of the wheels in the longitudinal case in Section 3, thus dividing the

state into a "free" (*F*) and "externally constrained" (*C*) subvector, and obtaining four submatrices per matrix as in the (4.52) and (4.53). Notice that due to the presence of an additional external action caused by the track irregularity $y_T$, the formulation changes slightly with respect to the longitudinal case; it is only thanks to the non-existant relation between $y_T$ and $\rho$ that it is possible to ignore the hypothetical lower component of the external actions matrix:

$$
\begin{bmatrix} M_{FF} & M_{FC} \\ M_{CF} & M_{CC} \end{bmatrix} \begin{Bmatrix} \ddot{x}_F \\ \ddot{x}_C \end{Bmatrix} + \begin{bmatrix} R_{FF} & R_{FC} \\ R_{CF} & R_{CC} \end{bmatrix} \begin{Bmatrix} \dot{x}_F \\ \dot{x}_C \end{Bmatrix} + ...
$$

$$
... + \begin{bmatrix} K_{FF} & K_{FC} \\ K_{CF} & K_{CC} \end{bmatrix} \begin{Bmatrix} x_F \\ x_C \end{Bmatrix} = \begin{bmatrix} \dfrac{\partial F}{\partial y_T} \\ [0] \end{bmatrix} y_T
$$

(4.52)

$$
M_{FF} \ddot{x}_F + R_{FF} \dot{x}_F + K_{FF} x_F = ...
$$

$$
... - M_{FC} \ddot{x}_C - R_{FC} \dot{x}_C - K_{FC} x_C + \dfrac{\partial F}{\partial y_T} y_T
$$

(4.53)

Once the matrix has been divided into its free and externally constrained components, the same modifications made for the longitudinal case must be repeated. First of all, the relation between the roll rotation $\rho$ and its derivative must be taken into account (just like was previously done in Section 3.2 for the longitudinal kinematics) by extending the state from a 17+17 to a 17+17+4=38 variables vector as represented below in (4.54) and (4.55):

$$
x = \{ y_{CB} \, \sigma_{CB} \, \rho_{CB} \, y_{B1} \, \sigma_{B1} \, \rho_{B1} \, y_{B2} \, \sigma_{B2} \, \rho_{B2}
$$

$$
y_{W1} \, \sigma_{W1} \, y_{W2} \, \sigma_{W2} \, y_{W3} \, \sigma_{W3} \, y_{W4} \, \sigma_{W4} \}^T
$$

(4.54)

$$
\rho = \{ \rho_{W1} \, \rho_{W2} \, \rho_{W3} \, \rho_{W4} \}^T
$$

$$
\dot{x}_{extended} = \begin{Bmatrix} \ddot{x} \\ \dot{x} \\ \dot{\rho} \end{Bmatrix} = A_{extended} \begin{Bmatrix} \dot{x} \\ x \\ \rho \end{Bmatrix} + E_{extended} \begin{Bmatrix} \dot{\rho} \\ y_T \end{Bmatrix}
$$

(4.55)

The resulting extended state and input matrices are the following (4.56) and (4.57):

$$A_{extended} = \begin{bmatrix} -M_{FF}^{-1} R_{FF} & -M_{FF}^{-1} K_{FF} & -M_{FF}^{-1} K_{FC} \\ I & [0] & [0] \\ [0] & [0] & [0] \end{bmatrix} \tag{4.56}$$

$$E_{extended} = \begin{bmatrix} -M_{FF}^{-1} R_{FC} & M_{FF}^{-1} \dfrac{\partial F}{\partial y_T} \\ [0] & [0] \\ I & [0] \end{bmatrix} \tag{4.57}$$

The second aspect to be taken care of is the Padé Approximation, in order to take equal delayed inputs into account. From the experiences relative to the vertical case, the full-delayed system (i.e. featuring only 1 input and all of the following being only the result of said approximation) will not be tried, while instead the double input formulation will be immediately employed; with respect to the vertical case, though, in this case the inputs to be duplicated are not single variables, but are represented by a vector of length 2 comprising both the derivative of roll rotation $\rho$ and the rail lateral irregularity $y_T$. In the matrix $E$ (4.58), the two inputs are alternated to keep the pair referring to the same wheelset in the same 2-columns submatrix. This means the formulation of Padé Approximation (4.59), despite remaining unvaried on the theoretical side, gets somewhat more cluttered in practice:

$$E = \begin{bmatrix} E_{\rho 1} E_{yT1} E_{\rho 2} E_{yT2} E_{\rho 3} E_{yT3} E_{\rho 4} E_{yT4} \end{bmatrix} \tag{4.58}$$

$$\begin{Bmatrix} \dot{x}_{extended} \\ \dot{x}_{P\rho 2} \\ \dot{x}_{PyT2} \\ \dot{x}_{P\rho 4} \\ \dot{x}_{PyT4} \end{Bmatrix} = \begin{bmatrix} A & E_{\rho 2} C_P & E_{yT2} C_{irr} & E_{\rho 4} C_P & E_{yT4} C_P \\ [0] & A_P & [0] & [0] & [0] \\ [0] & [0] & A_P & [0] & [0] \\ [0] & [0] & [0] & A_P & [0] \\ [0] & [0] & [0] & [0] & A_P \end{bmatrix} \begin{Bmatrix} x_{extended} \\ x_{P\rho 2} \\ x_{PyT2} \\ x_{P\rho 4} \\ x_{PyT4} \end{Bmatrix}$$

$$+ \begin{bmatrix} E_{\rho 1}+\ldots & E_{yT1}+\ldots & E_{\rho 3}+\ldots & E_{yT3}+\ldots \\ +E_{\rho 2} D_P & +E_{yT2} D_P & +E_{\rho 4} D_P & +E_{yT4} D_P \\ B_P & [0] & [0] & [0] \\ [0] & B_P & [0] & [0] \\ [0] & [0] & B_P & [0] \\ [0] & [0] & [0] & B_P \end{bmatrix} \begin{Bmatrix} \rho_1 \\ y_{T1} \\ \rho_3 \\ y_{T3} \end{Bmatrix} \tag{4.59}$$

## 4.4. Model Validation

Just as in the vertical model, it was decided to approach the problem in a conservative way; thus, the simplified model was first validated by comparing the accelerations it generates with the ones derived from the PoliMi multibody model. Although results are promising (pictured in Figure 4.7 are the accelerations relative to the front bogie), the bogies' roll suffers from an overdamping of high frequency inputs, as made evident in the spectral comparison at Figure 4.8; said figure, though, also highlights that lateral and especially yaw acceleration do not suffer from the same inaccuracy:
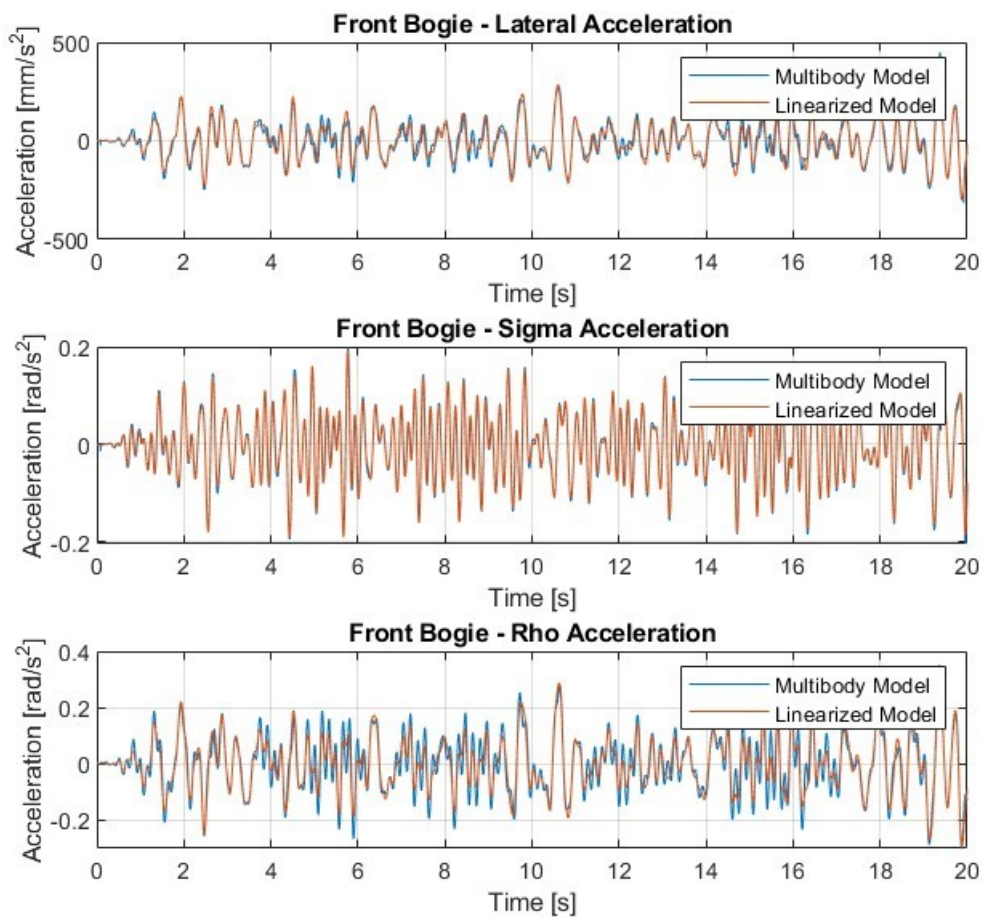


Figure 4.7: Comparison of Lateral, Yaw and Roll Acceleration of the front bogie between multibody and simplified models
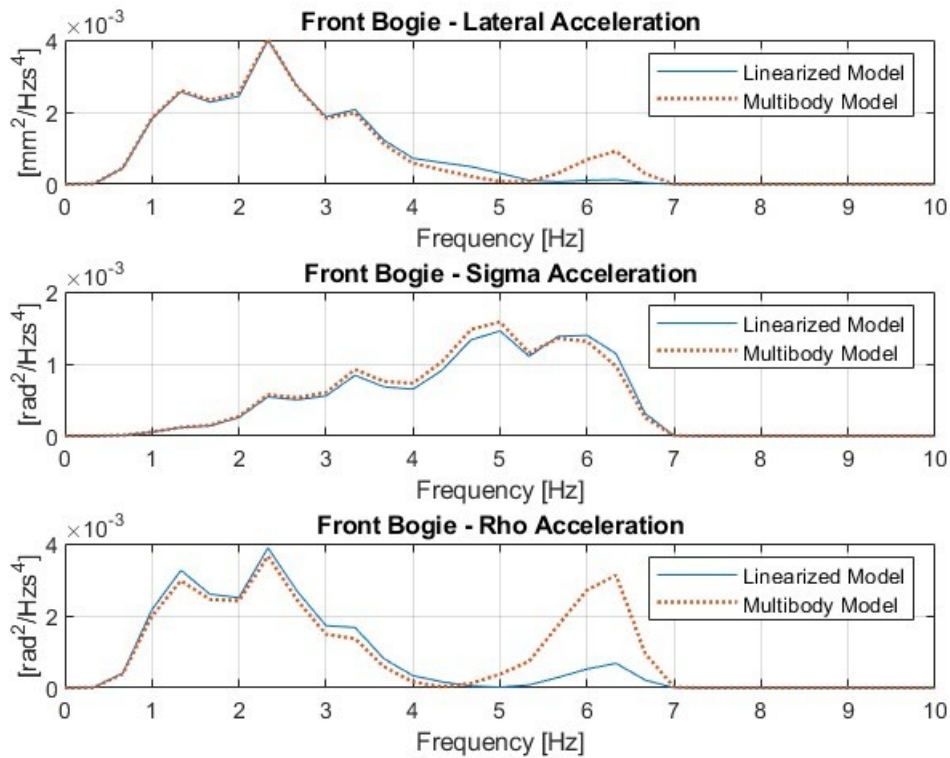
Figure 4.8: Power Spectral Density of Lateral, Yaw and Roll Acceleration of the front bogie

This is a problem connected with the way the multiple delayed inputs are being dealt with. If the Bode Diagrams at Figure 4.9 are analyzed, in fact, it can be noticed that Padé Approximation, since it estimates delays through a number of zeroes and poles equal to its order (that is, the size of matrices $A_P$ and the like employed to express it in linear form), can in no case correctly estimate phase delays up to 180° times this number. That being said, in this particular case (in which delay $\tau$ is equal to 2,15m / 70km/h, that is around 0,11s) this means that after around 3Hz 2$^{nd}$ order approximation starts diverging from the real delay phase diagram due to its asymptotic nature; this results in any input signal over that threshold being heavily distorted.

However, the same Figure 4.9 highlights that by increasing the order of Padé Approximation it is possible to much more effectively estimate the delay trend even at higher frequencies. As it is quite evident from Figure 4.10 and Figure 4.11, switching to a 3$^{rd}$ order approximation allows for the linear system to much more accurately approximate the behaviour of the multibody one, in particular fixing the aforementioned issues with the bogies' roll at higher frequencies.
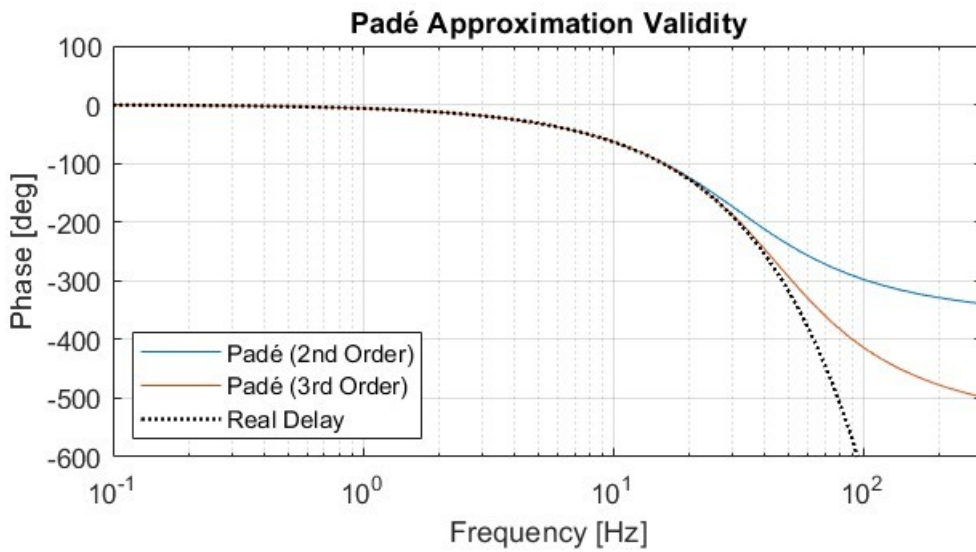
Figure 4.9: Padé Approximation Validity depending on its order – notice that at 6Hz the second order Approximation is not accurate anymore
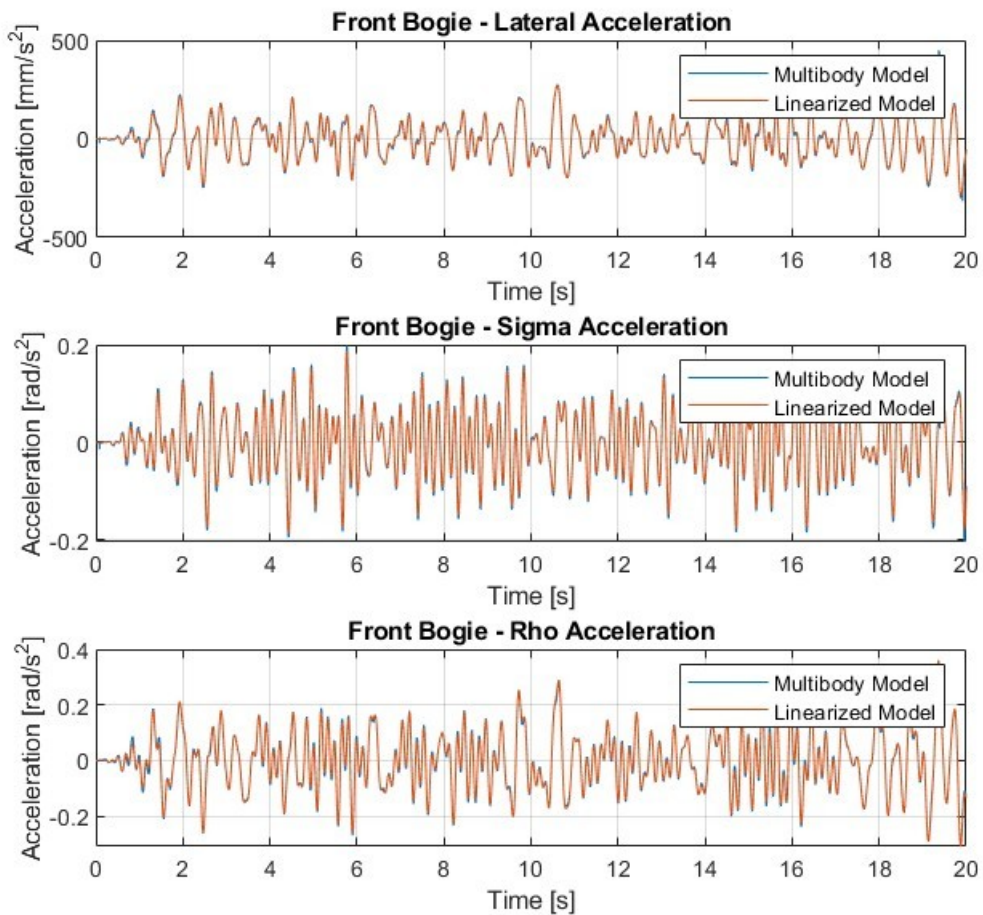


Figure 4.10: Comparison of Lateral, Yaw and Roll Acceleration of the front bogie between multibody and simplified models (3rd order Padé Approximation)
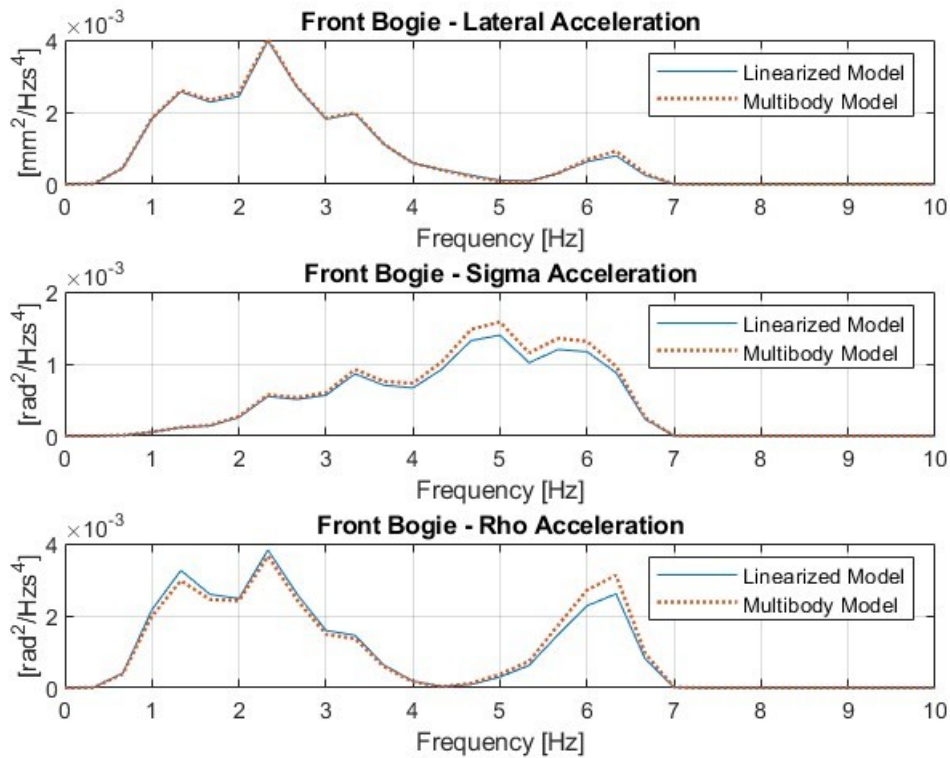
Figure 4.11: Power Spectral Density of Lateral, Yaw and Roll Acceleration of the front bogie (3rd order Padé Approximation)

It should be reminded that the matrix $D_P$, which was equal to *1* for the $2^{nd}$ order approximation (and assumes the same value for all even values of said order) becomes instead equal to *-1* for all odd numbers of the order (thus its apparently unnecessary explicitation in the (4.59)).

Notice, though, that increasing the order of Padé Approximation also means to furtherly extend the state vector and thus enlarge the state matrix, an operation which is not without its own consequences (as will be furtherly discussed upon in Section 4.5.2).

## 4.5.  Results

The particular case for which the estimation will be performed is a straight track section traversed at a constant speed of 70km/h. In order to proceed, it was decided to employ all possible measurements, thus all 17 acceleration values from the carbody, the bogies and the wheelsets (for the latter, obviously only lateral and yaw, the unconstrained degrees of freedom). As per the considerations made when presenting the results, only the front bogie results will be pictured.

### 4.5.1.  2$^{nd}$ Order Padé Approximation

Despite the moderately conflicting results regarding the accelerations' comparison discussed in the previous section, the use of 2$^{nd}$ order Padé Approximation was tried first for the estimation, due to the general trend of accelerations being quite accurate, at least at low frequency. As per the gain matrix, it was decided for the time being to keep using the same pole placement as in Section 3.4, that is, doubling the negative real part of observable poles and then furtherly subtracting their imaginary one.

As expected, the results pictured in Figure 4.12 are not particularly accurate; nonetheless, it can be qualitatively appreciated that the general trend is indeed being estimated, if almost constantly with excessively high values.
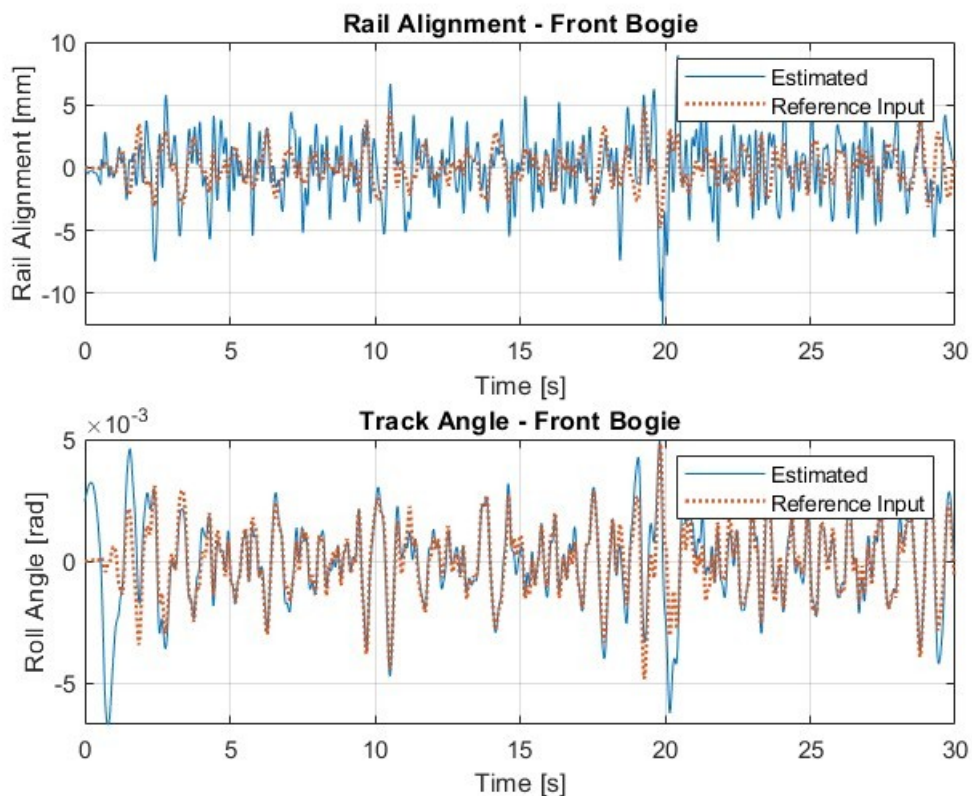


Figure 4.12: 21 D.o.F. Model - U.I.O. results (17 Accelerations)

Furthermore, while the lateral irregularity estimation is plagued by severe inaccuracies, the roll angle is already being estimated in quite satisfactory way; this is not entirely unexpected, being the latter a much easier quantity to be reconstructed due to it having a relation with the system much more akin to the vertical displacement in Section 3, unlike the lateral motion for which the somewhat approximated contact dynamics have been introduced.

The main reason for inaccuracy is the inadequacy of the $2^{nd}$ order Padé Approximation used in the linearized model to correctly describe the system behaviour at higher frequencies, as amply demonstrated by comparing its accelerations with those of the multibody model in the previous section. In particular, since the linearized system predicts lower high-frequency accelerations for the given disturbances (see the previous section), it associates much higher irregularities with the actual values of acceleration; this is made evident by the comparison of Power Spectral Density at Figure 4.13:
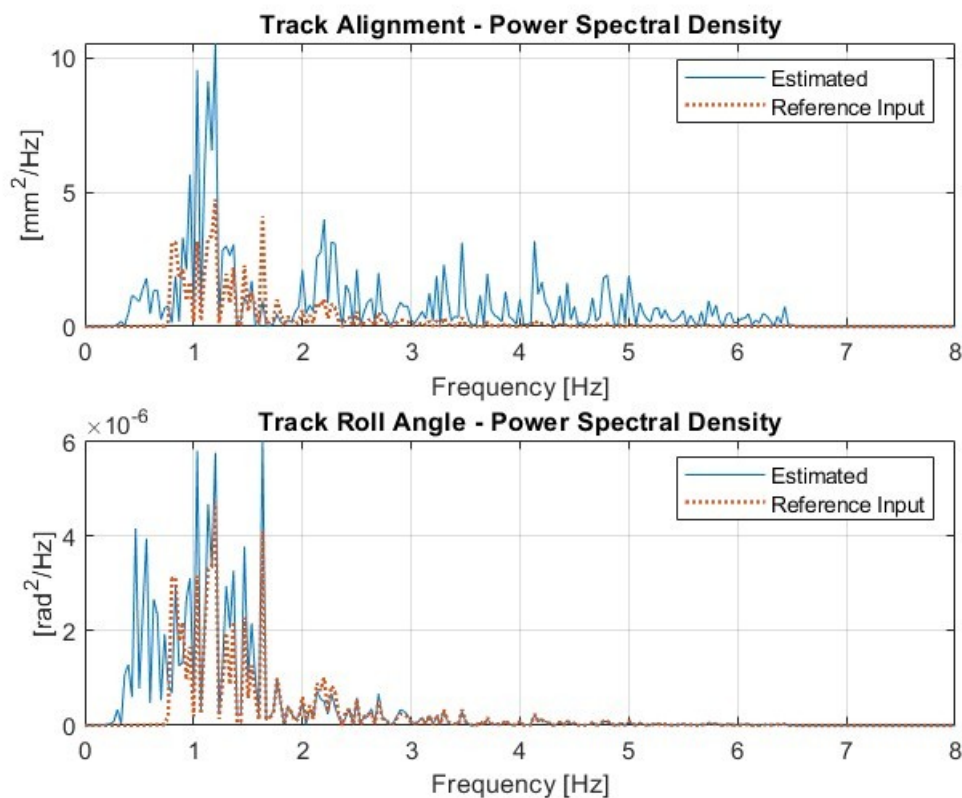


Figure 4.13: 21 D.o.F. Model – Estimation Power Spectral Density

In order to try and solve these issues, the natural next step is to try the same procedure using a third-order approximation instead of a quadratic one.

### 4.5.2. 3rd Order Padé Approximation

Changing the order of the Padé Approximation, however, is not without consequences. Due to the increase in size of the state matrix (mainly because of the enlarged Padé Approximation matrices), and most importantly due to having added several almost empty rows, the system becomes almost unobservable, therefore using the same set of measurements as before does not allow for the calculation of an adequate $L$ matrix, which turns out to be mostly composed of abnormally high values. By switching to control for an analogy, that's exactly the same as trying to control a vibrational mode through the application of a force which is almost uncorrelated with that mode – which should then be almost infinite to provide any effect.

This issue seems almost entirely uncorrelated with the criterion employed to move the poles to desired locations; even trying to simply displace the unstable poles towards the negative real part of the Gaussian Plane results in an unsuitable $L$ matrix, hindering any possibility of estimation.

As exposed in Section 2.1, precisely with the (2.6), it can be deduced that by uncautiously increasing the gains, the estimator becomes all but driven entirely by measurements, instead of combining them with the actual model; even worse, the gain actually multiplies the *difference* between said measurements and the estimated values of the measured quantities, effectively creating a system which only amplifies whatever inaccuracy we are feeding it with. Problem is, what is being employed is just a simplified linear model of the real vehicle, thus it is inevitable for some inaccuracies to be featured, them being related to non-linear effects, measurement noise or other causes. Therefore, the quantity which gets amplified by the aforementioned overly high gain matrix, however small, will never be equal to zero, resulting in a divergent estimation.

Although the U.I.O. is unable to provide an estimation for this particular set of measurement, there is an alternative way to proceed, although unorthodox. All 17 available measurements have been already used, so there are no more accelerations to be added to increase robustness; however, nothing prevents to extend the set of employed measurements for the estimation to the second half of the original state vector, thus taking also some velocities into account. This might seem counterintuitive given the premise of the study, it being the reconstruction of irregularity through accelerometers' measurations, but just as was done since the beginning to exploit the "derivative" requirement, the "velocity measurements" can once again be obtained as just the integration of the corresponding acceleration ones. In particular, all 8 accelerations relative to the four wheelsets (thus both lateral and yaw ones) were processed in this way to bring the total number of inputs to 25. A quick schematization of the solution is proposed in the Figure 4.14 in the next page:
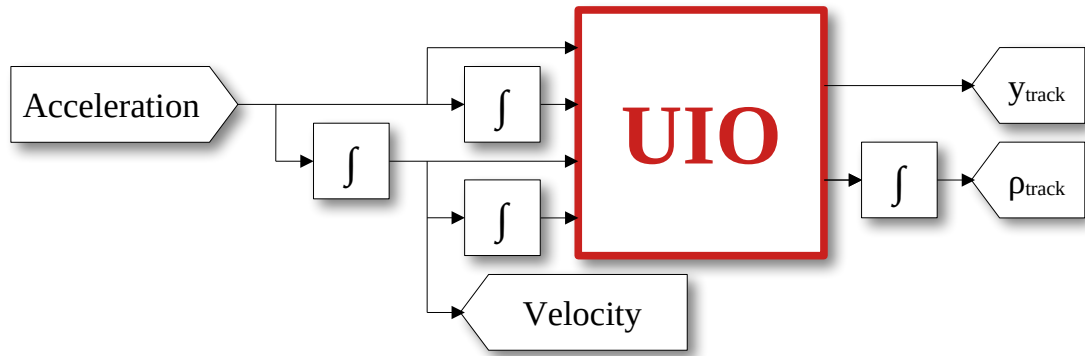
Figure 4.14: U.I.O. structure taking as inputs Acceleration and Velocity

Problem is, this means that the velocity measurements will have to be integrated twice (one from acceleration to velocity, and another one to convert this "derivative of the input" into the input itself); hence, any discrepancy between the expected value and the actual one (it being measurement noise or the linear model inaccuracy) would result in a very noticeable drift.

In order to solve this issue and obtain the result we are looking for, our filtering capabilities must be drastically increased; the simple double zero high-pass filter employed in Section 3.5 will not be good enough anymore, but instead a fourth-order Butterworth Filter will be used, with a cutoff frequency much less inclusive of potential deceleration and instead quite close to actual operation – corresponding to the traversing of a 25m-wavelength irregularity at a speed of *40km/h* (by comparison, cutoff frequency in the vertical case was defined at the same wavelength but for a *10km/h* speed). Furthermore, due to the increased size of matrix *L*, the pole placement was phased out in favour of a more robust Riccati-based positioning system using weighted identity matrices (weight=1 for *Q*, 0,0001 for *R*) as tentative variances.

The results pictured in Figure 4.15 are highly promising; it is noticeable, once again, that track roll has been accurately estimated (an expected outcome given the difference in complexity between the two parallel systems) while rail lateral alignment suffers from a general overestimation which, by looking at the PSD in Figure 4.16, seems to be an issue plaguing all frequency range, thus a more refined and less "brutal" filtering could furtherly improve it.
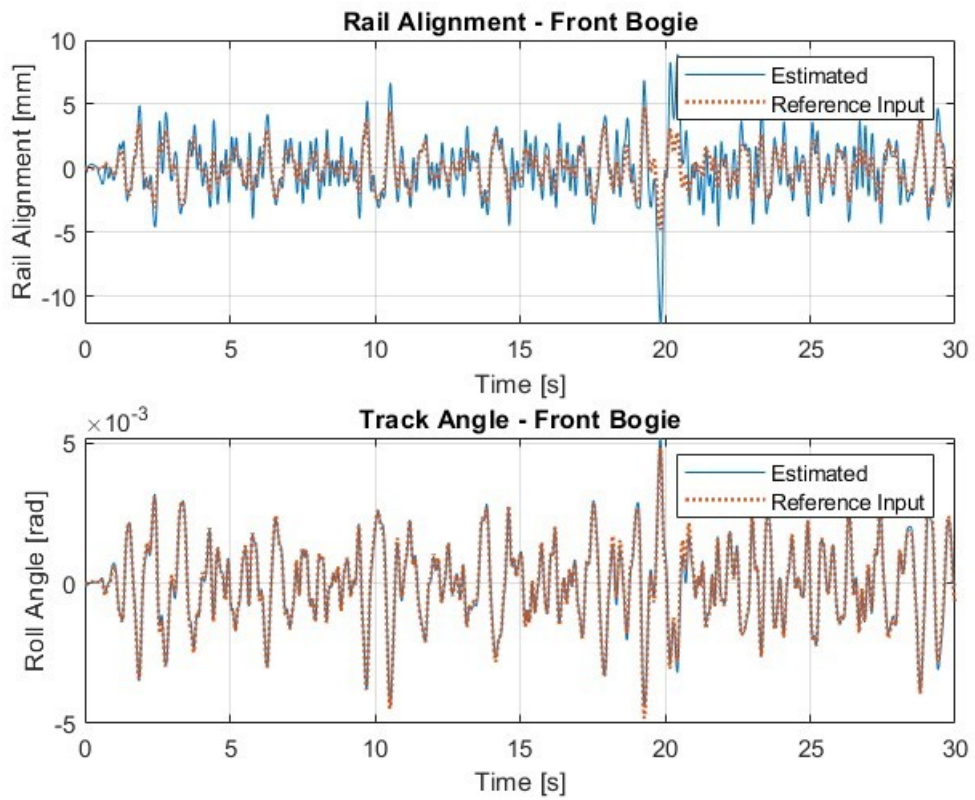
Figure 4.15: 21 D.o.F. Model - U.I.O. results (17 Accelerations + 8 Wheelset Velocities)
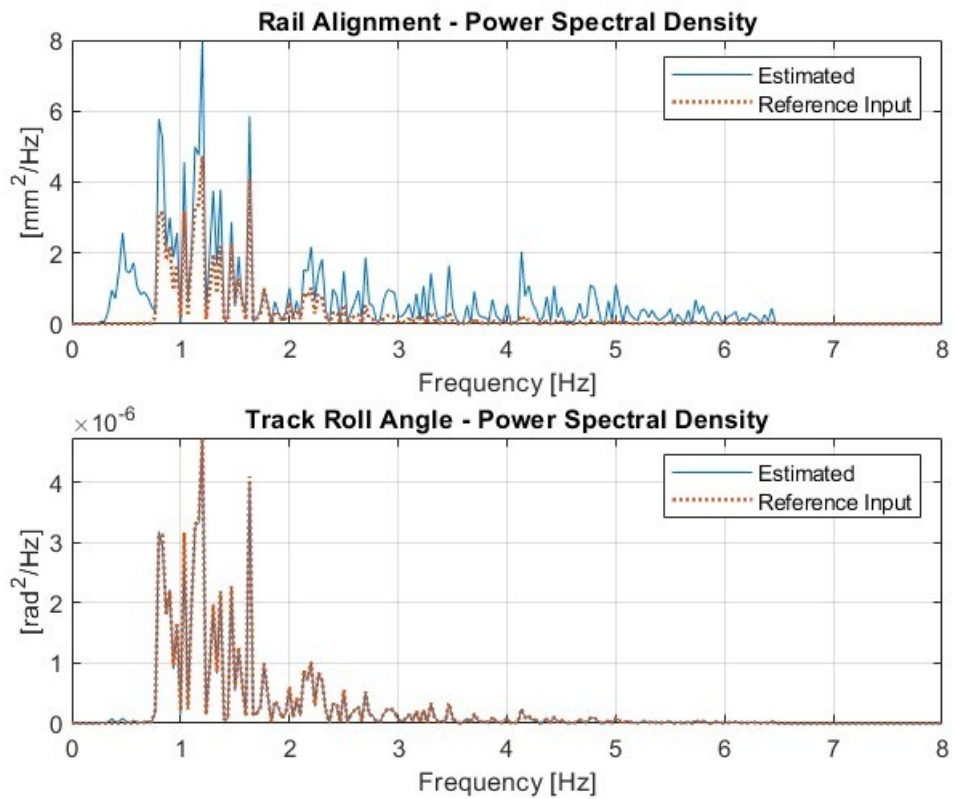


Figure 4.16: 21 D.o.F. Model – Estimation Power Spectral Density

That being said, even the less precise lateral geometry estimation is qualitatively correct in shape, although overestimated; the main difference between estimation and reference, as per the error trend in Figure 4.17, is clearly happening at T = 20s;
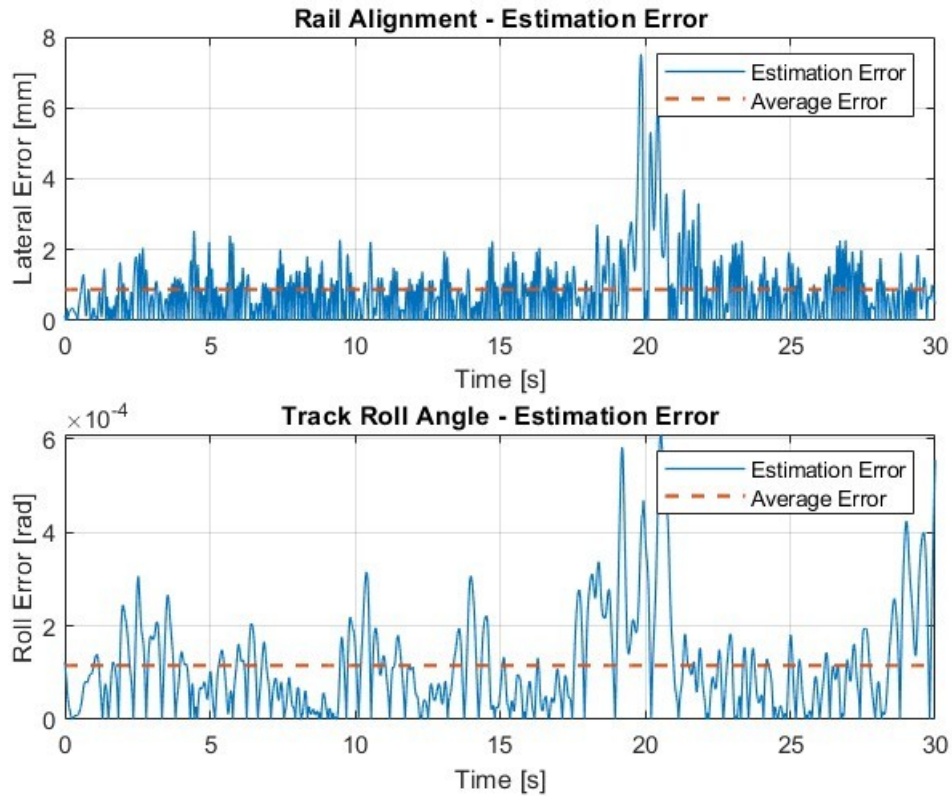


Figure 4.17: 21 D.o.F. Model – Estimation Error

This, however, is widely to be expected; if the provided wheelset accelerations are analyzed, in particular the lateral accelerations of the rear bogie (Figure 4.18), it can be distinctively observed that a rather pronounced spike is featured exactly at around 20s, determining these issues.
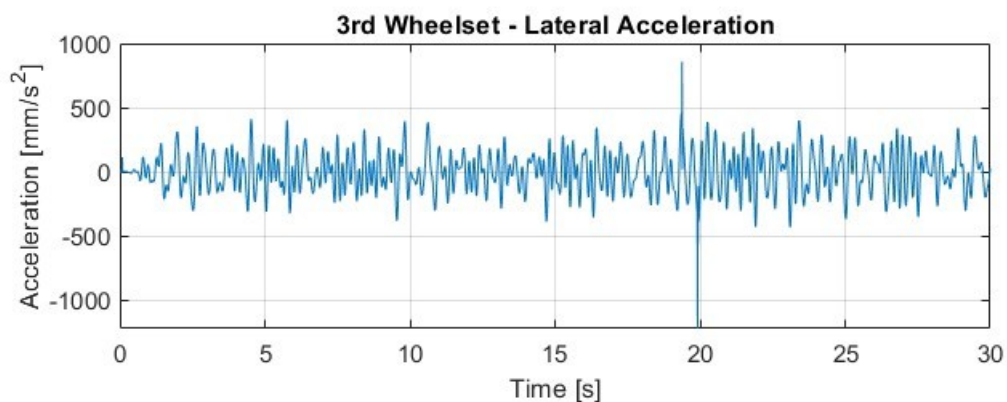


Figure 4.18: 21 D.o.F. Model – 3rd Wheelset Lateral Acceleration

It can however still be noticed that average error (represented by the dotted red line in the Figure 4.17 in the previous page) is well below the 1mm threshold, therefore providing a fairly valuable first-guess result. As per the roll angle, average error is almost neglectable, it being around 0,1mrad in value (against actual roll values spanning in the -5 to +5mrad range).

In order to have a second confirmation of the validity of this procedure, another simulation was run at a lower speed, this time 40km/h. In this case, too, the results (Figure 4.19 to Figure 4.21) seem to be highly accurate for the roll and moderately so – if not generally overestimated – when looking at the lateral irregularity. The filtering speed this time has been reduced to 30km/h to accommodate for the lowered vehicle velocity.
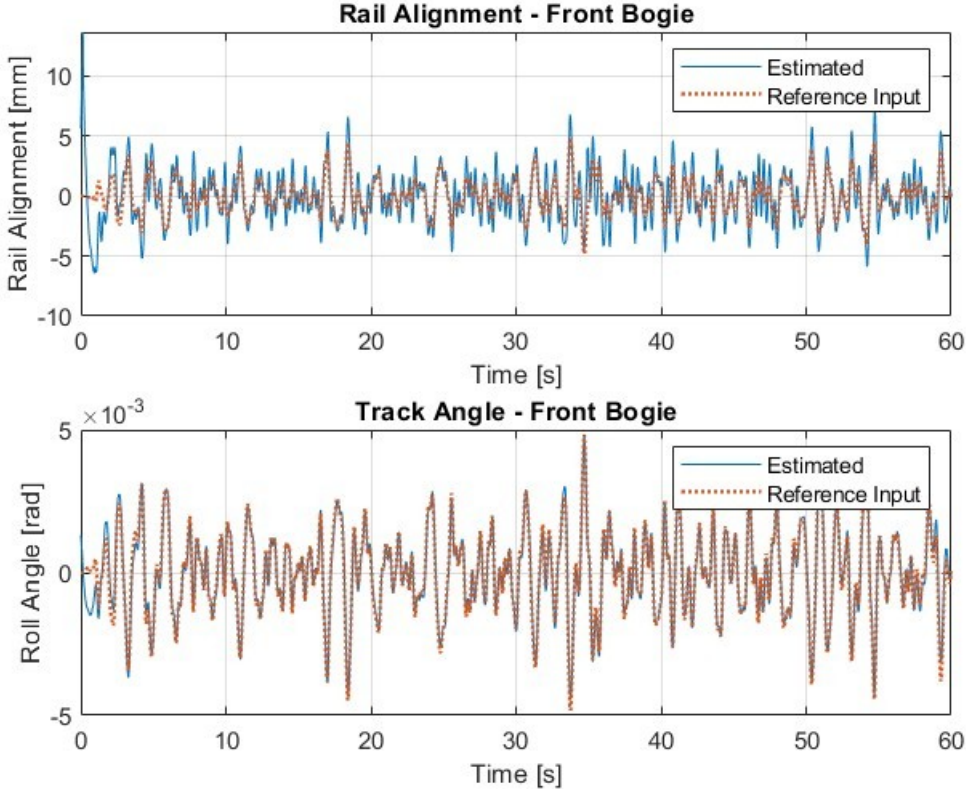


Figure 4.19: 21 D.o.F. Model - U.I.O. results (40km/h simulation)

It can immediately be noticed that in this case no spikes are featured along all the simulation time, and that the average error is fundamentally unchanged from the previously discussed 70km/h case (less than 1mm for lateral alignment, around 0,2mrad for roll angle).
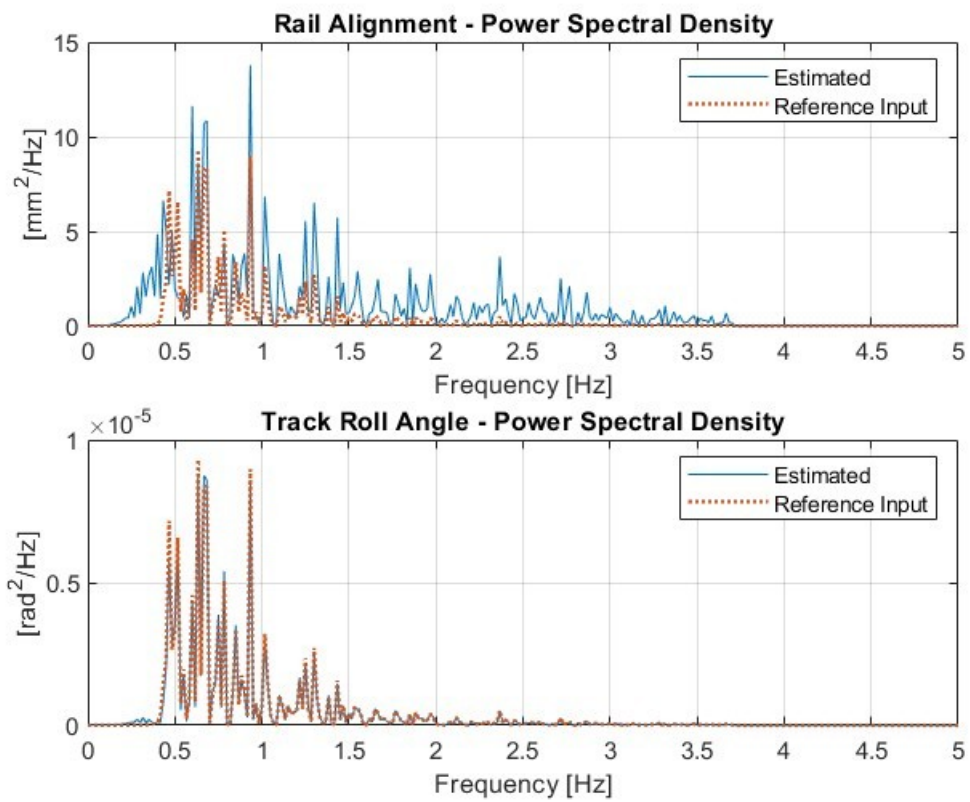
Figure 4.20: 21 D.o.F. Model - Estimation Power Spectral Density (40km/h simulation)
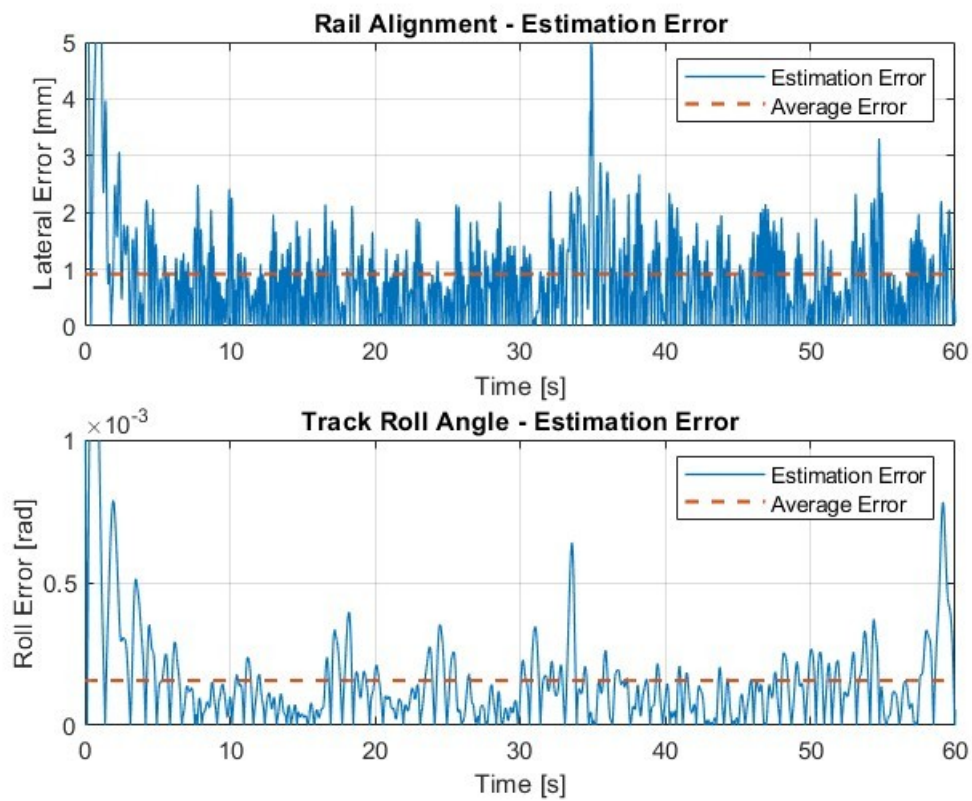


Figure 4.21: 21 D.o.F. Model – Estimation Error (40km/h simulation)

The values reported in Table 4.11 below describe the general validity of the approximation through the same coefficients used for Section 3.5, this time calculated for both the lateral alignment and the roll estimation in both the simulations:

Table 4.11: Values of indices for the 70km/h and 40km/h case

| Index | Value (70km/h) | Value (40km/h) |
|---|---|---|
| $\alpha_{\text{LATERAL}}$ | 0,726 | 0,827 |
| $\alpha_{\text{ROLL}}$ | 0,012 | 0,028 |
| $\beta_{\text{LATERAL}}$ | 0,562 | 0,631 |
| $\beta_{\text{ROLL}}$ | $3{,}3\times10^{-3}$ | $9{,}1\times10^{-3}$ |

All of this allows to conclude that the system is able to very accurately estimate roll track angle, while suffering from a tendency to overestimate track irregularity particularly when encountering sudden change in accelerational values (i.e. discontinuities or anyhow extremely localized peaks). Since the problem seems generalized to all the relevant frequency spectrum, this could be linked to the use of the same filtering technique for both roll and $y_{track}$. Moreover, it can be said with a certain degree of safety that the higher the speed, the better the results (since the indices values in the table above are constantly higher for the lower speed simulation); then again, this is not unexpected due to Padé Approximation being more adequate to model delays when said delay has a lower value.

# 5 Conclusion and future developments

The present thesis work aimed at demonstrate whether it is possible to employ the Unknown Input Observer algorithm to reconstruct the geometry of a railtrack through measurement of accelerations on a rail vehicle during its normal operation, specifically the 900 Series Meneghino model currently serving on 3 out of 5 lines of the Milan Metro. First, the vertical alignment estimation was performed through a U.I.O. based on a 10 D.o.F. linearized system; Padé Approximation was thus used to take multiple delayed inputs into account, but only between front and rear wheelsets of the same bogie due to its intrinsic accuracy limitations and the vehicle low speed. A 5km/h threshold-based gain selection algorithm was employed to take variable velocity into account, so to replicate the real operational conditions. A multibody model provided by PoliMi was used to generate virtual measurements, and the input it was fed with was thus compared with the U.I.O. estimated values. Results were deemed more than acceptable both in straight sections and turns, although the former noticeably more so.

Next, the estimation of lateral and roll irregularities was considered. A U.I.O. based on a 21 D.o.F. linear model was used for this task, taking into account the friction contact dynamics through the application of the creepages theory; Padé Approximation was once again employed, but its order had to be increased from 2 to 3 to take higher frequency disturbances into account. This, however, resulted in a nearly unobservable system, making it impossible for the system to generate a valuable gain matrix and making it necessary to increase the set of measurements to 25, thus including the 8 unconstrained wheelset velocities. Through adequate filtering, this made it possible to proceed with a remarkably accurate roll angle estimation and a rather promising first estimation of lateral irregularity, although the latter suffering from overestimation along a wide frequency range.

In general, it can be said that the U.I.O. works at its best when dealing with simple enough systems, as testified by both vertical dynamics and roll track angle. However, if the more strict conditions on its application are relaxed (i.e., through external methods for the gain matrix calculation and the employment of more advanced filtering techniques), even more complex structures can be dealt with; it is also true, though, that other methods such as the one based on Kalman Filter does not require particular modifications to adapt to the system complexity. One possible further step in this analysis would be, in fact, to repeat the same procedures with said Kalman

Observer and compare the results; nonetheless, it is already possible to make some consideration.

On one hand, it is unquestionable that Kalman does provide generally more accurate results, and countless works on the same topic seem to confirm this. That being said, though, until the very end the main point of U.I.O. - that is, its deterministic behaviour, thus not requiring prior knowledge of the to-be-estimated quantities' statistical behaviour – has been preserved. It is also true, on the opposite, that further refinement of the variance values used to calculate the extended $L$ matrix through stochastic methods *could* have a beneficial effect on the estimation; however, this aspect has not been explored in this work, both to avoid excessive complications and to keep the aforementioned premise true.

There are further developments that could be built upon this experiences. In particular, some of the considerations which were made for the simpler vertical case could be extended for the lateral case: the variable velocity $L$ selection algorithm was not analyzed for the lateral case due to the straight condition not featuring significant distinction from the previously done vertical case (i.e. velocity effect being mostly relegated to the Padé Approximation effect). However, if a curved track was analyzed instead (thus requiring a more extended set of steady-state conditions around which to linearize), matrices $A$ and $E$ would depend on velocity also through the contact dynamics themselves, making the application of speed-based gain scheduling a rather difficult but definitely interesting potential development.

# Bibliography

[1]     http://dati.istat.it/Index.aspx?DataSetCode=DCSC_TRAFERR

[2]     C. Esveld, *Modern Railway Track*, Version 3.8 (2015)

[3]     https://www.mermecgroup.com

[4]     M. Moretti, M. Triglia, G. Maffei, *ARCHIMEDE − The first European diagnostic train for global monitoring of the railway infrastructure*, in: 2004 IEEE Intelligent Vehicles Symposium, Parma, Italy (June 14-17 2004)

[5]     A. De Rosa, S. Alfi, S. Bruni, *Estimation of lateral and cross alignment in a railway track based on vehicle dynamics measurements* (2017)

[6]     P. Weston, C.S. Ling, C.J. Goodman, C. Roberts, P. Li, R.M. Goodall, *Monitoring lateral track irregularity from in-service railway vehicles*, Proc. Inst. Mech. Eng. Part F1: Rail Rapid Transit 221 (2007) 89–100.

[7]     J. Real, P. Salvador, L. Montalbán, M. Bueno, *Determination of rail vertical profile through inertial methods*, Proc. Inst. Mech. Eng. Part F: Rail Rapid Transit 225 (2011) 1337–1359.

[8]     S. Alfi, S. Bruni, *Estimation of long wavelength track irregularities from on board measurement*, in: Proceedings of 4th IET Int. Conference Railway Condition Monitoring (2008) pp. 1–6.

[9]     H. Tsunashima, Y. Naganuma, T. Kobayashi, *Track geometry estimation from car-body vibration*, Veh. Syst. Dyn. 52 (4) (2014) 207–219.

[10]    B. Friedland, *Control System Design: An Introduction to State-Space Methods*, Dover Publications (1986)

[11]    J. Chen, R.J. Patton, *Robust Model-Based Fault Diagnosis for Dynamic System*, Springer (1999)

[12]    S.X. Ding, *Model-based Fault Diagnosis Techniques*, Springer (2008)

[13]    G. Diana, F. Cheli, *Advanced Dynamics of Mechanical Systems*, Springer (2015)

# List of Figures

# List of Tables